FINITE ELEMENT SOLUTION FOR ELECTROMAGNETIC SCATTERING FROM TWO-DIMENSIONAL BODIES

by

John Lawrance Mason

A dissertation submitted in partial fulfillment
of the requirements for the degree of
Doctor of Philosophy
(Electrical Engineering)
in The University of Michigan
1982

Doctoral Committee:

Professor Thomas B.A. Senior (Co-Chairman)
Professor William J. Anderson (Co-Chairman) (Aerospace Engineering)
Associate Professor Valdis V. Liepa
Professor Ronald J. Lomax
Professor Herschel Weil

For Linda, Jane, and David

ACKNOWLEDGEMENTS

The author wishes to acknowledge the financial support provided in the early stages of the research by the Radiation Laboratory of the Department of Electrical and Computer Engineering at The University of Michigan (a stipend) and by Western Michigan University, his employer (a sabbatical leave). At Western, Dean W. Chester Fitch and Assistant Dean Robert E. Boughner of the College of Applied Sciences, and Professor Cassius A. Hesselberth, Chairman of the Electrical Engineering Department were particularly helpful in obtaining support.

The author is grateful for the aid and advice given him by the Doctoral Committee. He also received advice from the following individuals: Professor C. Bruce Sharpe of The University of Michigan, and Professor Paul J. Eenigenburg and Assistant Professor Dean R. Johnson, both of Western Michigan University. Assistance with the computer program was received from the staff at the Western Michigan University Computer Center, particularly from William Granet, George R. Kohrman, and Brian T. Mitchell. The author wishes to thank Linda Mason and Wanita Rasey for typing the first and final versions of the dissertation respectively and for their editorial assistance. Also, the author is grateful for the overnight accommodations provided by Leroy and Sara Kottke on numerous occasions. Finally, the author wishes to thank his wife and children for their patience and understanding during the time this work was in progress.

TABLE OF CONTENTS

LIST OF ILLUSTRATIONS

LIST OF TABLES

LIST OF APPENDICES

ABSTRACT

FINITE ELEMENT SOLUTION FOR ELECTROMAGNETIC

SCATTERING FROM TWO-DIMENSIONAL BODIES

by

John Lawrance Mason

Co-Chairmen: Thomas B.A. Senior, William J. Anderson

The problem of two-dimensional electromagnetic scattering from bodies in free space has been formulated using a differential equation finite element method. An incident plane wave polarized so as to excite only E-wave fields has been assumed. A weak integral statement was obtained using an approach equivalent to the weighted residuals method, the weighting functions being selected by Galerkin's method. The finite element mesh of general first-order quadrilaterals extended outward into the far field region of the scattering body, where the boundary condition at the outer boundary was obtained from the asymptotic expression for the scattered field.

In order to compare the finite element method with an integral equation moment method, a special case was solved numerically, namely that of a thin, infinitely long resistive strip. Accurate numerical results from a moment method solution were available to serve as a check on the accuracy of the finite element method results. For a perfectly conducting strip (the limiting case of a resistive strip) the finite element mesh contained special triangular elements at the edges of the strip to model the singularities in the magnetic field

which occur there. Two important disadvantages of the finite element solution became apparent. First, the boundary condition used at the outer boundary leads to the presence of standing waves in the computed scattered field, a non-physical result. Second, the computer memory required increased much more rapidly with strip width than in the moment method solution.

The finite element method used was thus unable to compete with the moment method solution for the thin strip problem. However, to demonstrate a problem for which a moment method solution may be less attractive because of its increased memory requirements, numerical results were obtained using the finite element method for scattering from a body consisting of a thin resistive strip embedded in a dielectric cylinder.

CHAPTER I. INTRODUCTION

1.1 Historical Background

The scattering of electromagnetic waves from bodies consisting of a simple shape of homogeneous material has been studied for years. Much of the early work focussed on bodies whose geometry coincided with coordinate surfaces of systems for which the wave equation is separable. Typically, modal expansions of the fields were written, followed by application of boundary conditions. The solution was in the form of an infinite series. Numerical values of the fields were then obtained by summing a finite number of terms of the series, which was generally a time-consuming process. The solution of scattering problems using integral equation formulations was not accomplished except in two cases. In these cases the body surfaces were complete coordinate surfaces of a system where the wave equation is separable. An integral transform was found to invert the equation for a solution.

The techniques mentioned above are usually called analytical techniques, even though they are often followed by a numerical procedure to evaluate the resulting expressions at particular points. For bodies having complicated shapes and/or inhomogeneous material properties, these techniques fail. Instead, so-called numerical techniques are used. Until about 1970, most electromagnetic scattering problems which were solved numerically involved finite

difference, variational, or moment methods (Wexler, 1969; Jones, 1956; Harrington, 1968). Since 1970 the finite element method, utilized earlier in applied mechanics, has been applied to scattering problems with some success. All of these numerical methods provide a procedure for converting a scattering problem, formulated in terms of either a differential equation or an integral equation, into a problem of solving a system of linear algebraic equations.

1.2 Formulation of Scattering Problems

For numerical solutions of scattering problems involving bodies in unbounded space, integral equation formulations have been preferred to those of differential equation formulations. The solution region for the integral equation is confined to the surface of the scattering body with boundary and radiation conditions automatically taken into account. Integral equation formulations are well suited for scattering by thin sheets and by bodies into which the field does not penetrate. However, it is more difficult to obtain such formulations for scattering problems involving thick, inhomogeneous bodies into which the field does penetrate.

The most commonly used numerical technique for the solution of integral equations arising from scattering problems is the method of moments. The resultant system of linear algebraic equations has a dense matrix of coefficients. In view of the current computer hardware available, this method can be applied to scattering bodies with surface areas up to about one square wavelength or, in the case of two-dimensional problems, to lengths of about five

wavelengths. A characteristic of the method is that the solution becomes non-unique at frequencies for which the interior of the scattering body is resonant (Klein and Mittra, 1975).

Differential equation formulations have been used primarily for interior scattering problems when numerical solutions have been made. For exterior problems, the solution region for the differential equation is unbounded, requiring application of the radiation condition at infinity. The solution region is thus larger than that for an integral equation formulation and is of higher dimension. However, a differential equation formulation is convenient for inhomogeneous media.

Interior problems formulated in terms of a differential equation are usually solved numerically with finite difference, moment, or finite element methods. The finite difference algorithms are usually the simplest. However, the finite element method has advantages over both the other methods in terms of accuracy and ability to handle bodies having complex shapes. All of these methods lead to systems of linear algebraic equations having sparse matrices. Proper arrangement of the equations results in a banded matrix allowing use of efficient equation solvers so that computer time and memory requirements can be reduced. These comments apply to exterior problems for which, however, all the methods require application of the radiation condition and, in general, require a large system of equations due to the large solution region. Difficulties associated with these two requirements for an

exterior problem may easily overshadow the advantages of a differential equation formulation over an integral equation formulation, except for the ability to handle inhomogeneous media.

The work reported here is an effort to determine if, and under what conditions, a finite element differential equation solution might be more economical than a moment-method integral equation solution for exterior scattering by electrically large bodies (dimensions of one half wavelength or greater). Also a finite element solution is demonstrated for a case involving a thick body for which a moment method integral equation solution may not be practical.

1.3 Previous Work

The finite element method has seen limited application in solution of integral equations (for example, Jeng and Wexler, 1977, and Sankar and Tong, 1975) because of the efficiency of the method of moments. The finite element method was first applied successfully to interior boundary value problems because of the difficulty in handling the radiation condition in exterior problems. For example, Arlett et al., (1968) solved the Helmholtz equation in a waveguide using a variational formulation combined with a finite element discretization.

Silvester and Hsieh (1971) reported solving Laplace's equation for an exterior problem using a variational formulation. They divided the solution region into two parts, one part being a local region containing, for example, sources, conductors and dielectrics. The local region was treated using finite elements.

The other region, extending to infinity was treated as a single exterior element. In the portion of the formulation related to this element it was necessary to require that the stored energy in the exterior region be finite, a requirement which is met by solutions of Laplace's equation. Determination of the element matrix involved the solution of an integral equation.

McDonald and Wexler (1972) also divided the solution region into a local region and external region. An integral equation using a free-space Green's function was used to relate the field at points within the local regions to points on the boundary of the external region. Examples of cases satisfying the Laplace and Helmholtz equations were solved using a variational formulation. As a result of the use of the integral equation, the global matrix obtained was more dense than the typical banded matrix of a finite element solution.

The works of Silvester and Hsieh, and McDonald and Wexler are examples of the combined use of finite element and boundary integral methods. Another example is the study by Berkhoff (1975) on linear water wave propagation. A survey of work using this combined approach was given by Zienkiewicz, Kelly and Bettess (1977). The technique was also discussed by Brebbia and Walker (1980), Zienkiewicz (1977), and McDonald and Wexler (1980).

In another approach known as the unimoment method and developed by Mei (1974), the fields in the exterior region are expressed in a modal expansion and the interior region is handled using finite element or finite difference techniques. The interior

and exterior problems are then coupled together by enforcing boundary conditions for the fields at the boundary between the regions. The resulting system of equations has a banded matrix. The unimoment method has been applied to the scattering of dielectric cylinders (Chang and Mei, 1976) and to inhomogeneous penetrable bodies of revolution (Morgan and Mei, 1979).

Another way of handling the outer boundary condition for an exterior problem, proposed by Ungless (1973) and applied by Bettess (1977), involves the use of elements extending to infinity. The shape functions for such infinite elements must realistically model the behavior of the unknown as the distance increases from the local region of interest and should lead to integrals over the element domain which are finite. Bettess and Zienkiewicz (1977) used a combination of finite and infinite elements in a study of water waves. Included in the infinite element shape functions was an exponential factor with a decay length. Although this method does not require detailed knowledge of the form of the solution in the outer region, some knowledge of the exact solution is required to be able to select the decay length. This approach does not give an accurate indication of the behavior of the unknown towards infinity; however, the effect of the far region on the local region of interest is introduced.

Thatcher (1978) used an infinite number of elements defined in a systematic way to solve Laplace's equation in an unbounded region. This method will also handle singularities occurring at

boundaries of the solution region. Application of this method to the solution of the Helmholtz equation in unbounded regions has apparently not been made.

Other work has been reported on absorbing or non-reflecting boundary conditions for use with finite difference or finite element solution of wave propagation problems, whereby the exterior problem is converted to a pseudo-interior problem. Smith (1974) proposed the superposition of the solutions of Dirichlet and Neumann problems to completely eliminate reflections at a plane boundary of a half space. However, this approach does not seem applicable to other geometries. Orlanski (1976) used the Sommerfeld radiation condition and a numerical evaluation of phase velocity in the vicinity of the boundary. In a mechanics problem involving determination of strain, Hanson and Petschek (1976) used a spring-dashpot system as a terminating network on a one-dimensional system to absorb a single wavelength. They reported successfully using a similar technique on a two-dimensional problem. Engquist and Majda (1977) developed "perfectly absorbing" boundary conditions for general classes of wave equations. They then derived local boundary conditions, suitable for numerical calculations, which approximate the theoretical boundary conditions.

1.4 Objectives of the Present Study

The first objective of the present study is to develop a finite element formulation for an exterior scattering problem.

Specifically, a differential equation formulation is used. The variational method, typical of finite element work, is replaced by a Green's identity and Galerkin's method. This amounts to using the method of weighted residuals. Also, the handling of the boundary condition at the edge of the finite element region is performed in such a manner that: (1) the influence of the boundary condition is made through individual element contributions and (2) the band nature of the global system matrix is preserved. This rules out the use of boundary integral techniques.

The second objective is to apply the finite element formulation to the solution of a specific scattering problem to determine if it has an advantage over a moment method integral equation solution for electrically large bodies. Scattering from an infinitely long, finite width, infinitesimally thin, flat resistive strip is considered since an integral equation formulation and accurate moment method numerical solution (Knott, Liepa and Senior, 1973) are available. Briefly a resistive sheet has the properties that: (1) the component of the electric field tangent to the surface has no discontinuity at the surface, and (2) the component of the magnetic field tangent to the surface has a discontinuity at the surface which is directly proportional to the tangential electric field. A perfectly conducting sheet can be considered as a resistive strip with zero resistivity. Both formulations are capable of handling a strip whose resistivity varies in the direction perpendicular to the axis of the strip. Further,

since a singularity in the magnetic field occurs at the edge of a perfectly conducting strip, the finite element discretization includes special elements to accurately model this behavior.

The practical requirement of each solution method is to compute the far scattered field and the radar cross section. The effect of the element density on the accuracy of these results for various strip widths and resistivities, and for different angles of incidence is investigated. In order to accomplish this, an automatic element mesh generator is included in the computer program so that the element density, the length-to-width ratio of the elements, and the distance outward to which the finite element region extends can be easily changed. The effect of the element density on the computer memory requirements and CPU time is also examined.

The third objective is to apply the finite element formulation to the solution of scattering from a thick body into which the field penetrates so as to demonstrate a case where the moment method integral equation approach may not be practical. The specific case of a resistive strip embedded in a dielectric cylinder is considered.

CHAPTER II. FORMULATION OF THE SCATTERING PROBLEM

2.1 Statement of the Problem

An infinitely long, infinitesimally thin strip of width w lying parallel to the z-axis and in the x-z plane is immersed in an infinite, uniform medium with permeability μ_0 and permittivity ε_0 (Fig. 2.1). The strip is a resistive sheet whose resistivity in ohms per square is RZ_0, where $Z_0 = \sqrt{\mu_0/\varepsilon_0}$. The sheet is defined by its boundary conditions

$$[\hat{n} \times \underline{E}]^+_- = 0 \qquad (2.1)$$

and

$$RZ_0 \hat{n} \times [\underline{H}]^+_- = -\hat{n} \times (\hat{n} \times \underline{E}) \quad , \qquad (2.2)$$

where $\hat{n}$ is a unit normal to the strip in the positive y direction and the notation $[\ ]^+_-$ represents a discontinuity across the strip. $\underline{E}$ and $\underline{H}$ are, respectively, the total electric and magnetic field strengths. The normalized resistivity R may be a function of x, i.e., $R = R(x)$.

A plane wave, whose direction of propagation is perpendicular to the z-axis, is incident on the strip. The polarization is such that

$$\underline{E}^i = E^i_z \hat{z} = \hat{z}\, e^{-ik_0(x \cos \phi_0 + y \sin \phi_0)} \quad , \qquad (2.3)$$

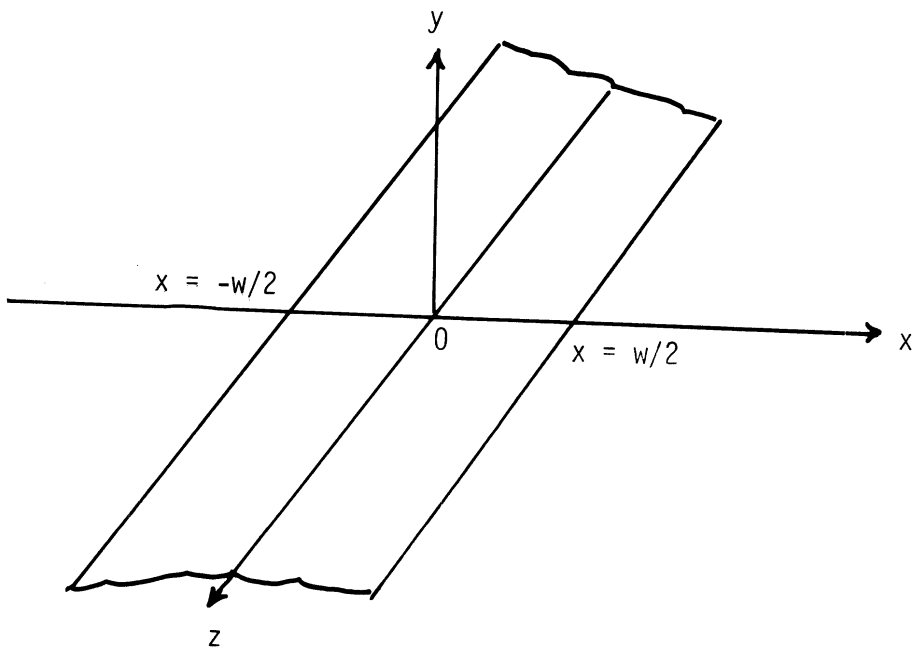

Fig. 2.1: A strip lying in the x-z plane.

where ϕ_0 is the angle that the direction of propagation makes with the plane of the strip (Fig. 2.2). An $e^{-i\omega t}$ time dependence is assumed for all time-varying quantities.

The incident fields $\underline{E}^i$ and $\underline{H}^i$ are the fields which would exist everywhere if the strip was not present. In the presence of the strip, the total fields are $\underline{E}$ and $\underline{H}$ which are the sums of the incident and scattered fields:

$$\underline{E} = \underline{E}^i + \underline{E}^{sc} \tag{2.4}$$

and

$$\underline{H} = \underline{H}^i + \underline{H}^{sc} \quad . \tag{2.5}$$

The scattered fields are associated with an outward radiation of energy and must satisfy a radiation condition at infinity. A surface current induced on the strip is given by

$$\underline{K} = \hat{n} \times [\underline{H}]_-^+ \quad , \tag{2.6}$$

but since the incident field has no discontinuity at the strip,

$$\underline{K} = \hat{n} \times [\underline{H}^{sc}]_-^+ \quad . \tag{2.7}$$

If a knowledge of the surface current density on the scattering body can be obtained, the far scattered field and the radar cross section can be determined using an integral representation such as that of Franz (1948, 1949).

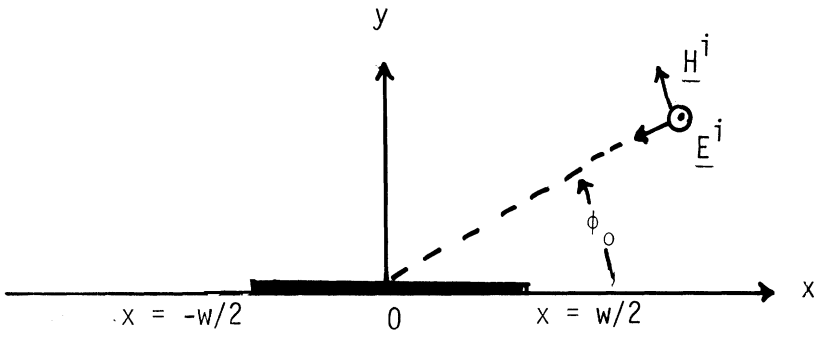

Fig. 2.2: An axial view of the strip.

Of interest here, is the prediction of the radar cross section of the strip for various angles of incidence, resistivities, and electrical strip widths.

2.2 Integral Equation Formulation

Formulation of a scattering problem in terms of an integral equation requires an integral representation (e.g., Stratton-Chu, 1939, or Franz) of the scattered field in terms of the surface current density on the scattering body. Expressions for the total fields in the space near the body can then be written. An integral equation for the surface current density is obtained if the observation point is allowed to approach the surface and the appropriate boundary conditions are applied (Maue, 1949 and Poggio and Miller, 1973).

A numerical solution of the integral equations of scattering problems is normally carried out using the method of moments (Harrington, 1968). Discretization of the equation and the unknown by this method results in a system of linear, algebraic equations which may be solved simultaneously using a digital computer.

2.3 Differential Equation Formulation

Maxwell's equations describing the electromagnetic field at any point in the region of free space surrounding the strip are

$$\nabla \times \underline{E} = i\omega\mu_0 \underline{H} \tag{2.8}$$

and

$$\nabla \times \underline{H} = -i\omega\varepsilon_0 \underline{E} \ . \tag{2.9}$$

The strip is assumed to be longitudinally invariant along z such that all field components are independent of z. Expanding (2.8) and (2.9) in component form yields

$$\frac{\partial E_z}{\partial y}\hat{x} - \frac{\partial E_z}{\partial x}\hat{y} + \left(\frac{\partial E_y}{\partial x} - \frac{\partial E_x}{\partial y}\right)\hat{z} = i\omega\mu_o(H_x\hat{x} + H_y\hat{y} + H_z\hat{z}) \qquad (2.10)$$

and

$$\frac{\partial H_z}{\partial y}\hat{x} - \frac{\partial H_z}{\partial x}\hat{y} + \left(\frac{\partial H_y}{\partial x} - \frac{\partial H_x}{\partial y}\right)\hat{z} = -i\omega\varepsilon_o(E_x\hat{x} + E_y\hat{y} + E_z\hat{z}) \quad . \qquad (2.11)$$

Decomposing (2.10) and (2.11) into scalar component equations yields the following two independent systems of equations:

$$\left.\begin{aligned} \frac{\partial E_z}{\partial y} &= i\omega\mu_o H_x \\ -\frac{\partial E_z}{\partial x} &= i\omega\mu_o H_y \\ \frac{\partial H_y}{\partial x} - \frac{\partial H_x}{\partial y} &= -i\omega\varepsilon_o E_z \end{aligned}\right\} \qquad (2.12)$$

and

$$\left.\begin{aligned} \frac{\partial H_z}{\partial y} &= -i\omega\varepsilon_o E_x \\ \frac{\partial H_z}{\partial x} &= i\omega\varepsilon_o E_y \\ \frac{\partial E_y}{\partial x} - \frac{\partial E_x}{\partial y} &= i\omega\mu_o H_z \end{aligned}\right\} \quad . \qquad (2.13)$$

Examination of the preceding equations reveals that (2.12) couple field components E_z, H_x, and H_y describing the field configuration of an E-wave, while (2.13) couple field components H_z, E_x and E_y describing the field configuration of an H-wave.

Since the incident plane wave has its electric field vector directed in the z-direction, only E-wave fields will be present. Eliminating H_x and H_y from (2.12) yields the following two-dimensional wave equation for E_z in which $k_o^2 = \omega^2 \mu_o \varepsilon_o$:

$$\frac{\partial^2 E_z}{\partial x^2} + \frac{\partial^2 E_z}{\partial y^2} + k_o^2 E_z = 0 \quad . \tag{2.14}$$

The incident plane wave field E_z^i satisfies the same wave equation, and thus it follows that the scattered field $E_z^{sc} = E_z - E_z^i$ satisfies

$$\frac{\partial^2 E_z^{sc}}{\partial x^2} + \frac{\partial^2 E_z^{sc}}{\partial y^2} + k_o^2 E_z^{sc} = 0 \quad . \tag{2.15}$$

Since the scattered field is an outwardly propagating wave, it satisfies the radiation condition (Bowman et al., 1969, p. 5):

$$\lim_{\rho \to \infty} \sqrt{\rho} \left[\frac{\partial E_z^{sc}(\underline{\rho})}{\partial \rho} - ik_o E_z^{sc}(\underline{\rho}) \right] = 0 \quad , \tag{2.16}$$

where $\underline{\rho}$ is a position vector in the x-y plane. At the strip the boundary conditions may be re-expressed as

$$[E_z^{sc}]_-^+ = 0 \tag{2.17}$$

and

$$R(x)Z_0\hat{n} \wedge [\underline{H}^{sc}]_-^+ = -\hat{n} \wedge (\hat{n} \wedge \underline{E}) \quad . \tag{2.18}$$

Since there is no discontinuity in the incident field and $\hat{n} = \hat{y}$, (2.18) becomes

$$-R(x)Z_0[H_x^{sc}]_-^+ = E_z = E_z^i + E_z^{sc} \quad . \tag{2.19}$$

Further, because (2.12) applies to the scattered fields,

$$H_x^{sc} = -\frac{i}{\omega\mu_0}\frac{\partial E_z^{sc}}{\partial y} \tag{2.20}$$

and

$$\frac{iR(x)}{k_0}\left[\frac{\partial E_z^{sc}}{\partial y}\right]_-^+ = E_z^i + E_z^{sc} \quad . \tag{2.21}$$

In the case of a perfectly conducting strip, $R(x) = 0$, implying that

$$E_z^{sc} = -E_z^i \tag{2.22}$$

at the strip.

Some symmetry properties of the scattered field evident from an integral representation (e.g., 2.38) should be noted at this point:

$$E_z^{sc}(x,y) = E_z^{sc}(x,-y) \quad , \tag{2.23}$$

$$H_x^{sc}(x,y) = -H_x^{sc}(x,-y) \quad . \tag{2.24}$$

This means that (2.19) can be written as

$$-2R(x)Z_o H_x^{sc}\big|_+ = E_z^i + E_z^{sc} \quad . \tag{2.25}$$

Using (2.20), this becomes

$$\frac{2iR(x)}{k_o} \left.\frac{\partial E_z^{sc}}{\partial y}\right|_+ = E_z^i + E_z^{sc} \tag{2.26}$$

on the strip. Further, from symmetry considerations, H_x^{sc} equals zero off the strip in the x-z plane, implying that

$$\frac{\partial E_z^{sc}}{\partial y} = 0 \tag{2.27}$$

for $|x| > w/2$, $y = 0$. These symmetry properties allow the solution of the problem by solving the wave equation only in the half-space $y \geq 0$.

The boundary conditions at the edge of the strip are not as easily deduced as they were elsewhere on the strip. At the edge there is some ambiguity concerning the definition of normal and tangent vectors. Meixner (1949) proposed an additional boundary condition which, when imposed, makes the solution to the boundary value problem unique. His "edge condition" states that the electromagnetic energy density must be integrable over any finite domain even if the domain contains singularities of the electromagnetic field. Bouwkamp (1946) showed that in the case of a perfectly conducting infinitesimally thin

plane surface with an edge, near the edge the singular components of the electric and magnetic field vectors are of the order of $r^{-1/2}$, where r is the distance from the edge, while components of the fields parallel to the edge are always finite. It should be noted here that the singularities which do occur are in the scattered field components and not in the incident field. Also, the induced surface current density parallel to the edge of a perfect conductor is infinite at the edge.

Extending the work of Meixner to deal with imperfectly conducting edges, Fawzi and Burke (1974) concluded that there are no singularities in any of the field components at the edge of a nonmagnetic, finite conductivity wedge. Senior (1979) found that the current density along the edge of a resistive sheet is always finite.

A numerical solution for the scattered field E_x^{sc} using the differential equation formulation is carried out by the finite element method as described in the following chapters.

2.4 Far Scattered Field and the Radar Cross-Section

In order to obtain the far scattered field, the induced surface current density K_z on the strip is calculated. Using (2.7) and (2.20)

$$K_z = -[H_x^{sc}]_-^+ = \frac{i}{k_o \bar{Z}_o}\left[\frac{\partial E_z^{sc}}{\partial y}\right]_-^+ . \qquad (2.28)$$

For a resistive sheet, (2.19) yields

$$K_z = \frac{1}{R(x)Z_0}(E_z^i + E_z^{sc}) \quad , \tag{2.29}$$

where $R(x) \neq 0$.

Using Franz's representation, the scattered field may be expressed as

$$\underline{E}^{sc}(\underline{r}) = \nabla \wedge \nabla \wedge \underline{\Pi}(\underline{r}) \quad , \tag{2.30}$$

where $\underline{\Pi}$ is a Hertz vector of the electric type given by

$$\underline{\Pi}(\underline{r}) = \frac{i}{\omega\varepsilon_0}\int_S \underline{K}(\underline{r}')G_0(\underline{r},\underline{r}')ds' \tag{2.31}$$

in which

$$G_0(\underline{r},\underline{r}') = \frac{e^{ik_0|\underline{r} - \underline{r}'|}}{4\pi|\underline{r} - \underline{r}'|}$$

is the free space Green's function. This field satisfies the radiation condition at infinity. Since

$$\nabla \wedge \nabla \wedge \underline{\Pi} = \nabla(\nabla \cdot \underline{\Pi}) - \nabla^2\underline{\Pi}$$

and

$$\nabla^2\underline{\Pi} + k_0^2\underline{\Pi} = 0 \tag{2.32}$$

in source-free regions,

$$\underline{E}^{sc} = \nabla(\nabla \cdot \underline{\Pi}) + k_o^2 \underline{\Pi} \tag{2.33}$$

at any point off the sheet S.

Since the problem being considered in the present work is two-dimensional (no variation in the z-direction) and since $\underline{K} = K_z \hat{z}$, then $\underline{\Pi} = \Pi_z \hat{z}$ and $\nabla \cdot \underline{\Pi} = 0$. Thus

$$\underline{E}^{sc} = E_z^{sc} \hat{z} = k_o^2 \Pi_z \hat{z} \quad , \tag{2.34}$$

where

$$\Pi_z = \frac{i}{\omega \varepsilon_o} \int_{\Gamma_p} K_z(\underline{\rho}') \frac{i}{4} H_o^{(1)}(k_o|\underline{\rho} - \underline{\rho}'|) d\rho' \quad . \tag{2.35}$$

Here Γ_p is the strip and $(i/4)H_o^{(1)}(k_o|\underline{\rho} - \underline{\rho}'|)$ is the free space Green's function in two dimensions.

In the far field region $k_o|\underline{\rho} - \underline{\rho}'| >> 1$ and $\rho >> \rho'$. Thus

$$H_o^{(1)}(k_o|\underline{\rho} - \underline{\rho}'|) \approx \sqrt{\frac{2}{\pi k_o \rho}} e^{ik_o\rho - i(\pi/4)} e^{-ik_o \hat{\rho} \cdot \underline{\rho}'} \quad . \tag{2.36}$$

In terms of source coordinates, $\underline{\rho}' = x'\hat{x}$ and $\hat{\rho} \cdot \underline{\rho}' = x' \cos \phi$. Figure 2.3 shows the relationship between these various quantities. Therefore, in the far field region

$$E_z^{sc}(\underline{\rho}) = \sqrt{\frac{2}{\pi k_o \rho}} e^{ik_o\rho - i(\pi/4)} P(\phi, \phi_o) \quad , \tag{2.37}$$

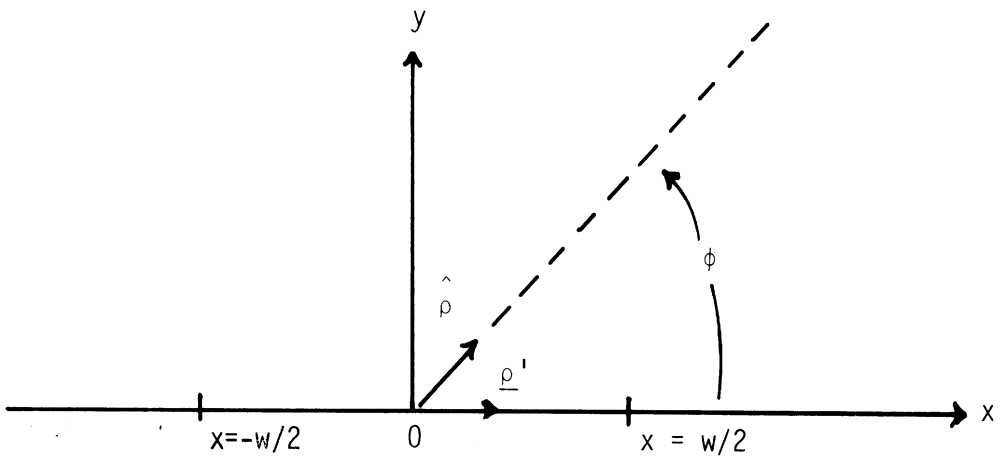

Fig. 2.3: A diagram for the far field computation.

where

$$P(\phi,\phi_o) = -\frac{k_o}{4}\int_{x'=-w/2}^{w/2} Z_o K_z(x')\, e^{-ik_o x' \cos\phi}\, dx' \quad . \tag{2.38}$$

The angle of incidence ϕ_o enters the integral by way of the current density. For a two-dimensional problem the radar cross section is defined (Bowman, 1969) as

$$\sigma(\phi,\phi_o) = \lim_{\rho \to \infty} 2\pi\rho \left| \frac{\underline{E}^{sc}}{\underline{E}^{i}} \right|^2 \tag{2.39}$$

which becomes

$$\sigma(\phi,\phi_o) = \frac{4}{k_o} \left| P(\phi,\phi_o) \right|^2 \tag{2.40}$$

in the present case.

CHAPTER III. SOLUTION BY THE FINITE ELEMENT METHOD

3.1 Summary of the Problem

The scattering problem formulated is essentially a scalar problem in two dimensions. The unknown field E_z^{sc} is denoted by the scalar u here and in the following chapters. The scalar u satisfies

$$\frac{\partial^2 u}{\partial x^2} + \frac{\partial^2 u}{\partial y^2} + k_o^2 u = 0 \quad . \tag{3.1}$$

On the strip located at $y = 0$ and $|x| \leq w/2$,

$$\frac{2iR(x)}{k_o} \left.\frac{\partial u}{\partial y}\right|_+ = u + u^i \quad . \tag{3.2}$$

Here $u^i = \exp[-ik_o(x \cos \phi_o + y \sin \phi_o)]$, the incident field. In addition on $y = 0$, $|x| > w/2$,

$$\frac{\partial u}{\partial y} = 0 \quad . \tag{3.3}$$

The field at the edge of the strip must satisfy Meixner's edge condition if the strip is a perfect conductor. Finally, the radiation condition

$$\lim_{\rho \to \infty} \sqrt{\rho} \left[\frac{\partial u(\underline{\rho})}{\partial \rho} - ik_o u(\underline{\rho}) \right] = 0 \tag{3.4}$$

must be satisfied.

3.2 Derivation of an Integral Statement of the Problem

The solution for the scalar field u is to be obtained in the region Ω bounded by the contour Γ as shown in Fig. 3.1. The region lies in the upper half-space $y \geq 0$. The contour Γ is composed of three sections:

1. Γ_p is the line $y = 0$, $-w/2 \leq x \leq w/2$.
2. Γ_0 are the lines $y = 0$, $|x| > w/2$.
3. Γ_B is a semicircle with a radius ρ_1 which is sufficiently large to place Γ_B in the far field region (see Section 5.2).

Green's first identity (Stratton, 1941, p. 165) indicates that for scalar functions u and v

$$\int_\Omega v\nabla_t^2 u \, d\Omega = -\int_\Omega \nabla_t v \cdot \nabla_t u \, d\Omega + \oint_\Gamma v \frac{\partial u}{\partial n} \, d\Gamma \quad , \tag{3.5}$$

where n is an outward normal to Γ and $\nabla_t = \hat{x}(\partial/\partial x) + \hat{y}(\partial/\partial y)$. The function u is the scattered field which is continuous and has continuous first and second derivatives in Ω expect at the edges of the strip ($x = \pm w/2$) if the strip is a perfect conductor. In this case singularities occur at the edges in the first derivatives which are integrable in accordance with Meixner's edge condition. The sum of the second derivative terms, $\nabla_t^2 u$, has no singularity anywhere since u has no singularity and u satisfies (3.1). The function v is an arbitrary function at this stage except that it must be sufficiently continuous so that any singularities in the first derivatives are integrable.

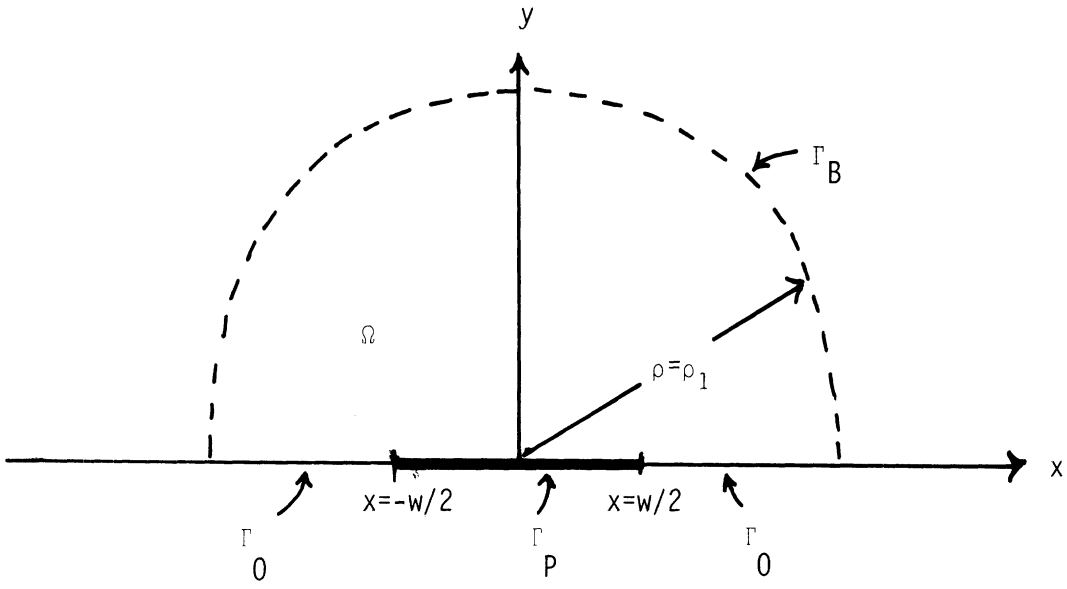

Fig. 3.1: The solution region.

Use of (3.1) through (3.3) results in

$$\int_{\Omega} (\nabla_t v \cdot \nabla_t u - k_o^2 vu)d\Omega - i\frac{k_o}{2}\int_{\Gamma_P}\frac{v(u+u^i)}{R(x)}\,d\Gamma - \int_{\Gamma_B} v\frac{\partial u}{\partial n}\,d\Gamma = 0 \quad . \tag{3.6}$$

In the far field region u is approximately given by (2.37) which satisfies (3.4). Then on Γ_B,

$$\frac{\partial u}{\partial n} = \frac{\partial u}{\partial \rho} = \left[-\frac{1}{2\rho_1} + ik_o\right] u\Big|_{\rho=\rho_1} \quad . \tag{3.7}$$

Using this, (3.6) becomes

$$\int_{\Omega} (\nabla_t v \cdot \nabla_t u - k_o^2 vu)d\Omega - i\frac{k_o}{2}\int_{\Gamma_P}\frac{v(u+u^i)}{R(x)}\,d\Gamma + \left[\frac{1}{2\rho_1} - ik_o\right]\int_{\Gamma_B}[vu]_{\rho=\rho_1}\,d\Gamma = 0 \quad . \tag{3.8}$$

This is known as a "weak form" integral statement (Zienkiewicz, 1977) since the order of the highest derivative is one lower than the order of the highest derivative in the original differential equation (3.1).

In the case of a perfectly conducting strip, R(x) = 0, and (3.8) cannot be used since R(x) is in the denominator. Returning to (3.5), and using (3.1) and (3.7) yields

$$\int_{\Omega} (\nabla_t v \cdot \nabla_t u - k_o^2 vu)d\Omega - \int_{\Gamma_\rho} v \frac{\partial u}{\partial n} d\Gamma + \left[\frac{1}{2\rho_1} - ik_o\right] \int_{\Gamma_B} [vu]_{\rho=\rho_1} d\Gamma = 0 \quad . \quad (3.9)$$

For the perfect conductor a prior knowledge of $\partial u/\partial n$ on the strip (Γ_p) does not exist, except that the derivative is proportional to the induced current on the strip, but the boundary condition, $u + u^i = 0$, on Γ_p is yet to be imposed. Equation (3.9) is the integral statement for the perfectly conducting case.

The derivations of (3.8) and (3.9) are essentially equivalent to the weighted residual method described in the finite element literature (Zienkiewicz, 1977, Chapter 3).

3.3 Interpolation Functions and Expansion of the Unknown

In order to solve for u, it is approximated by

$$u \approx \bar{u} = \sum_{n=1}^{I} N_n(x,y)a_n \quad (3.10)$$

and v is restricted to be $v = w_m$ ($m = 1,\ldots,I$) one of a set of weight functions yet to be prescribed. The domain Ω is divided into a number of small domains Ω^e called elements with nodes n on the element boundaries. As indicated in the summation above, there is a total of I nodes. For each node n there is an interpolation or shape function N_n which is unity at that node and zero at all other nodes. The value of the unknown u at node n is then approximately

a_n, a complex constant. Thus, the determination of the scattered field amounts to determining the value of each of the a_n constants.

Selection of interpolation functions and weight functions must be made in accordance with the necessity that the integrals of the weak form statement (3.8) or (3.9) be finite. In the weak form statement, the appearance of first derivatives requires that $\bar{u}$ and w_m must be continuous throughout Ω and on Γ, but allows discontinuities in their first derivatives. Further discussion on the selection of interpolation functions appears in Section 3.5.

Another name is often attached to the finite element weighted residual procedure depending on the choice of the weighting functions. If

$$w_m = N_m \quad , \tag{3.11}$$

the method of Galerkin is being used. In energy conserving problems, such as in a perfect dielectric medium, this method leads to a symmetric matrix of coefficients for the set of algebraic equations from which the a_n's are determined. Also, for this case, the method carries a guarantee of convergence to the proper numerical result, which other choices of weighting functions do not have (Zienkiewicz, 1977, Chapter 3).

3.4 Conversion to a Set of Algebraic Equations

Using the approximation $\bar{u}$ for u and Galerkin's method in selecting the weighting functions w_m one obtains for the weak form statement (3.8):

$$\int_{\Omega}\left\{\frac{\partial N_m}{\partial x}\ \frac{\partial}{\partial x}\left[\sum_{n=1}^{I} N_n a_n\right] + \frac{\partial N_m}{\partial y}\ \frac{\partial}{\partial y}\left[\sum_{n=1}^{I} N_n a_n\right]\right\} d\Omega$$

$$- k_o^2 \int_{\Omega} N_m \left[\sum_{n=1}^{I} N_n a_n\right] d\Omega - \frac{ik_o}{2} \int_{\Gamma_P} \frac{N_m}{R(x)} \left[\sum_{n=1}^{I} N_n a_n\right] d\Gamma$$

$$+ \left[\frac{1}{2\rho_1} - ik_o\right] \int_{\Gamma_B} N_m \left[\sum_{n=1}^{I} N_n a_n\right] d\Gamma = \frac{ik_o}{2} \int_{\Gamma_P} \frac{N_m u^i}{R(x)}\ d\Gamma \qquad (3.12)$$

for $m = 1,\ldots,I$.

Interchanging the order of integration and summation,

$$\sum_{n=1}^{I} \left\{\int_{\Omega}\left[\frac{\partial N_m}{\partial x}\ \frac{\partial N_n}{\partial x} + \frac{\partial N_m}{\partial y}\ \frac{\partial N_n}{\partial y} - k_o^2 N_m N_n\right] d\Omega\right\} a_n$$

$$- \sum_{n=1}^{I} \left\{\frac{ik_o}{2} \int_{\Gamma_P} \frac{N_m N_n}{R(x)}\ d\Gamma\right\} a_n + \sum_{n=1}^{I} \left\{\left(\frac{1}{2\rho_1} - ik_o\right) \int_{\Gamma_B} N_m N_n\ d\Gamma\right\} a_n$$

$$= \frac{ik_o}{2} \int_{\Gamma_P} \frac{N_m u^i}{R(x)}\ d\Gamma$$

for $m = 1,\ldots,I$. This is written as

$$\sum_{n=1}^{I} K_{mn} a_n = f_m \quad , \qquad m = 1,\ldots,I \ , \tag{3.13}$$

where

$$K_{mn} = \int_{\Omega} \left[\frac{\partial N_m}{\partial x} \frac{\partial N_n}{\partial x} + \frac{\partial N_m}{\partial y} \frac{\partial N_n}{\partial y} - k_o^2 N_m N_n \right] d\Omega$$

$$- \frac{ik_o}{2} \int_{\Gamma_P} \frac{N_m N_n}{R(x)} \, d\Gamma + \left(\frac{1}{2\rho_1} - ik_o \right) \int_{\Gamma_B} N_m N_n \, d\Gamma \tag{3.14}$$

and

$$f_m = \frac{ik_o}{2} \int_{\Gamma_P} \frac{N_m u^i}{R(x)} \, d\Gamma \quad . \tag{3.15}$$

Equations (3.13) represent a set of linear algebraic equations to be solved for the unknown a_n's, the values of the scattered field at the nodes.

Calculation of the coefficients K_{mn} and f_m in the finite element method is done by an element-by-element procedure. The integrals over the entire region Ω are replaced by sums of integrals over individual elements making up the domain. Thus

$$K_{mn} = \sum_{e=1}^{J} K_{mn}^e \tag{3.16}$$

and

$$f_m = \sum_{e=1}^{J} f_m^e \quad , \tag{3.17}$$

where J is the number of elements,

$$K_{mn}^e = \int_{\Omega^e} \left[\frac{\partial N_m}{\partial x} \frac{\partial N_n}{\partial x} + \frac{\partial N_m}{\partial y} \frac{\partial N_n}{\partial y} - k_o^2 N_m N_n \right] d\Omega$$
$$- \frac{ik_o}{2} \int_{\Gamma_P^e} \frac{N_m N_n}{R(x)} \, d\Gamma + \left(\frac{1}{2\rho_1} - ik_o \right) \int_{\Gamma_B^e} N_m N_n \, d\Gamma \tag{3.18}$$

and

$$f_m^e = \frac{ik_o}{2} \int_{\Gamma_P^e} \frac{N_m u^i}{R(x)} \, d\Gamma \quad . \tag{3.19}$$

For a perfectly conducting strip, the set of algebraic equations should be modified by removing equations corresponding to nodes where

the field strength a_n is known. The values of a_n for nodes on the strip is known due to the boundary condition $u + u^i = 0$ on Γ_p. Thus on Γ_p

$$a_n = -u^i(x_n,0) = -u_n^i \quad . \tag{3.20}$$

In this case (3.10) can be written as

$$\bar{u} = -\sum_{n=I'+1}^{I} N_n(x,y)u_n^i + \sum_{n=1}^{I'} N_n(x,y)a_n \quad , \tag{3.21}$$

where I - I' is the number of nodes on the strip. Proceeding as with the resistive strip using $\bar{u}$ for u and Galerkin's method in selecting w_m, the weak form (3.9) becomes

$$\int_\Omega \left[\frac{\partial N_m}{\partial x} \frac{\partial}{\partial x}\left(-\sum_{n=I'+1}^{I} N_n u_n^i + \sum_{n=1}^{I'} N_n a_n\right) + \frac{\partial N_m}{\partial y}\right.$$

$$\left. \cdot \frac{\partial}{\partial y}\left(-\sum_{n=I'+1}^{I} N_n u_n^i + \sum_{n=1}^{I'} N_n a_n\right)\right] d\Omega - k_o^2 \int_\Omega N_m \left(-\sum_{n=I'+1}^{I} N_n u_n^i\right.$$

$$\left. + \sum_{n=1}^{I'} N_n a_n\right) d\Omega - \int_{\Gamma_p} N_m \frac{\partial}{\partial n}\left(-\sum_{n=I'+1}^{I} N_n u_n^i + \sum_{n=1}^{I'} N_n a_n\right) d\Gamma$$

$$+ \left(\frac{1}{2\rho_1} - ik_o\right) \int_{\Gamma_B} N_m \left(-\sum_{n=I'+1}^{I} N_n u_n^i + \sum_{n=1}^{I'} N_n a_n\right) d\Gamma = 0 \tag{3.22}$$

for $m = 1,\ldots,I'$. After interchanging the order of integration and summation, and transferring the terms corresponding to the nodes on the strip to the right-hand side, the resulting set of linear algebraic equations is

$$\sum_{n=1}^{I'} K_{mn} a_n = g_m \quad , \qquad m = 1,\ldots,I' \quad , \tag{3.23}$$

where

$$K_{mn} = \int_{\Omega} \left[\frac{\partial N_m}{\partial x} \frac{\partial N_n}{\partial x} + \frac{\partial N_m}{\partial y} \frac{\partial N_n}{\partial y} - k_o^2 N_m N_n \right] d\Omega + \left(\frac{1}{2\rho_1} - ik_o \right) \int_{\Gamma_B} N_m N_n \, d\Gamma \quad , \tag{3.24}$$

and

$$g_m = \sum_{n=I'+1}^{I} K_{mn} u_n^i \quad . \tag{3.25}$$

3.5 The Element Mesh

The selection of a particular type of element and its interpolation functions for a particular problem depends on, in addition to the nature of the integral statement, the geometry of the problem, the nature of the medium, the desired accuracy of the solution, and the computer facilities available for the computation. In the present study, the geometry of the problem and the desire for computerized mesh generation lead to the selection of the elements.

Most of the elements are general quadrilaterals having a node at each corner. In order that the node locations be generated automatically in the computer program, the nodes are placed at the intersections of the ellipses and hyperbolas of an elliptic coordinate system (Stratton, 1941, p. 52). The sides of the elements are straight lines between the nodes (Fig. 3.2).

Triangular elements are used at the edges of the strip. This is done because of the need to properly model the behavior of the fields at the edge of a perfectly conducting strip. Since some components of the fields become infinite at the edge, an element is needed with shape functions whose derivatives have appropriate singularities. Such elements have been developed by W. S. Blackburn (1973) and a number of others (Zienkiewicz, 1977, Chapter 23).

It can be stated as a general rule that use of higher-order interpolation functions requires fewer elements to achieve a given degree of accuracy of solution. Thus savings in computation time and computer memory requirements can be obtained. On the other hand, the higher-order functions lead to more complicated computations for the element matrix coefficients (Zienkiewicz, 1977, Chapter 7). In this work the quadrilaterals used are of higher order than the more commonly used linear triangular elements and offer the potential of greater accuracy. Linear interpolation is used in the quadrilaterals rather than higher order interpolation functions in the interest of keeping the element matrix computations simple.

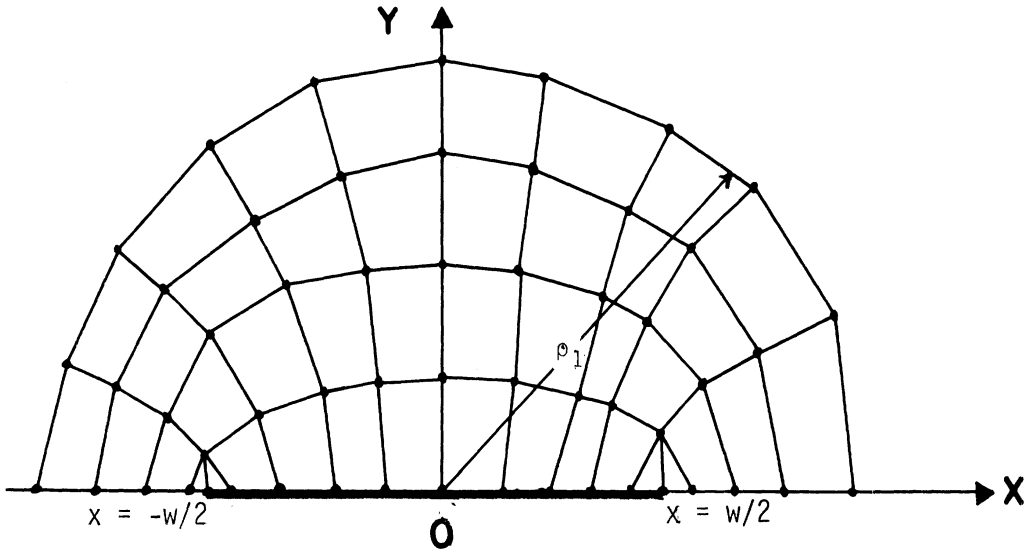

Fig. 3.2: The element mesh.

3.6 Quadrilateral Finite Elements

As can be seen in Fig. 3.2, the quadrilateral elements are of various sizes and shapes. Rather than write interpolation functions for each of these elements, a transformation of the elements to a set of normalized coordinates allows the writing of the interpolation functions for all the quadrilaterals in a single concise form.

A general quadrilateral in the x-y plane is shown in Fig. 3.3. The x- and y-coordinates of the nodes are known values. A transformation of coordinates is used to map this quadrilateral into a square element in the α-β coordinate system as shown in Fig. 3.4. That is, the x-coordinate of any point in the element is a function of α and β. The same is true for the y-coordinate. Thus,

$$x = x(\alpha,\beta) \tag{3.26}$$

and

$$y = y(\alpha,\beta) \quad . \tag{3.27}$$

Before the exact expressions for this coordinate transformation are stated, a discussion of the interpolation functions N_n for the quadrilateral elements will be given.

The simplest interpolation function is a linear function. It provides for continuity of $\bar{u}$ at element boundaries but will allow discontinuities in the first derivatives of $\bar{u}$. The function N_n must satisfy

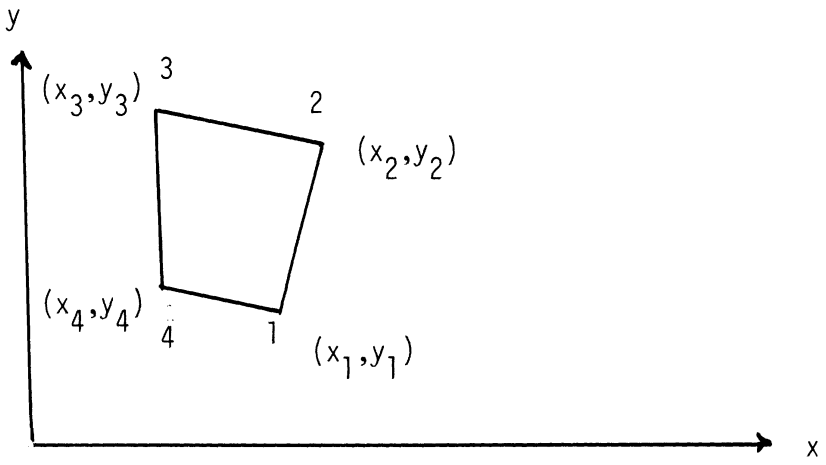

Fig. 3.3: A quadrilateral finite element.

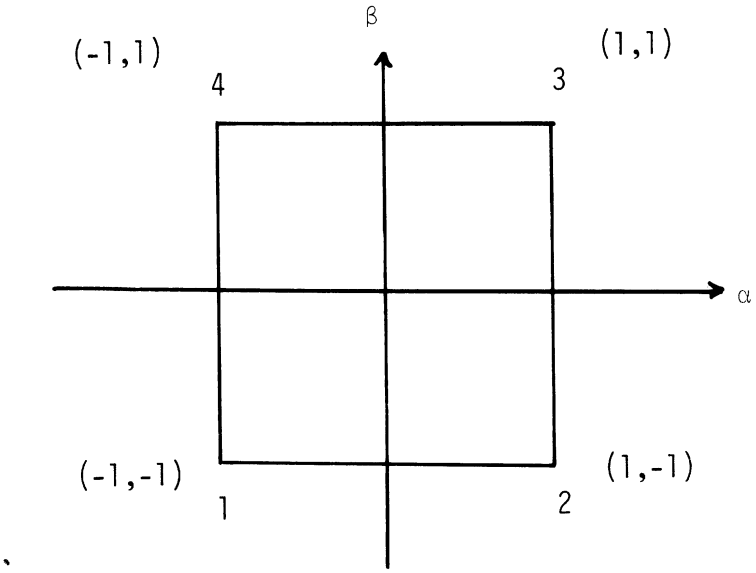

Fig. 3.4: A square element in normalized coordinates.

$$N_n = \begin{cases} 1 & \text{at node } n \\ \\ 0 & \text{at all other nodes} \end{cases} . \qquad (3.28)$$

A function meeting this requirement and having a linear variation with position

$$N_n = \frac{1}{4}(1 + \alpha\alpha_n)(1 + \beta\beta_n) \qquad (3.29)$$

is selected where,

α_n = value of α at node n,

β_n = value of β at node n.

Thus in the α-β coordinates the value of $\bar{u}$ at some point (α,β) in the square element is

$$\bar{u}(\alpha,\beta) = \sum_{n=1}^{4} N_n a_n \quad . \qquad (3.30)$$

Linear interpolation is also used for the coordinate transformation so that (3.26) and (3.27) become

$$x(\alpha,\beta) = \sum_{n=1}^{4} N_n(\alpha,\beta)x_n \qquad (3.31)$$

and

$$y(\alpha,\beta) = \sum_{n=}^{4} N_n(\alpha,\beta)y_n \quad , \qquad (3.32)$$

where x_n and y_n are the x- and y-coordinates of node n. Because the same interpolation functions are used for the function u and for the coordinates x and y, these elements are said to be "isoparametric".

In order to carry out the integrations for the element matrix coefficients K^e_{mn} (3.18) or (3.22) and the incident field term f^e_m (3.19), the integrals are transformed to the α-β coordinates, simplifying the specification of the limits of the integrals. The details of these calculations are presented in Chapter IV.

3.7 Triangular Elements at the Strip Edge

At both edges of the strip are regions which may be conveniently divided into two triangular elements rather than one quadrilateral element (Fig. 3.5). Integrations over these elements are most easily handled if the elements are transformed in a manner similar to that used for the quadrilateral elements. A general triangular element is shown in Fig. 3.6. This element is transformed into an α-β coordinate system as shown in Fig. 3.7 using linear interpolation functions:

$$x(\alpha,\beta) = (1 - \alpha - \beta)x_1 + \alpha x_2 + \beta x_3$$

and

$$y(\alpha,\beta) = (1 - \alpha - \beta)y_1 + \alpha y_2 + \beta y_3 \quad . \tag{3.33}$$

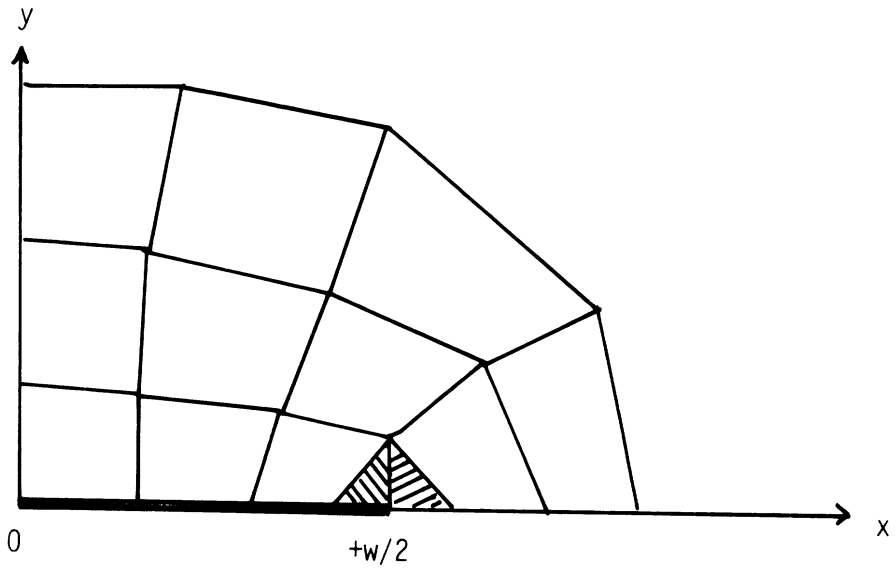

Fig. 3.5: Triangular elements in mesh at strip edge.

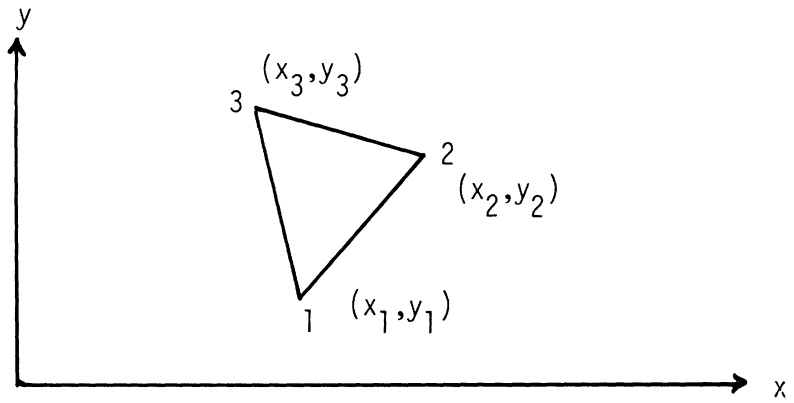

Fig. 3.6: A general triangular element.

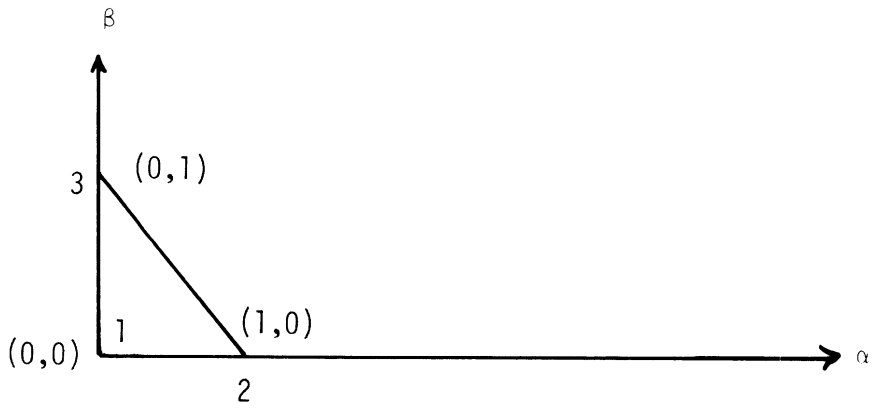

Fig. 3.7: A triangular element in normalized coordinates.

The interpolation functions N_n are

$$\left.\begin{aligned} N_1 &= 1 - \alpha - \beta \ , \\ N_2 &= \alpha \ , \\ N_3 &= \beta \ . \end{aligned}\right\} \tag{3.34}$$

The field is interpolated with the same shape functions

$$\bar{u}(\alpha,\beta) = \sum_{n=1}^{3} N_n a_n \ , \tag{3.35}$$

and the element is isoparametric.

This approximation for (3.35) is valid for a resistive strip, but for a perfectly conducting strip a special set of interpolation functions

$$\left.\begin{aligned} N_1 &= 1 - \sqrt{\alpha + \beta} \\ N_2 &= \alpha/\sqrt{\alpha + \beta} \\ N_3 &= \beta/\sqrt{\alpha + \beta} \end{aligned}\right\} \tag{3.36}$$

are used to model the behavior of the fields near the edge. Following the method of Blackburn (1973) this set of functions not only models the behavior of u near the edge, but also has a linear variation along the side of the triangle opposite the node at the edge of the strip to assure continuity of $\bar{u}$ at the element's boundary with the adjacent quadrilateral element. Since the interpolation functions (3.34) and (3.36) are not the same, this special element is not isoparametric.

CHAPTER IV. SOLUTION PROCEDURE

4.1 The Computer Program

The computer program for the numerical solution generates the mesh of nodes and elements by calculating x and y coordinates of every node. The elements and nodes are then automatically numbered. Each node is given a unique global node number and a local node number associated with each element of which it is a corner. Next, the element matrix coefficients K^e_{mn} and incident field terms f^e_m are calculated for one element and inserted into the proper location of the global matrix for the system of equations (3.13) or (3.23). This process is repeated for all the elements.

The resulting global matrix has all its nonzero coefficients in a relatively narrow band centered on the principal diagonal. Computer memory requirements are kept to a minimum by storing only the band of nonzero coefficients. The system of equations is solved by a procedure beginning with a triangular decomposition of the matrix followed by a variation of Gauss elimination.

Solution of the system of algebraic equations yields the value of the scattered field at every node. The induced current on the strip is then calculated, and from this the radar cross section is obtained. Details of the calculation of element matrix coefficients, the incident field terms, induced currents, and the

radar cross section are given in the remaining sections of this chapter.

4.2 Element Matrix Coefficients for Quadrilateral Elements

The integrals for the element matrix coefficients K_{mn}^e (3.18) or (3.24) are transformed to the α-β coordinates using (3.31) and (3.32). The first portion of K_{mn}^e

$$\int_{\Omega^e} \left[\frac{\partial N_m}{\partial x} \frac{\partial N_n}{\partial x} + \frac{\partial N_m}{\partial y} \frac{\partial N_n}{\partial y} - k_o^2 N_m N_n \right] dx\, dy$$

$$= \int_{\alpha=-1}^{1} \int_{\beta=-1}^{1} \left[\frac{\partial N_m}{\partial x} \frac{\partial N_n}{\partial x} + \frac{\partial N_m}{\partial y} \frac{\partial N_n}{\partial y} - k_o^2 N_m N_n \right] |J| \, d\alpha \, d\beta \quad , \tag{4.1}$$

where $|J|$ is the determinant of the Jacobian matrix J.

$$J = \begin{bmatrix} \frac{\partial x}{\partial \alpha} & \frac{\partial y}{\partial \alpha} \\ \\ \frac{\partial x}{\partial \beta} & \frac{\partial y}{\partial \beta} \end{bmatrix} \tag{4.2}$$

and

$$|J| = \det J = \frac{\partial x}{\partial \alpha} \frac{\partial y}{\partial \beta} - \frac{\partial x}{\partial \beta} \frac{\partial y}{\partial \alpha} \quad . \tag{4.3}$$

Using (3.31) and (3.32), the partial derivatives of J are

$$\left.\begin{aligned} \frac{\partial x}{\partial \alpha} &= \frac{1}{4}(D_1 + \beta D_2) \\ \frac{\partial x}{\partial \beta} &= \frac{1}{4}(D_3 + \alpha D_2) \\ \frac{\partial y}{\partial \alpha} &= \frac{1}{4}(D_4 + \beta D_5) \\ \frac{\partial y}{\partial \beta} &= \frac{1}{4}(D_6 + \alpha D_5) \end{aligned}\right\}, \tag{4.4}$$

where

$$\left.\begin{aligned} D_1 &= -x_1 + x_2 + x_3 - x_4 \\ D_2 &= x_1 - x_2 + x_3 - x_4 \\ D_3 &= -x_1 - x_2 + x_3 + x_4 \\ D_4 &= -y_1 + y_2 + y_3 - y_4 \\ D_5 &= y_1 - y_2 + y_3 - y_4 \\ D_6 &= -y_1 - y_2 + y_3 + y_4 \end{aligned}\right\}. \tag{4.5}$$

The terms in (4.5) are the coordinates of the nodes.

The partial derivatives in the integral of (4.1) are

$$\frac{\partial N_n}{\partial x} = \frac{1}{|J|}\left(\frac{\partial N_n}{\partial \alpha}\frac{\partial y}{\partial \beta} - \frac{\partial N_n}{\partial \beta}\frac{\partial y}{\partial \alpha}\right) \tag{4.6}$$

and

$$\frac{\partial N_n}{\partial y} = \frac{1}{|J|}\left(\frac{\partial N_n}{\partial \beta}\frac{\partial x}{\partial \alpha} - \frac{\partial N_n}{\partial \alpha}\frac{\partial x}{\partial \beta}\right). \tag{4.7}$$

Since N_n is given by (3.29), then

$$\frac{\partial N_n}{\partial \alpha} = \frac{1}{4}\alpha_n(1 + \beta\beta_n) \tag{4.8}$$

and

$$\frac{\partial N_n}{\partial \beta} = \frac{1}{4}\beta_n(1 + \alpha\alpha_n) \quad . \tag{4.9}$$

Although the transformation of the integral (4.1) to the α-β variables simplifies the limits of integration, the integral is not easily evaluated due to the complexity of the integrand. Numerical integration (Gaussian quadrature) is used in the computer program.

The next portion of K^e_{mn} given in (3.18) is the integral across the resistive strip. This integral has a nonzero result for only those elements adjacent to the strip. For a perfectly conducting strip, K^e_{mn} has no such integral on the strip as can be seen in (3.24). Figure 4.1 shows a typical element adjacent to the strip. From Fig. 4.1 it is apparent that

$$-\frac{ik_o}{2}\int_{\Gamma_p^e}\frac{N_m N_n}{R(x)}\,dx = \frac{ik_o}{2}\int_{x_1}^{x_4}\frac{[N_m N_n]_{y=0}}{R(x)}\,dx \quad . \tag{4.10}$$

Transforming the integral to the α-β variables and using

$$dx = \frac{\partial x}{\partial \alpha}\,d\alpha + \frac{\partial x}{\partial \beta}\,d\beta \tag{4.11}$$

yields

$$-\frac{ik_o}{2}\int_{\Gamma_p^e}\frac{N_m N_n}{R(x)}\,dx = \frac{ik_o}{2}\int_{\beta=-1}^{1}\left[\frac{N_m N_n}{R(\alpha,\beta)}\,\frac{\partial x}{\partial \beta}\right]_{\alpha=-1}d\beta \tag{4.12}$$

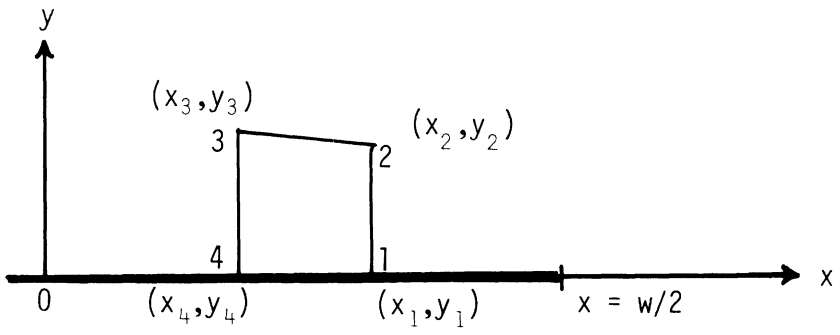

Fig. 4.1: The quadrilateral element adjacent to the strip.

since the line between nodes 1 and 4 corresponds to the line α=-1 in the α-β coordinate system.

To allow for a number of different resistivity profiles, R at node n is assumed to be of the form

$$R_n = A + BX_n + CX_n^2 \quad , \tag{4.13}$$

where A, B and C are constants which are part of the input data for the computer program. If A, B and C are zero, the computer program interprets the data to indicate a perfectly conducting strip. The expression for $R(\alpha,\beta)$ along the line α = -1 between nodes 1 and 4 is a linear interpolation in terms of R_1 and R_4.

$$[R(\alpha,\beta)]_{\alpha=-1} = N_1 R_1 + N_4 R_4 \quad ,$$

or

$$[R(\alpha,\beta)]_{\alpha=-1} = \frac{1}{2}(R_1 + R_4) - \frac{1}{2}\beta(R_1 - R_4) \quad . \tag{4.14}$$

Using (4.4) and (4.5) yields

$$\left.\frac{\partial x}{\partial \beta}\right|_{\alpha=-1} = -\frac{1}{2}(x_1 - x_4) \tag{4.15}$$

and using (3.29) yields

$$[N_m N_n]_{\alpha=-1} = \frac{1}{16}(1 - \alpha_m)(1 + \beta\beta_m)(1 - \alpha_n)(1 + \beta\beta_n) \quad . \tag{4.16}$$

Thus (4.12) becomes

$$-\frac{ik_o}{2}\int_{\Gamma_P^e}\frac{N_m N_n}{R(x)}\,dx = -\frac{ik_o(1-\alpha_m)(1-\alpha_n)(x_1-x_4)}{32}\cdot\int_{\beta=-1}^{1}\frac{(1+\beta\beta_m)(1+\beta\beta_n)d\beta}{(R_1+R_4)-\beta(R_1-R_4)} \qquad (4.17)$$

using (4.14), (4.15) and (4.16). This integral is also evaluated by numerical integration.

The final portion of K_{mn}^e given in (3.18) or (3.24) is the integral along the contour Γ_B in the far field region. This integral has a nonzero result only for the elements adjacent to this contour. Figure 4.2 shows a typical element adjacent to the strip. The integral is transformed to the α-β coordinates. If Γ is the distance along Γ_B^e from node 2, the integral is

$$\left(\frac{1}{2\rho_1}-ik_o\right)\int_{\Gamma_B^e}N_m N_n\,d\Gamma = \left(\frac{1}{2\rho_1}-ik_o\right)\int_{\beta=-1}^{1}\left[N_m N_n\frac{d\Gamma}{d\beta}\right]_{\alpha=1}d\beta \quad . \qquad (4.18)$$

The expression for Γ is

$$\Gamma = \frac{1}{2}\sqrt{(x_3-x_2)^2+(y_3-y_3)^2}\,(1+\beta) \quad . \qquad (4.19)$$

However,

$$x_2 = \rho_1\cos\phi_1 \;,\; y_2 = \rho_1\sin\phi_1 \;,\; x_3 = \rho_1\cos\phi_2$$

and

$$y_3 = \rho_1\sin\phi_2 \quad .$$

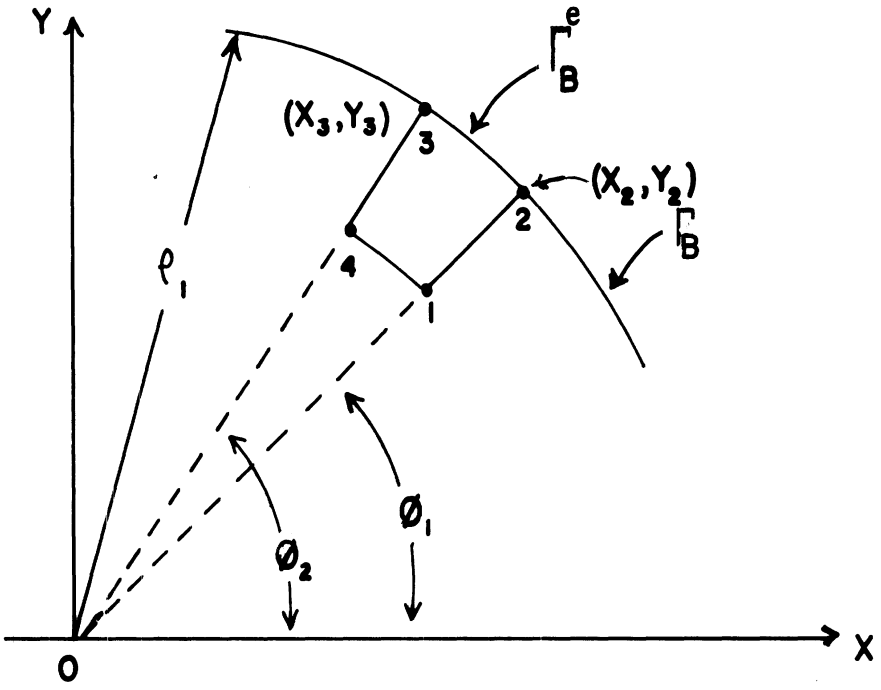

Fig. 4.2: A quadrilateral element adjacent to the contour Γ_B.

Thus (4.19) becomes

$$\Gamma = \frac{\rho_1}{\sqrt{2}} \sqrt{1 - \cos(\phi_2 - \phi_1)} \; (1 + \beta) \quad . \tag{4.20}$$

Then

$$\left.\frac{d\Gamma}{d\beta}\right|_{\alpha=1} = \frac{\rho_1}{\sqrt{2}} \sqrt{1 - \cos(\phi_2 - \phi_1)} \; d\beta \quad . \tag{4.21}$$

Using (3.29) yields

$$[N_m N_n]_{\alpha=1} = \frac{1}{16} (1 + \alpha_m)(1 + \beta\beta_m)(1 + \alpha_n)(1 + \beta\beta_n) \quad . \tag{4.22}$$

The integral in (4.18) becomes

$$\int_{\Gamma_B^e} N_m N_n \, d\Gamma = \frac{\rho_1 \sqrt{1 - \cos(\phi_2 - \phi_1)}}{16 \sqrt{2}} \cdot (1 + \alpha_m)(1 + \alpha_n) \int_{\beta=-1}^{1} (1 + \beta\beta_m)(1 + \beta\beta_n) d\beta \tag{4.23}$$

when (4.21) and (4.22) are used with (4.18). The integral in (4.23) is evaluated exactly so that

$$\left(\frac{1}{2\rho_1} - ik_o\right) \int_{\Gamma_B^e} N_m N_n \, d\Gamma = \left(\frac{1}{2\rho_1} - ik_o\right) \frac{\rho_1 \sqrt{1 - \cos(\phi_2 - \phi_1)}}{8 \sqrt{2}} \cdot (1 + \alpha_m)(1 + \alpha_n)\left(1 + \frac{1}{3} \beta_m \beta_n\right) \tag{4.24}$$

In summary, the element matrix coefficient K_{mn}^e (3.18) for a quadrilateral element is the sum of three terms given by (4.1), (4.17) and (4.24) for a resistive strip. For a perfectly conducting strip K_{mn}^e (3.24) is the sum of (4.1) and (4.24).

4.3 Element Matrix Coefficients for Triangular Elements

The integrals for the element matrix coefficients K_{mn}^e for the triangular elements are handled in much the same manner as those for the quadrilateral elements. The first portion of K_{mn}^e is transformed to the α-β coordinates

$$\int_{\Omega^e} \left[\frac{\partial N_m}{\partial x} \frac{\partial N_n}{\partial x} + \frac{\partial N_m}{\partial y} \frac{\partial N_n}{\partial y} - k_o^2 N_m N_n \right] dx\, dy$$

$$= \int_{\alpha=0}^{1} \int_{\beta=0}^{1-\alpha} \left[\frac{\partial N_m}{\partial x} \frac{\partial N_n}{\partial x} + \frac{\partial N_m}{\partial y} \frac{\partial N_n}{\partial y} - k_o^2 N_m N_n \right] |J|\, d\alpha\, d\beta \quad , \tag{4.25}$$

where integration is over the triangle shown in Fig. 3.7. Using (3.33) yields

$$\left.\begin{aligned} \frac{\partial x}{\partial \alpha} &= x_2 - x_1 \qquad \frac{\partial y}{\partial \alpha} = y_2 - y_1 \\ \frac{\partial x}{\partial \beta} &= x_3 - x_1 \qquad \frac{\partial y}{\partial \beta} = y_3 - y_1 \end{aligned}\right\} \tag{4.26}$$

so that

$$|J| = (x_2 - x_1)(y_3 - y_1) - (x_3 - x_1)(y_2 - y_1) \quad . \quad (4.27)$$

The interpolation functions (3.34) are written in a general form

$$N_n = \alpha_n\beta_n - \alpha_n\alpha - \beta_n\beta \quad , \quad (4.28)$$

where

$$\alpha_1 = 1 \qquad \beta_1 = 1$$
$$\alpha_2 = -1 \qquad \beta_2 = 0$$
$$\alpha_3 = 0 \qquad \beta_3 = -1$$

The partial derivatives in (4.25) are given by (4.6) and (4.7). Using (4.26) and (4.28) yields

$$\frac{\partial N_n}{\partial x} = \frac{1}{|J|}[\alpha_n(y_1 - y_3) + \beta_n(y_2 - y_1)] \quad (4.29)$$

and

$$\frac{\partial N_n}{\partial y} = \frac{1}{|J|}[\alpha_n(x_3 - x_1) + \beta_n(x_1 - x_2)] \quad . \quad (4.30)$$

Then using (4.28) through (4.30), the integral (4.25) becomes

$$\int_{\Omega^e} \left[\frac{\partial N_m}{\partial x} \frac{\partial N_n}{\partial x} + \frac{\partial N_m}{\partial y} \frac{\partial N_n}{\partial y} - k_o^2 N_m N_n \right] dx\, dy$$

$$= \frac{1}{2|J|} \Big\{ \alpha_m \alpha_n [(x_3 - x_1)^2 + (y_3 - y_1)^2] - (\alpha_m \beta_n + \beta_m \alpha_n)$$

$$\cdot [(x_2 - x_1)(x_3 - x_1) + (y_2 - y_1)(y_3 - y_1)] + \beta_m \beta_n [(x_2 - x_1)^2$$

$$+ (y_2 - y_1)^2] \Big\} - k_o^2 |J| \Big\{ \frac{1}{2} \alpha_m \beta_m \alpha_n \beta_n - \frac{1}{6} (\alpha_m \beta_m \alpha_n + \alpha_n \beta_n \alpha_m)$$

$$- \frac{1}{6} (\alpha_m \beta_m \beta_n + \alpha_n \beta_n \beta_m) + \frac{1}{24} (\alpha_m \beta_n + \alpha_n \beta_m) + \frac{1}{12} (\alpha_m \alpha_n + \beta_m \beta_n) \Big\} . \quad (4.31)$$

The next portion of K_{mn}^e given in (3.18) is the integral on the resistive strip. This integral is nonzero only for the triangles which are adjacent to the strip. Figure 4.3 shows a triangular element adjacent to the strip at x = w/2. From the figure it is apparent that

$$- \frac{ik_o}{2} \int_{\Gamma_P^e} \frac{N_m N_n}{R(x)} dx = \frac{ik_o}{2} \int_{x=x_1}^{x_3} \frac{[N_m N_n]_{y=o}}{R(x)} dx . \quad (4.32)$$

Transforming the integral to the α-β coordinates yields

$$- \frac{ik_o}{2} \int_{\Gamma_P^e} \frac{N_m N_n}{R(x)} dx = \frac{ik_o}{2} \int_{\beta=o}^{1} \left[\frac{N_m N_n}{R(\alpha,\beta)} \right]_{\alpha=o} \left(\frac{\partial x}{\partial \beta} \right) d\beta , \quad (4.33)$$

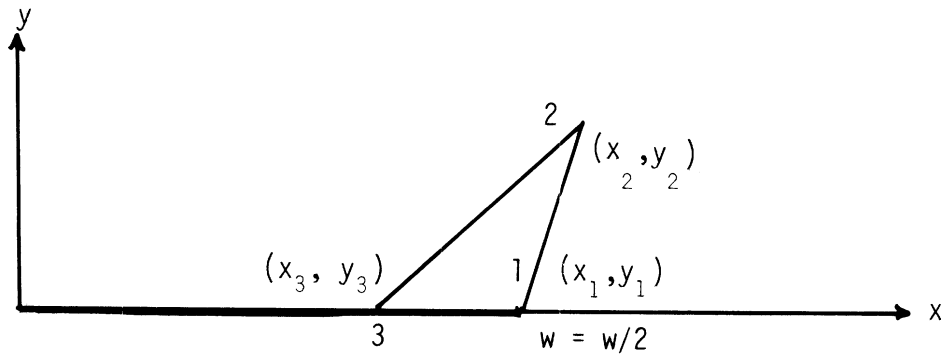

Fig. 4.3: A triangular element adjacent to the strip at x = w/2.

since the line between nodes 1 and 3 corresponds to the line $\alpha = 0$ in the α-β coordinate system. The expression for $R(\alpha,\beta)$ along the line $\alpha = 0$ is a linear interpolation from R_1 and R_3:

$$[R(\alpha,\beta)]_{\alpha=0} = R_1 + \beta(R_3 - R_1) \quad . \tag{4.34}$$

Using (4.26), (4.28) and (4.34), the integral (4.33) becomes

$$-\frac{ik_o}{2}\int_{\Gamma_p^e}\frac{N_m N_n}{R(x)}\,dx = -\frac{ik_o(x_1 - x_3)}{2}\int_{\beta=0}^{1}\frac{(\alpha_m - \beta)\beta_m(\alpha_n - \beta)\beta_n}{R_1 + \beta(R_3 - R_1)}\,d\beta \quad . \tag{4.35}$$

A change of variable in the integral, $\beta = (\sigma + 1)/2$, yields

$$-\frac{ik_o}{2}\int_{\Gamma_p^e}\frac{N_m N_n}{R(x)}\,dx$$

$$= -\frac{ik_o(x_1 - x_3)}{8}\int_{\sigma=-1}^{1}\frac{(2\alpha_m - 1 - \sigma)\beta_m(2\alpha_n - 1 - \sigma)\beta_n}{(R_1 + R_3) + \sigma(R_3 - R_1)}\,d\sigma \quad , \tag{4.36}$$

a form which is convenient for numerical integration.

Figure 4.4 shows the triangular element adjacent to the strip at $x = -w/2$. The equivalent of (4.36) for this triangle is

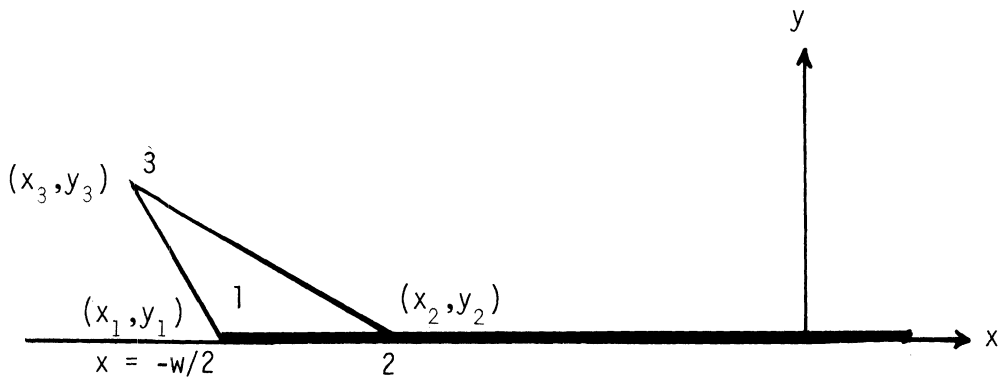

Fig. 4.4: A triangular element adjacent to the strip at x = -w/2.

$$-\frac{ik_o}{2}\int_{\Gamma_p^e}\frac{N_m N_n}{R(x)}\,dx$$

$$=-\frac{ik_o(x_2-x_1)}{8}\int_{\sigma=-1}^{1}\frac{(2\beta_m-1-\sigma)\alpha_m(2\beta_n-1-\sigma)\alpha_n}{(R_1+R_2)+\sigma(R_2-R_1)}\,d\sigma\quad,\qquad(4.37)$$

which is evaluated in the computer program by numerical integration.

In the case of a perfectly conducting strip, the element matrix coefficient (3.24) for the triangular elements becomes

$$K_{mn}^e=\int_{\Omega^e}\left[\frac{\partial N_m}{\partial x}\frac{\partial N_n}{\partial x}+\frac{\partial N_m}{\partial y}\frac{\partial N_n}{\partial y}-k_o^2N_mN_n\right]dx\,dy\quad.\qquad(4.38)$$

This integral is transformed to α-β coordinates using (3.33):

$$K_{mn}^e=\int_{\alpha=0}^{1}\int_{\beta=0}^{1-\alpha}\left[\frac{\partial N_m}{\partial x}\frac{\partial N_n}{\partial x}+\frac{\partial N_m}{\partial y}\frac{\partial N_n}{\partial y}-k_o^2N_mN_n\right]|J|\,d\alpha\,d\beta\quad,\qquad(4.39)$$

where $|J|$ is given by (4.27). The interpolation function N_n is given by (3.36) or can be written in a general form

$$N_n=\alpha_n\beta_n-\frac{\alpha_n\alpha+\beta_n\beta}{\sqrt{\alpha+\beta}}\quad,\qquad(4.40)$$

where α_n and β_n are given by

$$\alpha_1 = 1 \qquad \beta_1 = 1$$
$$\alpha_2 = -1 \qquad \beta_2 = 0$$
$$\alpha_3 = 0 \qquad \beta_3 = -1$$

The partial derivatives in (4.39) are given by (4.6) and (4.7). From (4.40),

$$\frac{\partial N_n}{\partial \alpha} = -\frac{\alpha_n \alpha + (-2\alpha_n + \beta_n)\beta}{2(\alpha + \beta)^{3/2}} \tag{4.41}$$

and

$$\frac{\partial N_n}{\partial \beta} = \frac{(\alpha_n - 2\beta_n)\alpha - \beta_n \beta}{2(\alpha + \beta)^{3/2}} \quad . \tag{4.42}$$

Then using (4.26), the partial derivatives (4.6) and (4.7) become

$$\frac{\partial N_n}{\partial x} = \frac{1}{|J|}\left[-\frac{\alpha_n \alpha + (-2\alpha_n + \beta_n)\beta}{2(\alpha + \beta)^{3/2}}(y_3 - y_1) - \frac{(\alpha_n - 2\beta_n)\alpha - \beta_n \beta}{2(\alpha + \beta)^{3/2}}(y_2 - y_1)\right] \tag{4.43}$$

and

$$\frac{\partial N_n}{\partial y} = \frac{1}{|J|}\left[\frac{(\alpha_n - 2\beta_n)\alpha - \beta_n \beta}{2(\alpha + \beta)^{3/2}}(x_2 - x_1) - \frac{-\alpha_n \alpha + (-2\alpha_n + \beta_n)\beta}{2(\alpha + \beta)^{3/2}}(x_3 - x_1)\right] . \tag{4.44}$$

K^e_{mn} (4.39) is evaluated by exact integration and using (4.40), (4.43) and (4.44). Defining

$$\left.\begin{aligned} F_1 &= (x_3 - x_1)^2 + (y_3 - y_1)^2 \\ F_2 &= (x_2 - x_1)(x_3 - x_1) + (y_2 - y_1)(y_3 - y_1) \\ F_3 &= (x_2 - x_1)^2 + (y_2 - y_1)^2 \end{aligned}\right\} \tag{4.45}$$

the coefficients K^e_{mn} for the triangular element are

$$\left.\begin{aligned} K^e_{11} &= \frac{1}{4|J|}(F_1 - 2F_2 + F_3) - \frac{k_0^2|J|}{30} \\ K^e_{12} &= \frac{1}{4|J|}\left(-\frac{3}{2}F_1 + F_2 + \frac{1}{2}F_3\right) - \frac{k_0^2|J|}{30} \\ K^e_{13} &= \frac{1}{4|J|}\left(\frac{1}{2}F_1 + F_2 - \frac{3}{2}F_3\right) - \frac{k_0^2|J|}{30} \\ K^e_{21} &= \frac{1}{4|J|}\left(-\frac{3}{2}F_1 + F_2 + \frac{1}{2}F_3\right) - \frac{k_0^2|J|}{30} \\ K^e_{22} &= \frac{1}{4|J|}\left(\frac{7}{3}F_1 + \frac{4}{3}F_2 + \frac{1}{3}F_3\right) - \frac{k_0^2|J|}{9} \\ K^e_{23} &= -\frac{1}{4|J|}\left(\frac{5}{6}F_1 + \frac{7}{3}F_2 + \frac{5}{6}F_3\right) - \frac{k_0^2|J|}{18} \\ K^e_{31} &= \frac{1}{4|J|}\left(\frac{1}{2}F_1 + F_2 - \frac{3}{2}F_3\right) - \frac{k_0^2|J|}{30} \\ K^e_{32} &= -\frac{1}{4|J|}\left(\frac{5}{6}F_1 + \frac{7}{3}F_2 + \frac{5}{6}F_3\right) - \frac{k_0^2|J|}{18} \\ K^e_{33} &= \frac{1}{4|J|}\left(\frac{1}{3}F_1 + \frac{4}{3}F_2 + \frac{7}{3}F_3\right) - \frac{k_0^2|J|}{9} \end{aligned}\right\}. \tag{4.46}$$

In summary, the element matrix coefficient K^e_{mn} (3.18) for a triangular element is the sum of two terms (4.31) and (4.36) or (4.37) for a resistive strip. For a perfectly conducting strip K^e_{mn} (3.24) is given by (4.46).

4.4 Incident Field Terms

The integral for the incident field terms (3.19) is evaluated for the element adjacent to the resistive strip. For a quadrilateral (Fig. 4.1), (3.19) becomes

$$f^e_m = \frac{ik_o}{2} \int_{\Gamma^e_p} \frac{N_m u^i}{R(x)}\, dx = -\frac{ik_o}{2} \int_{x_1}^{x_4} \frac{N_m u^i\, dx}{R(x)}$$

or

$$f^e_m = -\frac{ik_o}{2} \int_{\beta=-1}^{1} \left[\frac{N_m u^i(\alpha,\beta)}{R(\alpha,\beta)} \frac{\partial x}{\partial \beta}\right]_{\alpha=-1} d\beta \tag{4.47}$$

upon transformation to the α-β coordinates. The incident field in the α-β coordinates is

$$u^i(\alpha,\beta) = \exp[-ik_o x(\alpha,\beta)\cos\phi_o] , \tag{4.48}$$

where $x(\alpha,\beta)$ is given by (3.31). Then

$$u^i(\alpha,\beta)\Big|_{\alpha=-1} = \exp\left\{-ik_o(\cos\phi_o)\,\frac{1}{2}\,[(x_1 + x_4) - \beta(x_1 - x_4)]\right\} . \tag{4.49}$$

Using (3.29), (4.14), (4.15) and (4.49), the incident field term (4.47) becomes

$$f_m^e = \frac{ik_o(1 - \alpha_m)(x_1 - x_4)}{8} \exp\left[-ik_o\left(\frac{x_1 + x_4}{2}\right)\cos\phi_o\right]$$

$$\cdot \int_{\beta=-1}^{1} \frac{(1 + \beta\beta_m)\exp\left[ik_o\left(\frac{x_1 - x_4}{2}\right)(\cos\phi_o)\beta\right]}{(R_1 + R_4) - \beta(R_1 - R_4)} d\beta \ , \tag{4.50}$$

which is evaluated using numerical integration.

For the triangular element adjacent to the resistive strip at x = w/2 (Fig. 4.3),

$$f_m^e = -\frac{ik_o}{2} \int_{x=x_1}^{x_3} \frac{N_m u^i \, dx}{R(x)}$$

or

$$f_m^e = -\frac{ik_o}{2} \int_{\beta=0}^{1} \left[\frac{N_m u^i(\alpha,\beta)}{R(\alpha,\beta)}\right]_{\alpha=0} \left(\frac{\partial x}{\partial \beta}\right) d\beta \ . \tag{4.51}$$

In this case the incident field $u^i(\alpha,\beta)$ for $\alpha = 0$ is obtained using (3.33)

$$u^i(\alpha,\beta)\Big|_{\alpha=0} = \exp\left[-ik_o \cos\phi_o[(1 - \beta)x_1 + \beta x_3]\right] \ . \tag{4.52}$$

Using (4.26), (4.28), (4.34) and (4.52), the integral (4.51) becomes

$$f_m^e = \frac{ik_o(x_1 - x_3)}{2} \exp[-ik_o x_1 \cos\phi_o]$$

$$\cdot \int_{\beta=0}^{1} \frac{(\alpha_m - \beta)\beta_m \exp[ik_o(x_1 - x_3)(\cos\phi_o)\beta]}{R_1 + \beta(R_3 - R_1)} d\beta \tag{4.53}$$

or, if $\beta = (\sigma + 1)/2$,

$$f_m^e = \frac{ik_0(x_1 - x_3)}{4} \exp\left[-ik_0\left(\frac{x_1 + x_3}{2}\right)\cos\phi_0\right] \cdot \int_{\sigma=-1}^{1} \frac{(2\alpha_m - 1 - \sigma)\beta_m \exp\left[ik_0\left(\frac{x_1 - x_3}{2}\right)\cos\phi_0)\sigma\right]}{(R_1 + R_3) + \sigma(R_3 - R_1)} d\sigma \,, \tag{4.54}$$

which is evaluated using numerical integration.

For the triangular element adjacent to the strip at $x = -w/2$ (Fig. 4.4), a similar calculation yields

$$f_m^e = \frac{ik_0(x_2 - x_1)}{4} \exp\left[-ik_0\left(\frac{x_1 + x_2}{2}\right)\cos\phi_0\right] \cdot \int_{\sigma=-1}^{1} \frac{\alpha_m(2\alpha_m - 1 - \sigma)\exp\left[ik_0\left(\frac{x_1 - x_2}{2}\right)(\cos\phi_0)\sigma\right]}{(R_1 + R_2) + \sigma(R_2 - R_1)} d\sigma \,, \tag{4.55}$$

which is numerically evaluated.

In summary, the incident field terms are given by (4.50) for a quadrilateral, (4.54) for the triangle at $x = w/2$, and (4.55) for the triangle at $x = -w/2$.

4.5 Induced Current

The induced current in the resistive strip is obtained using (2.29) or

$$K_z = \frac{1}{R(x)Z_0}(u^i + u) \tag{4.56}$$

and is evaluated at the center of the side of each element adjacent to the strip. If the element is a quadrilateral (Fig. 4.1)

$$R(x) = N_1 R_1 + N_4 R_4 \quad , \tag{4.57}$$

where

$$N_1 = \frac{x - x_4}{x_1 - x_4} \quad , \tag{4.58}$$

and

$$N_4 = \frac{x_1 - x}{x_1 - x_4} \quad , \tag{4.59}$$

and R_n is given by (4.13). The scalar u on the strip is given by

$$u = N_1 a_1 + N_4 a_4 \tag{4.60}$$

and the incident field on the strip is given by

$$u^i = \exp[-ik_0 x \cos \phi_0] \quad . \tag{4.61}$$

Since the x-coordinate of the center of the side of the element which is along the x-axis is

$$x_c = \frac{x_1 + x_4}{2} \quad , \tag{4.62}$$

the current (4.56) at that point is written as

$$K_z = \frac{1}{Z_0}\left[\frac{\exp\left[-ik_0\left(\frac{x_1 + x_4}{2}\right)\cos\phi_0\right]}{\left(\frac{R_1 + R_4}{2}\right)} + \frac{\left(\frac{a_1 + a_4}{2}\right)}{\left(\frac{R_1 + R_4}{2}\right)}\right] \tag{4.63}$$

by using (4.57), (4.60) and (4.61). Similarly, the induced current at the center of the triangular element at x = w/2 (Fig. 4.3) is

$$K_z = \frac{1}{Z_0}\left[\frac{\exp\left[-ik_0\left(\frac{x_1 + x_3}{2}\right)\cos\phi_0\right]}{\left(\frac{R_1 + R_3}{2}\right)} + \frac{\left(\frac{a_1 + a_3}{2}\right)}{\left(\frac{R_1 + R_3}{2}\right)}\right] \tag{4.64}$$

and at the center of the triangular element at x = -w/2 (Fig. 4.4) is

$$K_z = \frac{1}{Z_0}\left[\frac{\exp\left[-ik_0\left(\frac{x_1 + x_2}{2}\right)\cos\phi_0\right]}{\left(\frac{R_1 + R_2}{2}\right)} + \frac{\left(\frac{a_1 + a_2}{2}\right)}{\left(\frac{R_1 + R_2}{2}\right)}\right] . \tag{4.65}$$

If the strip is a perfect conductor, the expressions for K_z having R(x) in the denominator cannot be used. Instead (2.28) is used. Due to symmetry (2.24) in the scattered field, (2.28) is rewritten using (2.20) to obtain

$$K_z = \frac{2i}{k_0 Z_0}\left.\frac{\partial u}{\partial y}\right|_+ . \tag{4.66}$$

For the quadrilateral elements (Fig. 4.1) the derivative in (4.66) is now evaluated. The scalar u is given by (3.10) or by

$$u \approx \bar{u} = \sum_{n=1}^{4} N_n a_n \tag{4.67}$$

in a single element. Thus the derivative can be expressed by

$$\left.\frac{\partial u}{\partial y}\right|_{+} \approx \sum_{n=1}^{4} \left.\frac{\partial N_n}{\partial y}\right|_{y=o} a_n \quad . \tag{4.68}$$

Here N_n is given by (3.29) and $(\partial N_n/\partial y)$ is given by (4.7). Since the element is adjacent to the x-axis, then $y_1 = 0$ and $y_4 = 0$. Noting that $\alpha = -1$, where $y = 0$, (4.68) is evaluated to be

$$\left.\frac{\partial u}{\partial y}\right|_{+} \approx \left\{ \left(- \frac{a_1 - a_4}{x_1 - x_4} \right) \left[(-x_1 + x_2 + x_3 - x_4) + \beta(x_1 - x_2 + x_3 - x_4) \right] + (a_2 - a_1)(1 - \beta) + (a_3 - a_4)(1 + \beta) \right\} \Big/ \left[(y_3 + y_2) + \beta(y_3 - y_2) \right] \tag{4.69}$$

At the center of the side of the quadrilateral, $\beta = 0$ and the induced current is

$$K_z \approx \frac{2i}{k_o Z_o} \left\{ \frac{\left(- \frac{a_1 - a_4}{x_1 - x_4} \right)(-x_1 + x_2 + x_3 - x_4) + (a_2 - a_1) + (a_3 - a_4)}{y_3 + y_2} \right\} . \tag{4.70}$$

For the triangular element (Fig. 4.3) adjacent to the strip at $x = w/2$, the derivative in (4.66) is now evaluated. The scalar u is given by

$$u \approx \bar{u} = \sum_{n=1}^{3} N_n a_n \quad , \tag{4.71}$$

where N_n is given by (4.40). Then

$$\left.\frac{\partial u}{\partial y}\right|_{+} \approx \sum_{n=1}^{3} \left.\frac{\partial N_n}{\partial y}\right|_{y=o} a_n \quad , \tag{4.72}$$

where $\partial N_n/\partial y$ is given by (4.44). Since nodes 1 and 3 are on the x-axis, $y_1 = 0$ and $y_3 = 0$. Noting again that $\alpha = -1$ where $y = o$, (4.72) is evaluated to be

$$\left.\frac{\partial u}{\partial y}\right|_{+} \approx -\frac{a_1(x_2 - x_3) + 2a_2(x_1 - x_3) + [(x_2 - x_1) + (x_3 - x_1)]a_3}{2\beta^{1/2}\, y_2 (x_1 - x_3)} \quad . \tag{4.73}$$

At the center of the side of the triangle, $\beta = 1/2$ and the induced current is

$$K_z \approx \frac{2i}{k_o Z_o}\left\{\frac{-(x_2 - x_3)a_1 + 2(x_1 - x_3)a_2 + [(x_2 - x_1) + (x_3 - x_1)]a_3}{\sqrt{2}\,(x_1 - x_3)y_2}\right\}. \tag{4.74}$$

For the triangular element (Fig. 4.4) adjacent to the strip at $x = -w/2$, the derivative in (4.66) is now evaluated. Since nodes 1 and 2 are on the x-axis, y_1 and y_2 equal zero. Equation (4.72) becomes

$$\left.\frac{\partial u}{\partial y}\right|_{+} \approx \frac{-a_1(x_2 - x_3) - a_2[(x_2 - x_1) + (x_3 - x_1)] + 2a_3(x_2 - x_1)}{2\alpha^{1/2} y_3 (x_2 - x_1)} . \tag{4.75}$$

At the center of the side of the triangle, $\alpha = 1/2$ and

$$K_z = \frac{2i}{k_o Z_o}\left\{\frac{-(x_2 - x_3)a_1 - [(x_2 - x_1) + (x_3 - x_1)]a_2 + 2(x_2 - x_1)a_3}{\sqrt{2}\, y_3 (x_2 - x_1)}\right\}. \tag{4.76}$$

In summary, for a resistive strip the induced current K_z is given by (4.63) for a quadrilateral, (4.64) for the triangle at $x = w/2$, and (4.65) for the triangle at $x = -w/2$. For a perfectly conducting strip K_z is given by (4.70) for a quadrilateral, (4.74) for the triangle at $x = w/2$, and (4.76) for the triangle at $x = -w/2$.

4.6 Radar Cross Section

The radar cross section given by (2.40) requires evaluation of (2.38), the expression for $P(\phi,\phi_o)$. Using (4.56) yields

$$P(\phi,\phi_o) = -\frac{k_o}{4}\left\{\int_{x'=-w/2}^{w/2} \frac{\exp[-ik_o x'(\cos\phi_o + \cos\phi)}{R(x')}\, dx' + \int_{x'=-w/2}^{w/2} \frac{u(x',0)\exp[-ik_o x' \cos\phi]}{R(x')}\, dx'\right\} \tag{4.77}$$

for a resistive strip. These integrals can be converted to a series of integrals over individual element edges along the strip.

$$P(\phi,\phi_0) = \sum_{e=1}^{J} P_e(\phi,\phi_0) \quad , \tag{4.78}$$

where

$$P_e(\phi,\phi_0) = -\frac{k_0}{4}\left\{\int_{\Gamma_P^e} \frac{\exp[-ik_0x'(\cos\phi_0 + \cos\phi)]}{R(x')}\,dx' + \int_{\Gamma_P^e} \frac{u(x',0)\exp[-ik_0x'\cos\phi]}{R(x')}\,dx'\right\} \tag{4.79}$$

and J is the total number of elements. In (4.78) only those elements adjacent to Γ_P make a nonzero contribution to $P(\phi,\phi_0)$.

For a quadrilateral element (Fig. 4.1), the integrals in (4.79) are transformed to the α-β coordinates using (3.31) and (3.32).

$$P_e(\phi,\phi_0) = \frac{k_0}{4}\left\{\int_{\beta=-1}^{1}\left[\frac{\exp[-ik_0x(\alpha,\beta)(\cos\phi + \cos\phi_0)]}{R(\alpha,\beta)}\frac{\partial x}{\partial\beta}\right]_{\alpha=-1} d\beta + \int_{\beta=-1}^{1}\left[\frac{u(\alpha,\beta)\exp[-ik_0x(\alpha,\beta)\cos\phi_0]}{R(\alpha,\beta)}\frac{\partial x}{\partial\beta}\right]_{\alpha=-1} d\beta\right\} \quad . \tag{4.80}$$

Since $u(\alpha,\beta)$ is approximately given by (3.30), then

$$u(\alpha,\beta)\Big|_{\alpha=-1} \approx \frac{1}{2}(1-\beta)a_1 + \frac{1}{2}(1+\beta)a_4 \,. \qquad (4.81)$$

Using (4.14), (4.15), (4.49) and (4.81) yields

$$P_e(\phi,\phi_o) = -\frac{k_o}{4}\left\{(x_1 - x_4)\exp\left[-ik_o\left(\frac{x_1+x_4}{2}\right)(\cos\phi + \cos\phi_o)\right]\right.$$

$$\cdot \int_{\beta=-1}^{1} \frac{\exp\left[ik_o\left(\frac{x_1-x_4}{2}\right)(\cos\phi+\cos\phi_o)\beta\right]}{(R_1+R_4)-\beta(R_1-R_4)}\,d\beta$$

$$+\left(\frac{x_1-x_4}{2}\right)\exp\left[-ik_o\left(\frac{x_1+x_4}{2}\right)\cos\phi\right]$$

$$\left.\cdot \int_{\beta=-1}^{1} \frac{(a_1+a_4)-\beta(a_1-a_4)}{(R_1+R_4)-\beta(R_1-R_4)}\exp\left[ik_o\left(\frac{x_1-x_4}{2}\right)(\cos\phi)\beta\right]d\beta\right\}. \qquad (4.82)$$

For the triangular element adjacent to the strip at $x = w/2$ (Fig. 4.3)

$$P_e(\phi,\phi_o) = -\frac{k_o}{4}\left\{(x_1 - x_3)\exp\left[-ik_o\left(\frac{x_1 + x_3}{2}\right)(\cos\phi + \cos\phi_o)\right]\right.$$

$$\cdot \int_{\beta=-1}^{1} \frac{\exp\left[ik_o\left(\frac{x_1 - x_3}{2}\right)(\cos\phi + \cos\phi_o)\beta\right]}{(R_1 + R_3) - \beta(R_1 - R_3)}\, d\beta$$

$$+ \left(\frac{x_1 - x_3}{2}\right)\exp\left[-ik_o\left(\frac{x_1 + x_3}{2}\right)\cos\phi\right]$$

$$\left.\cdot \int_{\beta=-1}^{1} \frac{(a_1 + a_3) - \beta(a_1 - a_3)}{(R_1 + R_3) - \beta(R_1 - R_3)} \exp\left[ik_o\left(\frac{x_1 - x_3}{2}\right)(\cos\phi)\beta\right] d\beta\right\}, \quad (4.83)$$

and for the triangle adjacent to the strip at x = -w/2 (Fig. 4.4)

$$P_e(\phi,\phi_o) = -\frac{k_o}{4}\left\{(x_2 - x_1)\exp\left[ik_o\left(\frac{x_1 + x_2}{2}\right)(\cos\phi + \cos\phi_o)\right]\right.$$

$$\cdot \int_{\beta=-1}^{1} \frac{\exp\left[ik_o\left(\frac{x_2 - x_1}{2}\right)(\cos\phi + \cos\phi_o)\beta\right]}{(R_1 + R_2) - \beta(R_2 - R_1)}\, d\beta$$

$$+ \left(\frac{x_2 - x_1}{2}\right)\exp\left[-ik_o\left(\frac{x_1 + x_2}{2}\right)\cos\phi\right]$$

$$\left.\cdot \int_{\beta=-1}^{1} \frac{(a_1 + a_2) - \beta(a_2 - a_1)}{(R_1 + R_2) - \beta(R_2 - R_1)} \exp\left[ik_o\left(\frac{x_2 - x_1}{2}\right)(\cos\phi)\beta\right] d\beta\right\}. \quad (4.84)$$

For the case of a perfectly conducting strip, evaluation of (2.38) requires the use of (4.66) rather than (4.56). Thus

$$P(\phi,\phi_o) = -\frac{k_o}{4}\int_{x'=-w/2}^{w/2}\frac{2i}{k_o}\left.\frac{\partial u}{\partial y}\right|_+ \exp\left[-ik_o x'\cos\phi\right]dx' \ . \qquad (4.85)$$

As with the resistive strip, this integral is converted to a series of integrals along individual elements. Using (4.78) again,

$$P_e(\phi,\phi_o) = -\frac{k_o}{4}\int_{\Gamma_P^e}\frac{2i}{k_o}\left.\frac{\partial u}{\partial y}\right|_+ \exp\left[-ik_o x'\cos\phi\right]dx' \ . \qquad (4.86)$$

For a quadrilateral element adjacent to the strip (Fig. 4.1), transformation of (4.86) to α-β coordinates yields

$$P_e(\phi,\phi_o) = \frac{k_o}{4}\int_{\beta=-1}^{1}\frac{2i}{k_o}\left[\frac{\partial u}{\partial y}\exp\left[-ik_o x(\alpha,\beta)\cos\phi\right]\frac{\partial x}{\partial\beta}\right]_{\alpha=-1} d\beta \ . \qquad (4.87)$$

Since $x(\alpha,\beta)$ is given by (3.31), then

$$\exp\left[-ik_o x(\alpha,\beta)\cos\phi\right]\Big|_{\alpha=-1} = \exp\left[-ik_o\left(\frac{x_1+x_4}{2}\right)\cos\phi\right] \cdot \exp\left[ik_o\left(\frac{x_1-x_4}{2}\right)(\cos\phi)\beta\right]. \qquad (4.88)$$

Using (4.15), (4.69) and (4.88) yields

$$P_e(\phi,\phi_o) = -\frac{i(x_1 - x_4)}{4} \exp\left[-ik_o\left(\frac{x_1 + x_4}{2}\right)\cos\phi\right]$$

$$\cdot \int_{\beta=-1}^{1} \frac{\exp\left[ik_o\left(\frac{x_1 - x_4}{2}\right)(\cos\phi)\beta\right]}{(y_3 + y_2) + \beta(y_3 - y_2)}$$

$$\cdot \left[\left(-\frac{a_1 - a_4}{x_1 - x_4}\right)(D_1 + \beta D_2) + (-a_1 + a_2 + a_3 - a_4)\right.$$

$$\left. + \beta(a_1 - a_2 + a_3 - a_4)\right] d\beta \quad , \qquad (4.89)$$

where D_1 and D_2 are given by (4.5).

For the triangular element adjacent to the strip at x = w/2 (Fig. 4.3), transformation of (4.86) to α-β coordinates yields

$$P_e(\phi,\phi_o) = \frac{k_o}{4} \int_{\beta=0}^{1} \frac{2i}{k_o}\left[\frac{\partial u}{\partial y} \exp\left[-ik_o x(\alpha,\beta)\cos\phi\right]\frac{\partial x}{\partial \beta}\right]_{\alpha=0} d\beta \quad . \qquad (4.90)$$

Using (3.31), (4.26) and (4.73) yields

$$P_e(\phi,\phi_o) = -\frac{i(x_1 - x_3)}{2} \exp\left[-ik_o x_1 \cos\phi\right]$$

$$\cdot \left\{\frac{-a_1(x_2 - x_3) + 2a_2(x_1 - x_3) + [(x_2 - x_1) + (x_3 - x_1)]a_3}{2y_2(x_1 - x_3)}\right\}$$

$$\cdot \int_{\beta=0}^{1} \frac{\exp\left[ik_o(x_1 - x_3)(\cos\phi)\beta\right]}{\beta^{1/2}} d\beta \qquad (4.91)$$

or, if $\beta = (\sigma + 1)/2$,

$$P_e(\phi,\phi_o) = -\frac{i(x_1 - x_3)}{4} \exp\left[-ik_o\left(\frac{x_1 + x_3}{2}\right)(\cos\phi)\right]$$

$$\cdot\left\{\frac{-a_1(x_2 - x_3) + 2a_2(x_1 - x_3) + [(x_2 - x_1) + (x_3 - x_1)]a_3}{\sqrt{2}\ y_2(x_1 - x_3)}\right\}$$

$$\cdot\int_{\sigma=-1}^{1}\frac{\exp\left[ik_o\frac{x_1 - x_3}{2}(\cos\phi)\sigma\right]}{\sqrt{\sigma + 1}}\,d\sigma \quad . \qquad (4.92)$$

Using (4.74), $P_e(\phi,\phi_o)$ may be written as

$$P_e(\phi,\phi_o) = -\frac{k_o}{4} Z_o K_z\left(\frac{x_1 - x_3}{2}\right) \exp\left[-ik_o\left(\frac{x_1 + x_3}{2}\right)\cos\phi\right]$$

$$\cdot\int_{\sigma=-1}^{1}\frac{\exp\left[ik_o\left(\frac{x_1 - x_3}{2}\right)(\cos\phi)\sigma\right]}{\sqrt{\sigma + 1}}\,d\sigma \quad , \qquad (4.93)$$

where $Z_o K_z$ is the induced current at the center of the element.

For the triangular element adjacent to the strip at $x = -w/2$ (Fig. 4.4), the expressions for $P(\phi,\phi_o)$ are similar to (4.92) and (4.93), that is

$$P_e(\phi,\phi_o) = -\frac{i(x_2 - x_1)}{4} \exp\left[-ik_o\left(\frac{x_1 + x_2}{2}\right)(\cos\phi)\right]$$

$$\cdot \left\{-\frac{a_1(x_2 - x_3) - a_2[(x_2 - x_1) + (x_3 - x_1)] + 2a_3(x_2 - x_1)}{\sqrt{2}\ y_3(x_2 - x_1)}\right\}$$

$$\cdot \int_{\sigma=-1}^{1} \frac{\exp\left[ik_o\left(\frac{x_1 - x_2}{2}\right)(\cos\phi)\sigma\right]}{\sqrt{\sigma + 1}}\, d\sigma \qquad (4.94)$$

or

$$P_e(\phi,\phi_o) = -\frac{k_o}{4} Z_o K_z \left(\frac{x_2 - x_1}{2}\right) \exp\left[-ik_o\left(\frac{x_1 + x_2}{2}\right)\cos\phi\right]$$

$$\cdot \int_{\sigma=-1}^{1} \frac{\exp\left[ik_o\left(\frac{x_2 - x_1}{2}\right)(\cos\phi)\sigma\right]}{\sqrt{\sigma + 1}}\, d\sigma \quad , \qquad (4.95)$$

where $Z_o K_z$ is the induced current at the center of the element.

The radar cross section is frequently given as a dimensionless quantity $\sigma(\phi,\phi_o)/\lambda_o$ and is given in decibels. Since $k_o = 2\pi/\lambda_o$, (2.40) may be written as

$$\frac{\sigma(\phi,\phi_o)}{\lambda_o} = \frac{2}{\pi} |P(\phi,\phi_o)|^2 \quad . \qquad (4.96)$$

Expressed in decibels,

$$10 \log_{10} \left(\frac{\sigma(\phi,\phi_o)}{\lambda_o} \right) = 10 \log_{10} \frac{2}{\pi} + 20 \log_{10} |P(\phi,\phi_o)| \quad , \tag{4.97}$$

where $P(\phi,\phi_o)$ is given by (4.78).

In summary, for a resistive strip $P_e(\phi,\phi_o)$ is given by (4.82) for a quadrilateral, (4.83) for the triangle adjacent to the strip at x = w/2 and (4.84) for the triangle at x = -w/2. For a perfectly conducting strip, $P_e(\phi,\phi_o)$ is given by (4.89) for a quadrilateral, (4.93) for the triangle at x = w/2 and (4.95) for the triangle at x = -w/2. Numerical integration is used in the computer program to evaluate the integrals in these expressions for $P_e(\phi,\phi_o)$.

CHAPTER V. RESULTS OF THE NUMERICAL SOLUTION

5.1 Error Criteria for Numerical Results

The numerical results of the finite element method (FEM) were obtained using the DEC-10 computer at Western Michigan University. They are compared with results obtained from an integral equation formulation of the same problem. The integral equation was solved by the method of moments (MOM) at the Radiation Laboratory of the University of Michigan (Knott, Liepa and Senior, 1973). The moment method results for the radar cross section of the resistive strip are known to agree quite well with measurements.

The error in magnitude of any quantity Q calculated by the finite element method is defined as follows:

$$\text{percent error in } |Q| = \frac{|Q|_{FEM} - |Q|_{MOM}}{|Q|_{MOM}} \times 100 \quad . \tag{5.1}$$

The phase error is given by

$$\text{error in arg } Q = (\arg Q)_{FEM} - (\arg Q)_{MOM} \quad . \tag{5.2}$$

5.2 Selection of Element Mesh Parameters

The objective to be met in selection of the mesh parameters is to provide a sufficient density of elements so that the incident

field is adequately sampled at the strip, and so that magnitude and phase errors in the computed scattered field are not large, allowing a certain accuracy of solution to be obtained. Of course, the cost of the solution is also a consideration.

The semicircle Γ_B is to be in the far field region of the scattered field. Selection of the radius ρ_1 of Γ_B is made using the criterion $2d^2/\lambda_o$ for the near field radius, where d is the largest dimension of the scattering body (Kouyoumjian and Peters, 1965). There is no reason to extend the finite element region further outward because the accuracy of solution is not improved and the cost of solution is increased. Thus

$$\rho_1 \approx \frac{2w^2}{\lambda_o} \quad . \tag{5.3}$$

Along a radial line extending outward from the strip, the scattered field is essentially a decaying sinusoid of wavelength λ_o. The results of the one-dimensional problem (scattering from an infinite sheet) in Appendix C indicate that the maximum error in the magnitude of the scattered field is less than one percent if the density of the elements is 16 or more elements per wavelength. This density of elements is generally viewed as adequate for sampling a sinusoid. Thus if M_y is the number of elements in the radial direction, the selection is

$$M_y \geq 16 \frac{\rho_1}{\lambda_o} \quad . \tag{5.4}$$

Using (5.3) yields

$$M_y \geq \frac{32\ w^2}{\lambda_o^2} \quad . \tag{5.5}$$

In order to adequately sample the incident field on the strip, the density of elements there should also be about 16 elements per wavelength. If M_x is the number of elements adjacent to the strip, the selection is

$$M_x \geq 16\ \frac{w}{\lambda_o} \quad . \tag{5.6}$$

A lower density may be used for cases where the incidence is nearly broadside.

The element mesh, discussed in Section 3.5, has a nonuniform distribution of elements. Thus the element densities implied by (5.4) and (5.6) must be considered as average densities. Near the strip the density of elements is greater than near the semicircle Γ_B.

When ρ_1, M_x and M_y have been selected, computation of the parameters actually used in the computer program is begun. The integer number M_x is called NUMELS in the program. The semicircle of radius ρ_1 bounding the finite element region coincides approximately with an ellipse of eccentricity ξ^{-1}. For $\xi^{-1} < 0.5$, the ellipse is essentially a circle. Taking ρ_1 as the average of the semi-major and semi-minor axes of the ellipse yields

$$\rho_1 \approx \frac{w}{2}\,\xi \quad . \tag{5.7}$$

Using (5.3) yields

$$\xi^{-1} = \frac{1}{4\frac{w}{\lambda_o}} \tag{5.8}$$

which is the required eccentricity. This value is the computer program parameter SMEC:

$$\text{SMEC} = \frac{1}{4\frac{w}{\lambda_o}} \quad . \tag{5.9}$$

In order that the largest ellipse inside the circle $\rho = \rho_1$ be nearly a circle, SMEC must be 0.5 or less. A value of SMEC equal to 0.5 corresponds to $w/\lambda_o = 0.5$ according to (5.9) and $\rho_1 = w$ according to (5.3). Consequently, for $w/\lambda_o < 0.5$ the parameter SMEC must remain at 0.5 and ρ_1 must equal the strip width.

Another of the computer program parameters is an aspect ratio EL. It is the ratio of the dimension of a quadrilateral element in the direction parallel to the strip to the dimension in the direction perpendicular to the strip. Assuming values for M_y, NUMELS, and SMEC have been tentatively selected, an approximate value for EL can be obtained from

$$\text{EL} = \frac{M_y - 1}{(\text{NUMELS})A} = \frac{M_y - 1}{(M_x)A} \quad , \tag{5.10}$$

where $A = -0.83 \log_{10} \text{SMEC} + 0.17$. This expression for EL is due to the properties of the mesh generation portion of the computer program as explained in Appendix A.

5.3 Effects of Element Density

In order to examine the effect of element density on the accuracy of the solution, numerical values of the magnitude and phase of $P(\phi,\phi_0)$ for backscattering ($\phi = \phi_0$) were obtained for a strip of width $w/\lambda_0 = 0.5$. The radius in wavelengths of the finite element region ρ_1/λ_0 is 0.5 as specified by the selection rule (5.3). The errors in the numerical values are defined by (5.1) and (5.2).

The numerical results indicate that an increase in accuracy in both magnitude and phase of $P(\phi,\phi_0)$ for all angles of incidence is most economically accomplished, in terms of computer memory, by making element densities $(M_x)\lambda_0/w$ and $(M_y)\lambda_0/\rho_1$ equal and increasing them both. It is possible to make one density substantially larger than the other to reduce the errors at certain angles of incidence. However, the effects on the errors at other angles of incidence are not always predictable if this is done. Figures 5.1 and 5.2 show the errors in $P(\phi,\phi_0)$ versus element density for R = 1. For 50 degree and 90 degree angles of incidence, element densities of 16 elements per wavelength in both directions appear to be adequate to reduce the error in the magnitude of $P(\phi,\phi_0)$ to be less than one percent, and to reduce the phase error to 1.0 degree or less. The errors for incidence at zero degrees are larger, apparently due to the presence of a null in the radiation pattern near this angle.

The effect of the null can be seen in Figs. 5.3 and 5.4 which show the errors in $P(\phi,\phi_0)$ versus ϕ for backscattering. The errors at the null which occur at about $\phi = 25°$ can be reduced by

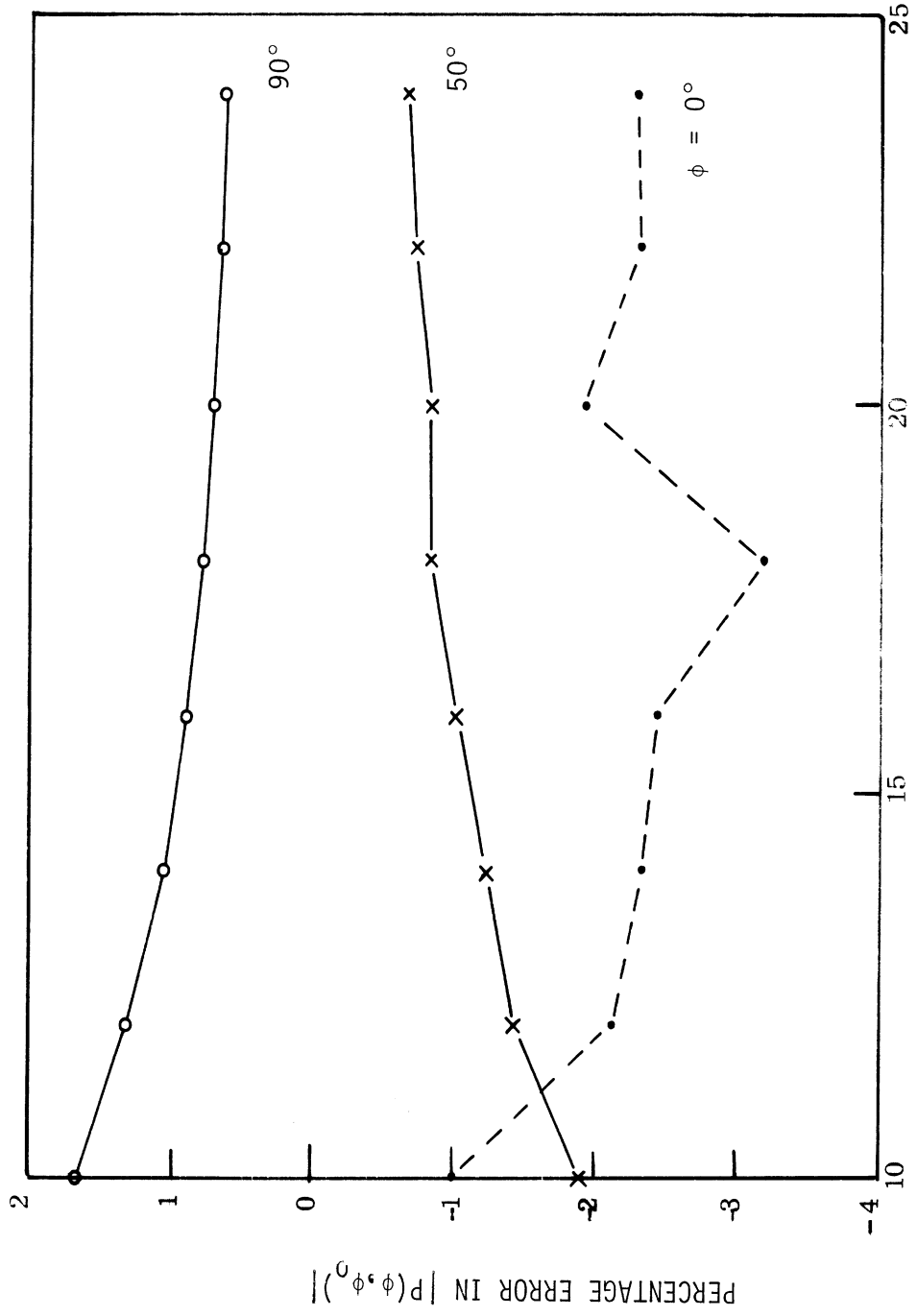

Fig. 5.1: Error in $|P(\phi,\phi_o)|$ vs. element density, $(M_x)(\lambda_o/w) = (M_y)(\lambda_o/\rho_1)$, R = 1.0, w/λ_o = 0.5, ρ_1/λ_o = 0.5, backscattering ($\phi = \phi_o$).

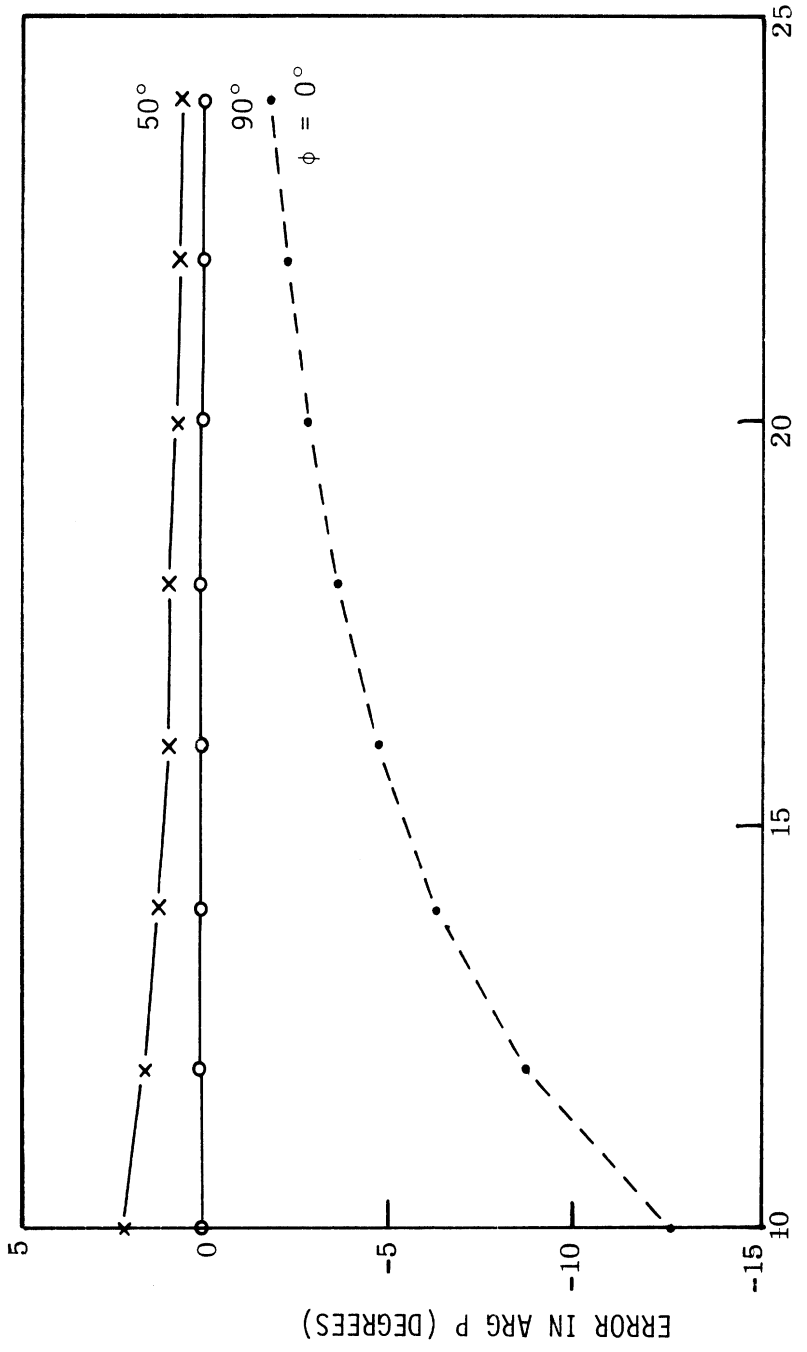

Fig. 5.2: Error in arg $P(\phi,\phi_o)$ vs. element density, $(M_x)(\lambda_o/w) = (M_y)(\lambda_o/\rho_1)$, R = 1.0, $w/\lambda_o = 0.5$, $\rho_1/\lambda_o = 0.5$, backscattering ($\phi = \phi_o$).

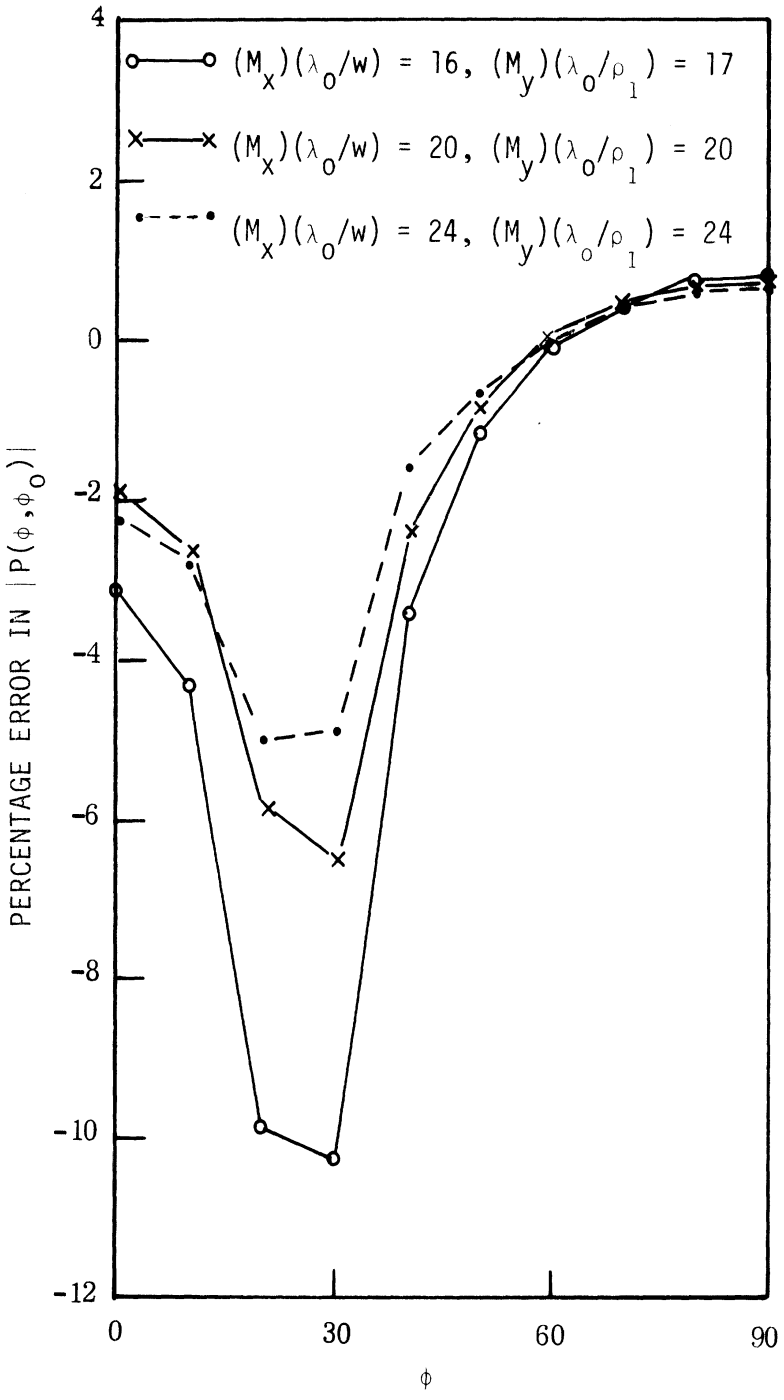

Fig. 5.3: Error in $|P(\phi,\phi_o)|$ vs. ϕ for R = 1.0, w/λ_o = 0.5, $\rho_1/\lambda_o \approx 0.5$, backscattering ($\phi = \phi_o$).

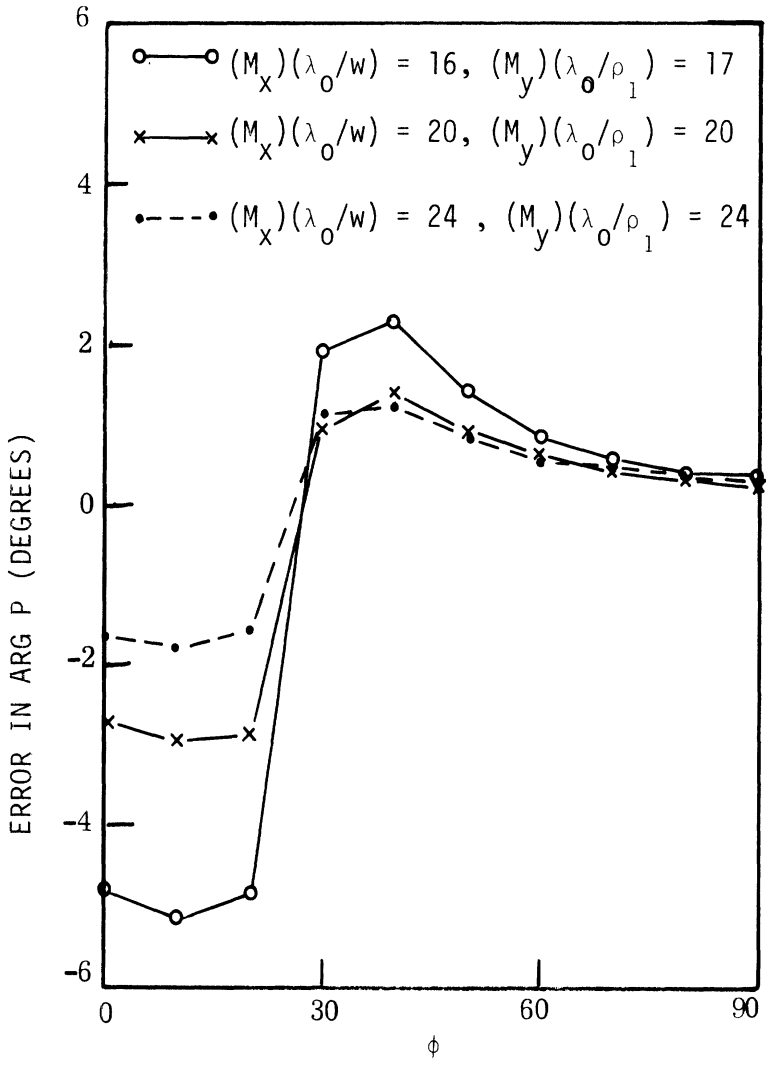

Fig. 5.4: Error in arg $P(\phi,\phi_o)$ vs. ϕ for R = 1.0, $w/\lambda_o = 0.5$, $\rho_1/\lambda_o \approx 0.5$, backscattering ($\phi = \phi_o$).

increasing the element densities. The same general results for R = 0 are shown in Fig. 5.5 and 5.6 except that the errors are larger than for R = 1.

The errors in $P(\phi,\phi_0)$ are plotted versus $(1/2)k_0 w \cos\phi$ for three different strip widths in Figs. 5.7 and 5.8. Here both the element densities are 16 elements per wavelength and R = 1. Data for strips wider than 0.71 wavelength could not be obtained due to large amount of computer memory required. These two figures show that for $(1/2)k_0 w \cos\phi < 0.3\,\pi$ the magnitude error is less than one percent and the phase error is less than 1.5 degrees for all strip widths. The wider strips have nulls in their radiation patterns for $(1/2)k_0 w \cos\phi \approx 0.5\,\pi$ and consequently have larger errors in $P(\phi,\phi_0)$ at certain angles due to the rapid changes in phase of the scattered field in the vicinity of a null. For the widest strip considered ($w/\lambda_0 = 0.71$), the errors for $(1/2)k_0 w \cos\phi > 0.6\,\pi$ are in approximately the same range as those for $(1/2)k_0 w \cos\phi < 0.3\,\pi$. Increasing the element density above 16 elements per wavelength will reduce errors mainly in the vicinity of a null.

5.4 Effects of Strip Resistivity

Table 5.1 shows the effect of changing the strip resistivity on the error in $P(\phi,\phi_0)$ for backscattering. The table shows that as R decreases below 0.1 the error grows significantly. In the range $0 < R \leq 0.05$ the numerical results are highly inaccurate, except for near-broadside incidence.

Two effects lead to the deterioration of the numerical results for low R. One can be explained by considering the finite element

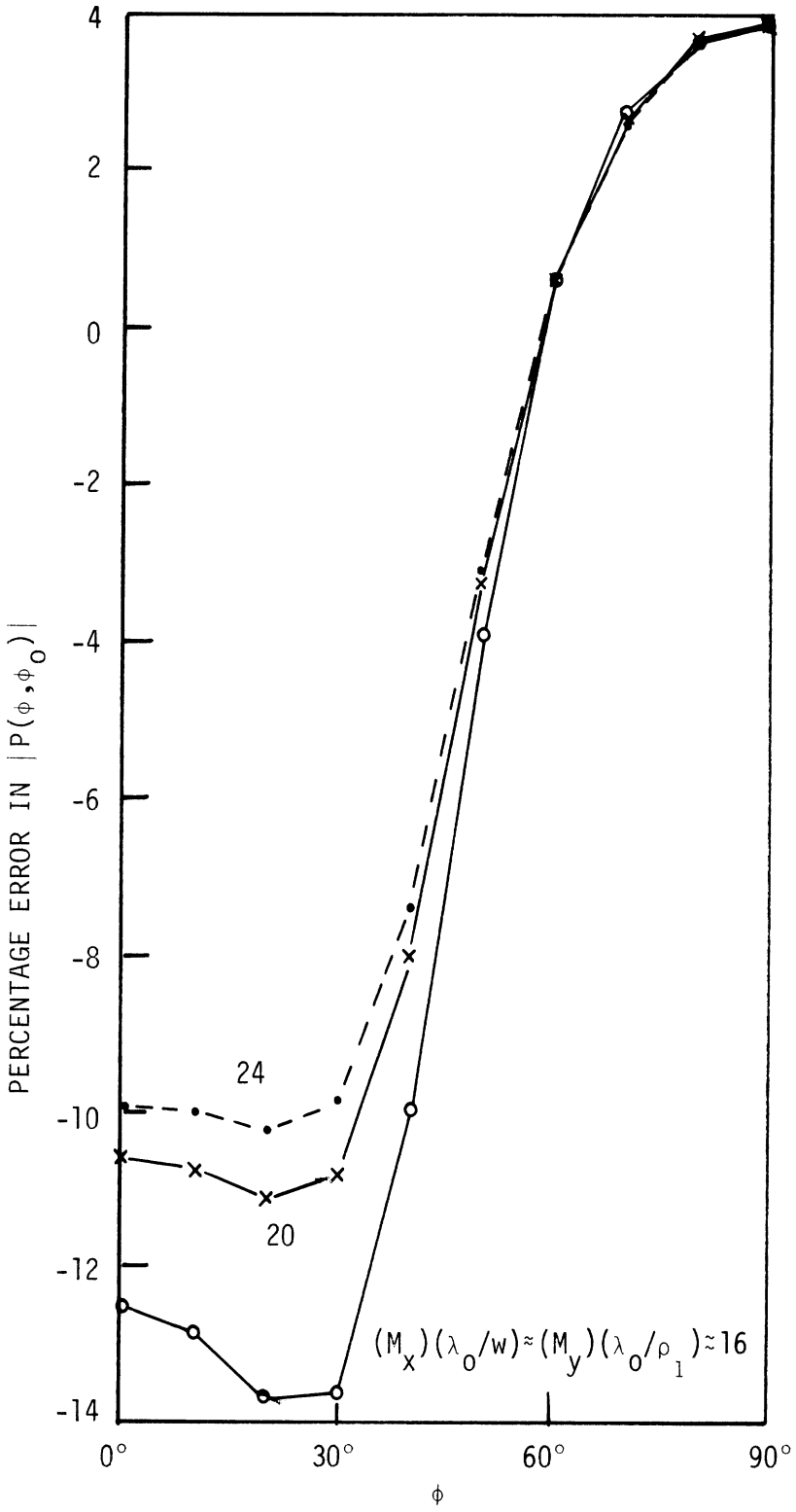

Fig. 5.5: Error in $|P(\phi,\phi_o)|$ vs. ϕ for R = 0.0, w/λ_o = 0.5, $\rho_1/\lambda_o \approx 0.5$, backscattering ($\phi = \phi_o$).

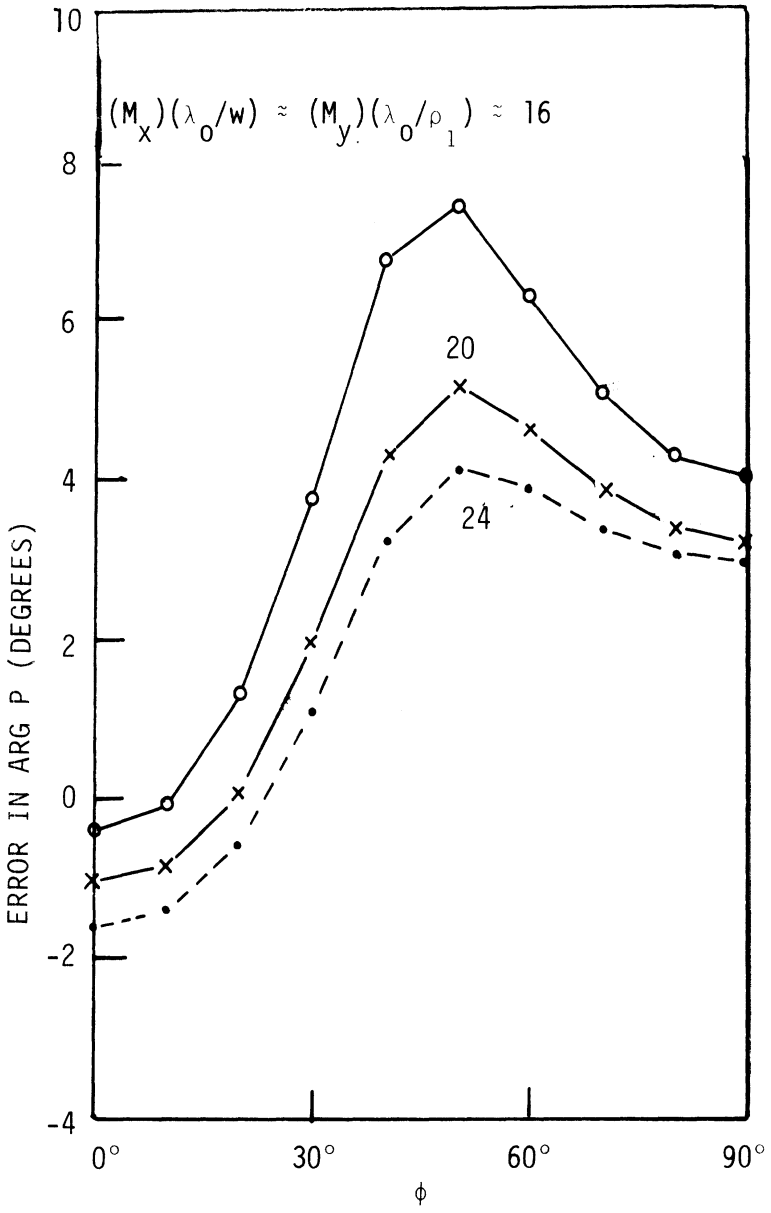

Fig. 5.6: Error in arg $P(\phi,\phi_o)$ vs. ϕ for R = 0.0, w/λ_o = 0.5, $\rho_1/\lambda_o \approx 0.5$, backscattering ($\phi = \phi_o$).

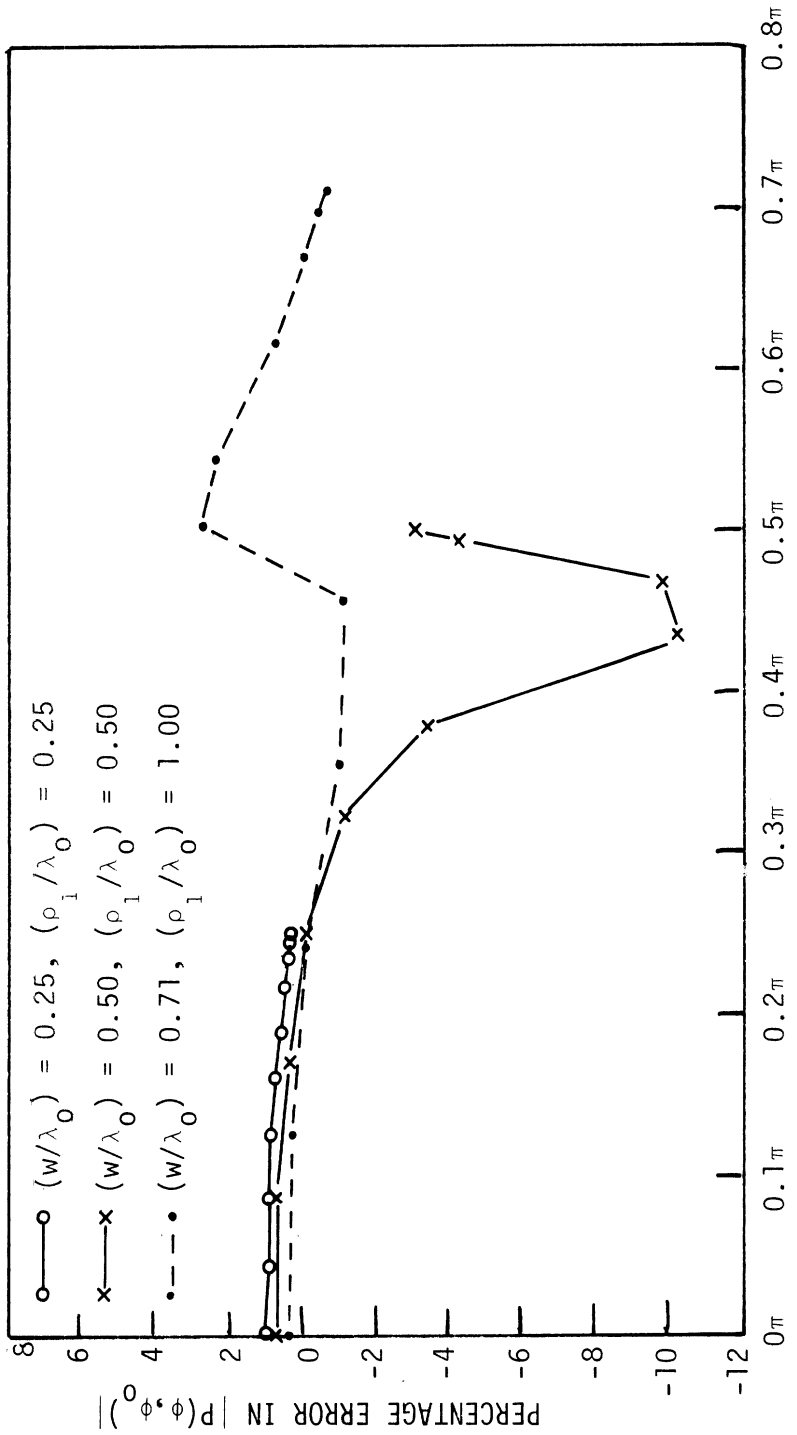

Fig. 5.7: Error in $|P(\phi,\phi_o)|$ vs. $(1/2)k_o w \cos\phi$ for R = 1.0, $(M_x)(\lambda_o/w) \approx 16$, $(M_y)(\lambda_o/\rho_1) \approx 16$, backscattering ($\phi = \phi_o$).

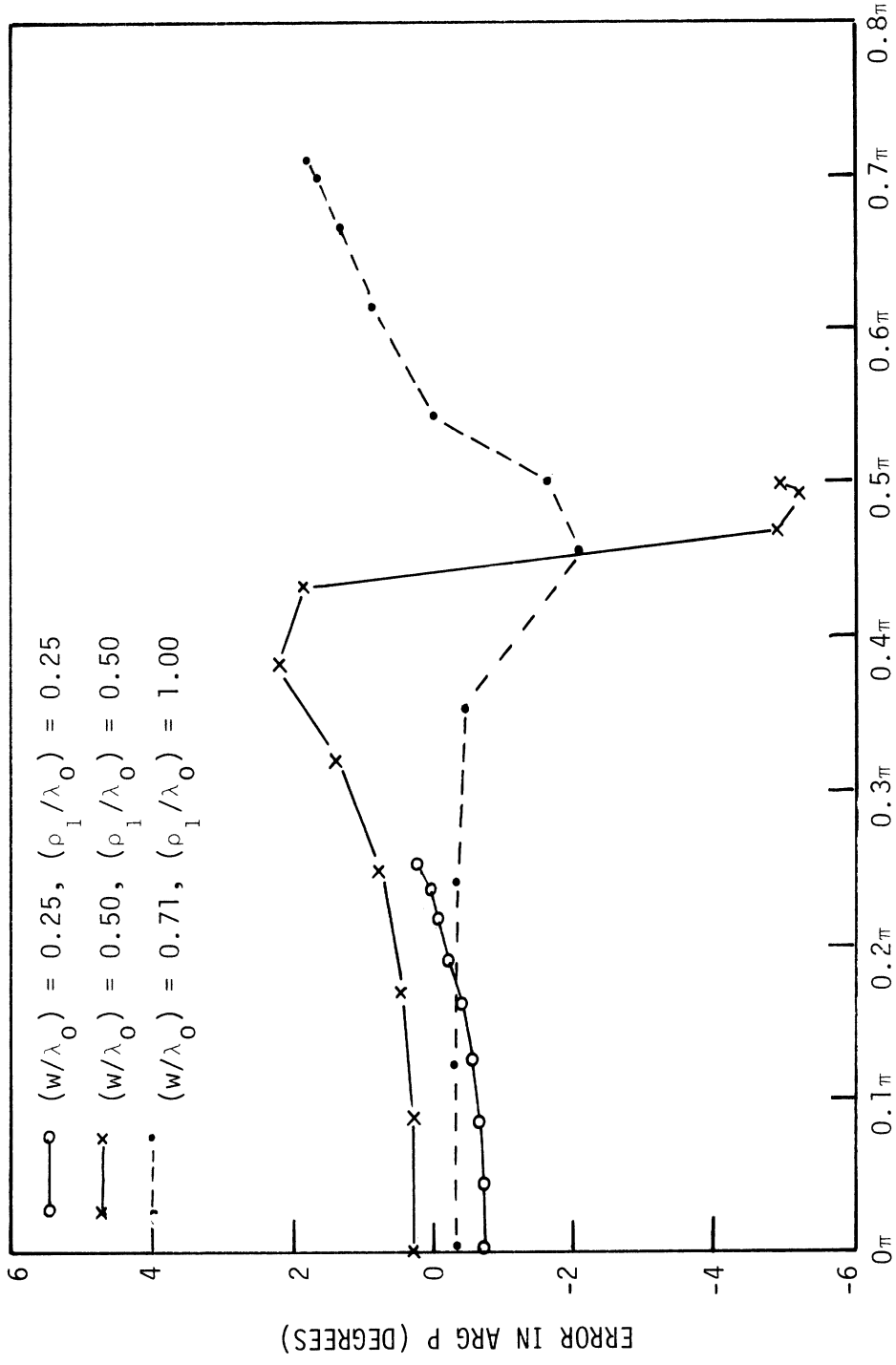

Fig. 5.8: Error in arg $P(\phi,\phi_o)$ vs. $(1/2)k_o w \cos\phi$ for R = 1.0, $(M_x)(\lambda_o/w) \approx 16$, $(M_y)(\lambda_o/\rho_1) \approx 16$, backscattering ($\phi = \phi_o$).

Table 5.1

Error in $P(\phi,\phi_o)$ for Backscattering ($\phi = \phi_o$)

$(M_x)\ \frac{\lambda_o}{w} = 18$, $(M_y)\ \frac{\lambda_o}{\rho_1} \approx 17$, $\frac{w}{\lambda_o} = 0.5$, $\frac{\rho_1}{\lambda_o} \approx 0.5$

R	Error in $\lvert P \rvert$ / Error in Arg P		
	$\phi = 0°$	$\phi = 50°$	$\phi = 90°$
0.0	-10.362% / -0.680°	-3.220% / 5.968°	4.288% / 3.720°
0.01	95.292% / -62.961°	-72.613% / -81.545°	6.530% / -0.985°
0.05	3.695% / -22.311°	-20.676% / -2.812°	4.115% / -0.726°
0.10	-0.554% / -12.293°	-10.779% / -0.257°	3.118% / -0.515°
0.5	-0.673% / -4.118°	-1.962% / 1.025°	1.283% / 0.054°
1.0	-1.345% / -3.499°	-0.891% / 0.802°	0.848% / 0.095°
2.0	-1.852% / 3.184°	-0.478% / -0.463°	0.533% / 0.071°

mesh as a radial transmission line. The boundary condition imposed at Γ_B acts as an imperfect termination for the transmission line. Multiple reflections occur at Γ_B and at the strip Γ_P so that standing waves appear in the numerical data. Lowering the value of R increases the magnitude of the wave reflected from the strip and thus increases the standing-wave ratio. The transmission line interpretation and the nature of the error caused by the standing waves are discussed in Appendix B.

The second effect leading to the poor numerical results for low R is due to the coefficients K_{mn} (3.14), corresponding to nodes on the strip, becoming much larger as R decreases. This results in the system of equations (3.13) becoming increasingly ill-conditioned. The effect can be partially offset by controlling the size of the term in (3.18) which contains R. This term is proportional to $[R(M_x)\lambda_0/w]^{-1}$, where $(M_x)\lambda_0/w$ is the density of elements along the strip. The data of Table 5.1 indicates that if $R(M_x)\lambda_0/w < 1$, there will be large errors in $P(\phi,\phi_0)$. A selection rule of

$$R(M_x)\lambda_0/w > 5 \tag{5.11}$$

is appropriate. Figures 5.9 and 5.10 show the errors in $P(\phi,\phi_0)$ versus the angle of incidence for backscattering with R = 0.1. The curves for constant $(M_x)(\lambda_0/w)R$ show how the accuracy improves as this parameter increases.

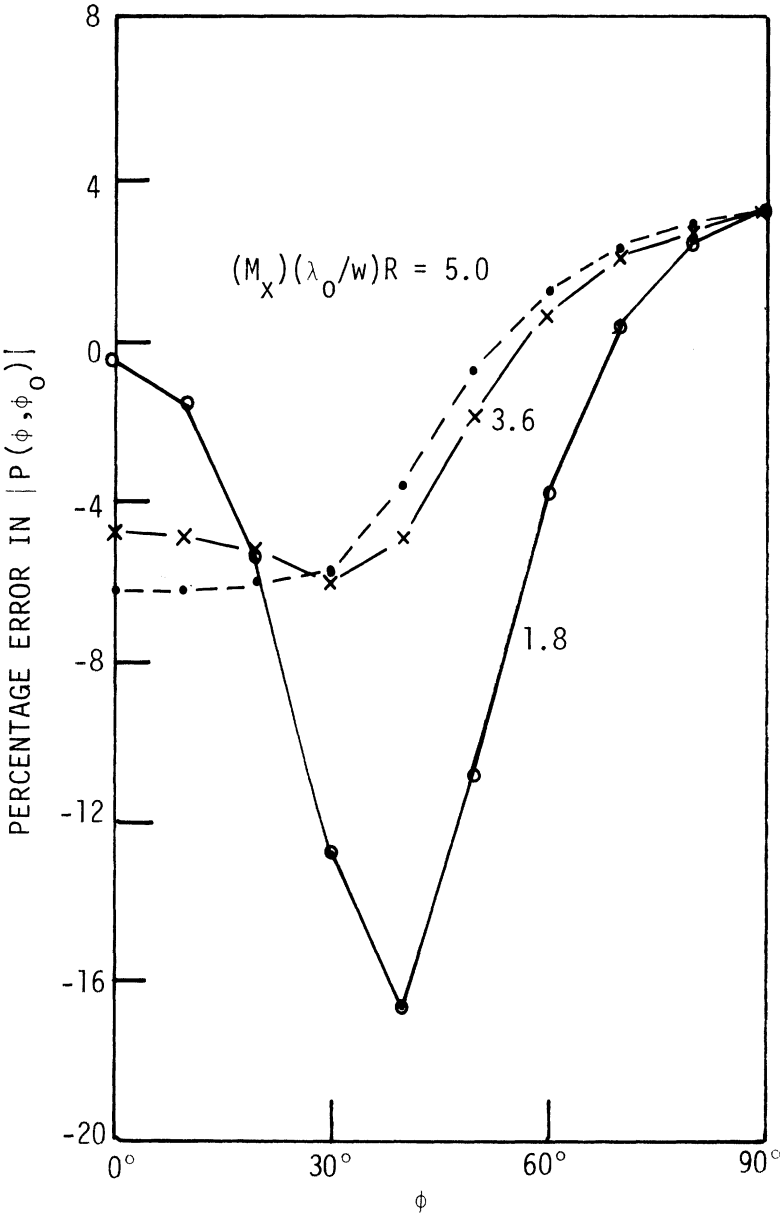

Fig. 5.9: Error in $|P(\phi,\phi_0)|$ vs. ϕ for R = 0.1, $w/\lambda_0 = 0.5$, $\rho_1/\lambda_0 \approx 0.5$, $(M_y)(\lambda_0/\rho_1) \approx 17$, backscattering ($\phi = \phi_0$).

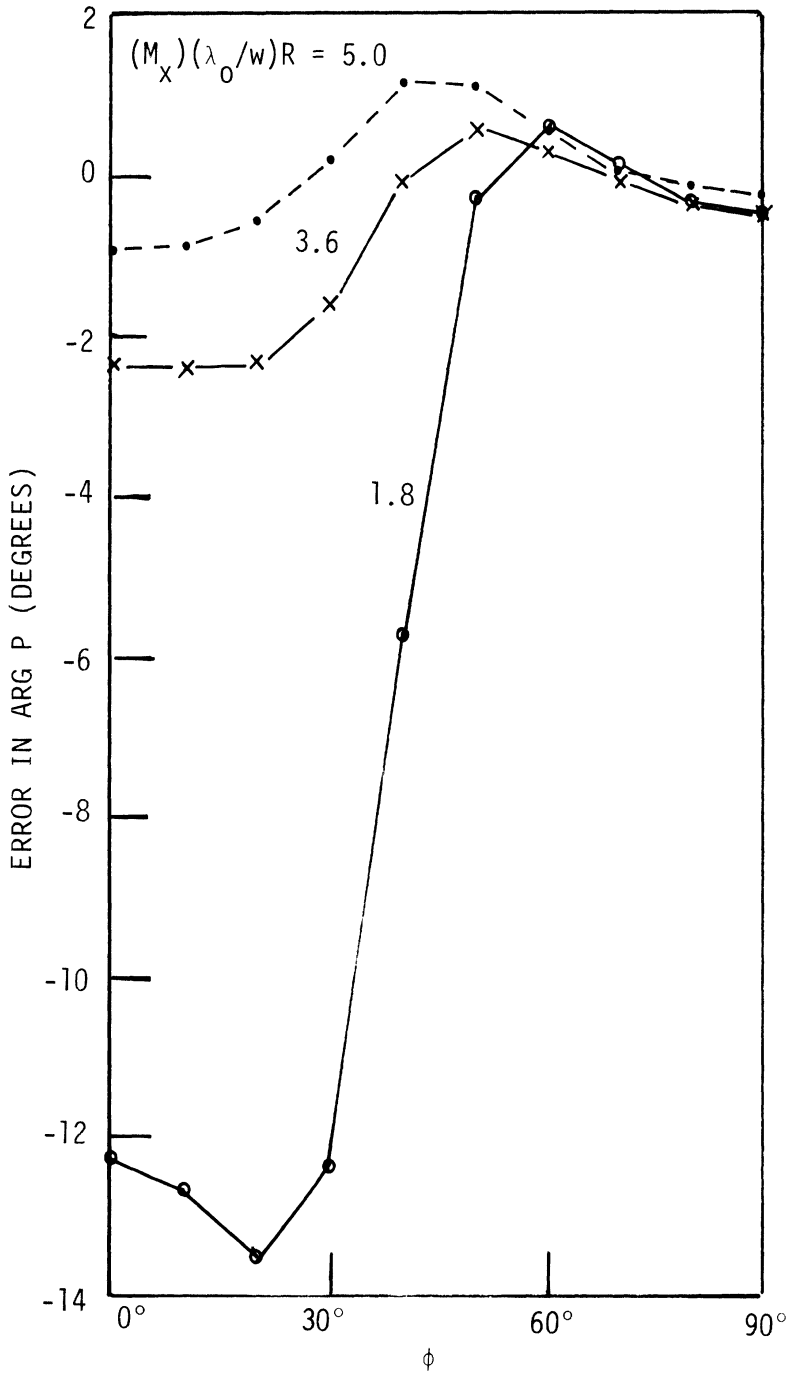

Fig. 5.10: Error in arg $P(\phi,\phi_o)$ vs. ϕ for $R = 0.1$, $w/\lambda_o = 0.5$, $\rho_1/\lambda_o \approx 0.5$, $(M_y)(\lambda_o/\rho_1) \approx 17$, backscattering ($\phi = \phi_o$).

5.5 Solution Cost Considerations

The cost of the numerical solution is a function of the number of elements used in the discretization of the space surrounding the scattering body. The number of elements is

$$J = M_x M_y + 2 \quad . \tag{5.12}$$

The actual number of unknowns, however, is equal to the number of nodes at which the scattered field is not known a priori. The number of unknowns for a resistive strip is

$$M_u = (M_x + 1)(M_y + 1) \quad . \tag{5.13}$$

For a perfect conductor the number is less,

$$M_u = (M_x + 1)M_y \quad , \tag{5.14}$$

since the scattered field at the nodes on the strip is specified by the boundary condition there.

The computer memory requirements for the finite element solution may be classified either as being fixed or as being variable with the number of elements. In the variable category, the largest block of memory is for band storage of the global matrix for the system of equations (3.13). The variable memory requirements (in words) are:

Resistive Strip

$$\left[\begin{array}{c}\text{Global Matrix} \\ \text{Memory} \\ \text{(band storage)}\end{array}\right] = 6M_xM_y^2 + 6M_y^2 + 20\,M_xM_y + 14\,M_x + 20\,M_y \tag{5.15}$$

$$\left[\begin{array}{c}\text{Memory, Other} \\ \text{Matrices}\end{array}\right] = 14\,M_xM_y + 10\,M_x + 10\,M_y \tag{5.16}$$

Perfectly Conducting Strip

$$\left[\begin{array}{c}\text{Global Matrix} \\ \text{Memory} \\ \text{(band storage)}\end{array}\right] = 6\,M_xM_y^2 + 6M_y^2 + 8\,M_xM_y + 8\,M_y \tag{5.17}$$

$$\left[\begin{array}{c}\text{Memory, Other} \\ \text{Matrices}\end{array}\right] = 2\,M_x^2M_y + 18\,M_xM_y + 5\,M_x + 11\,M_y \tag{5.18}$$

If the element densities $M_x\lambda_o/w$ and $M_y\lambda_o/\rho_1$ are to be kept equal in view of the results of Section 5.3, M_y may be written in terms of M_x using (5.3) if $w/\lambda_o \geq 0.5$.

$$M_y = 2M_x \frac{w}{\lambda_o} \quad . \tag{5.19}$$

For $w/\lambda_o < 0.5$, it is required that $\rho_1 = w$ instead of (5.3) as discussed in Section 5.2. In this case

$$M_y = M_x \quad . \tag{5.20}$$

The number of elements (5.12) becomes

$$J = 2M_x^2 \frac{w}{\lambda_o} + 2 \quad , \quad w/\lambda_o \geq 0.5$$
$$= M_x^2 + 2 \quad , \quad w/\lambda_o < 0.5 \qquad . \qquad (5.21)$$

Then for equal element densities, M_y may be eliminated from (5.15) through (5.18). For example, (5.15) and (5.16) may be written in terms of the element density $M_x\lambda_o/w$ and the strip width in wavelengths w/λ_o:

Resistive Strip ($w/\lambda_o \geq 0.5$)

$$\left[\begin{array}{c}\text{Global Matrix} \\ \text{Memory} \\ \text{(band storage)}\end{array}\right] = 24\left(M_x \frac{\lambda_o}{w}\right)^3 \left(\frac{w}{\lambda_o}\right)^5 + 24\left(M_x \frac{\lambda_o}{w}\right)^2 \left(\frac{w}{\lambda_o}\right)^4$$
$$+ 40\left(M_x \frac{\lambda_o}{w}\right)^2 \left(\frac{w}{\lambda_o}\right)^3 + 40\left(M_x \frac{\lambda_o}{w}\right)\left(\frac{w}{\lambda_o}\right)^2$$
$$+ 14\left(M_x \frac{\lambda_o}{w}\right)\left(\frac{w}{\lambda_o}\right) \qquad (5.22)$$

$$\left[\begin{array}{c}\text{Memory, Other} \\ \text{Matrices}\end{array}\right] = 28\left(M_x \frac{\lambda_o}{w}\right)^2 \left(\frac{w}{\lambda_o}\right)^3 + 20\left(M_x \frac{\lambda_o}{w}\right)\left(\frac{w}{\lambda_o}\right)^2$$
$$+ 10\left(M_x \frac{\lambda_o}{w}\right)\left(\frac{w}{\lambda_o}\right) . \qquad (5.23)$$

Table 5.2 shows the number of elements, number of unknowns and variable memory for different element densities and strip widths. Table 5.3 compares the memory requirement for the band-storage

Table 5.2

Variable Memory Requirement for a Resistive Strip

$$\left(M_x \frac{\lambda_o}{w} = M_y \frac{\lambda_o}{\rho_1}\right)$$

$M_x \frac{\lambda_o}{w}$	$\frac{w}{\lambda_o}$	Number of Elements, J	Number of Unknowns, M_u	Total Variable Memory (words)*
16	0.25	18	25	1,240
	0.50	66	81	6,064
	0.71	178	204	25,160
	1.00	514	561	123,200
20	0.25	27	36	2,020
	0.50	102	121	10,540
	0.71	282	315	47,762
	1.00	802	861	230,480

*Includes band-storage global matrix.

Table 5.3

Global Matrix Memory for a Resistive Strip for $M_x \frac{\lambda_o}{w} = 16$

$\frac{w}{\lambda_o}$	Global Matrix Memory (words)		
	F.E.M* Square Matrix	F.E.M.* Banded Matrix	M.O.M. Square Matrix
0.25	1,250	950	32
0.50	13,122	5,022	128
0.71	83,232	22,440	242
1.00	629,442	115,566	512

* $M_x \frac{\lambda_o}{w} = M_y \frac{\lambda_o}{\rho_1}$

global matrix to a full square matrix and to the matrix for a method of moments integral equation solution. Table 5.4 gives the actual computation time for three selected examples on the DEC-10 computer.

Table 5.4

Computation Time for a Resistive Sheet

$(M_x\lambda_o/w = M_y\lambda_o/\rho_1 \approx 16)$

w/λ_o	0.25	0.50	0.71
Number of elements, J	18	66	178
Number of unknowns, M_u	25	81	204
Matrix fill time (sec)	0.84	3.61	10.04
Solution of equations (sec)	0.19	1.10	6.22
Total CPU time* (sec)	1.41	5.10	16.60

*Backscattering for one angle of incidence.

CHAPTER VI. VOLUME SCATTERING EXAMPLE

6.1 Statement and Formulation of Example

One of the advantages of the finite element method lies in its ability to solve problems in which inhomogeneous media are present or multiple regions of differing homogeneous media are present. The distinction between these two types of problems is not important for a finite element solution. Only a minor difference in the computer program is needed in assigning material properties to particular finite elements. An example is considered here in which the resistive strip of the preceding chapters is embedded in a dielectric cylinder, radius w, of uniform relative permittivity ε_r and uniform permeability μ_o as shown in Fig. 6.1. The cylinder is, in turn, immersed in free space. The radar cross section of the combined dielectric cylinder and resistive strip is computed.

As before, the incident plane wave (2.3) will excite only E-wave fields. In this case the total field satisfies

$$\frac{\partial^2 E_z}{\partial x^2} + \frac{\partial^2 E_z}{\partial y^2} + \omega^2 \mu_o \varepsilon(x,y) E_z = 0 \quad . \tag{6.1}$$

The incident field E_z^i, which is the field present in the absence of the scattering body, satisfies

$$\frac{\partial^2 E_z^i}{\partial x^2} + \frac{\partial^2 E_z^i}{\partial y^2} + \omega^2 \mu_o \varepsilon_o E_z^i = 0 \quad . \tag{6.2}$$

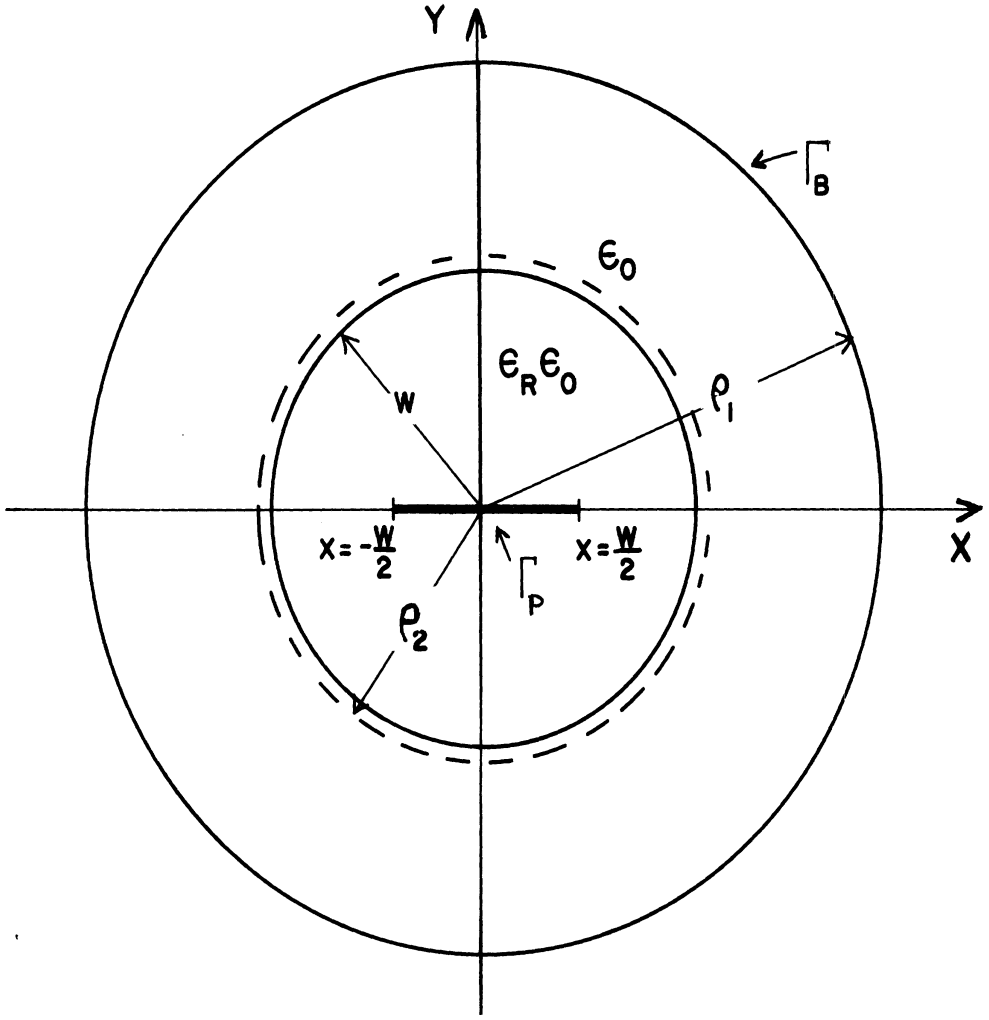

Fig. 6.1: The extended solution region.

The scattered field $E_z^{sc} = E_z - E_z^i$ then must satisfy

$$\frac{\partial^2 E_z^{sc}}{\partial x^2} + \frac{\partial^2 E_z^{sc}}{\partial y^2} + \omega^2 \mu_o \varepsilon(x,y) E_z^{sc} = -k_o^2 \chi_e(x,y) E_z^i \tag{6.3}$$

where

$$\chi_e = \frac{\varepsilon}{\varepsilon_o} - 1 = \varepsilon_R - 1 \tag{6.4}$$

is the electric susceptibility for the dielectric.

The derivation of an integral statement of the problem parallels that of Section 3.2. In this case however, the scattered field does not, in general, have the symmetry properties (2.24) and (2.27) which exist for the strip alone. Thus the region Ω must extend into the lower half space $y \leq 0$ as shown in Fig. 6.1. The region is bounded by the contour Γ which is composed of two sections:

1. Γ_P is the line $y = 0$, $-w/2 \leq x \leq w/2$.

2. Γ_B is a circle centered at the origin with a radius ρ_1 which is sufficiently large to place Γ_B in the far field region of the dielectric cylinder with the embedded strip.

Combining the Green's identity (3.5) and differential equation (6.3) yields

$$\int_\Omega [\nabla_t v \cdot \nabla_t u - k_o^2(1 + \chi_e(x,y))vu] d\Omega$$

$$= \oint_\Gamma v \frac{\partial u}{\partial n} d\Gamma + k_o^2 \int_\Omega \chi_e(x,y) v u^i \, d\Omega \quad . \tag{6.5}$$

where u and u^i are the scattered and incident fields as before. Of the contour integral, the portion on Γ_B is the same as before. On Γ_P, the boundary condition is

$$\frac{iR(x)}{k_o}\left[\frac{\partial u}{\partial y}\right]_-^+ = u + u^i \quad . \tag{6.6}$$

The contour integral on Γ_P is

$$\int_{\Gamma_P} v\,\frac{\partial u}{\partial n}\,d\Gamma = -\int_{x=-w/2}^{w/2} v\left[\frac{\partial u}{\partial y}\right]_-^+ dx \quad . \tag{6.7}$$

Combining (3.7),(6.6) and (6.7) with (6.5) yields the integral statement upon which the finite element solution is based. The result is

$$\int_\Omega [\nabla_t v \cdot \nabla_t u - k_o^2(1 + \chi_e(x,y))vu]d\Omega + \int_{\Gamma_B}\left(\frac{1}{2\rho_1} - ik_o\right) vu\,d\Gamma$$

$$- ik_o \int_{x=-w/2}^{w/2}\left[\frac{vu}{R(x)}\right]_{y=o} dx = ik_o\int_{x=-w/2}^{w/2}\left[\frac{vu^i}{R(x)}\right]_{y=o} dx$$

$$+ k_o^2\int_\Omega \chi_e(x,y)vu^i\,d\Omega \quad . \tag{6.8}$$

The remainder of the solution of this example closely parallels the procedure of Chapters III and IV. However, in order to calculate the far scattered field and the radar cross section, an integral such as (2.35) cannot be used because of the presence of the dielectric

cylinder. Instead, an integration of the scattered field values on a closed contour outside and surrounding the dielectric cylinder must be evaluated. If the contour is a circle of radius $\rho = \rho_2$ as shown in Fig. 6.1, the far scattered field is

$$E_z^{sc}(\underline{\rho}) = \sqrt{\frac{2}{\pi k_0 \rho}} \exp[ik_0\rho - i(\pi/4)]P(\phi,\phi_0) \quad , \tag{6.9}$$

where, from the integral representation of the field,

$$P(\phi,\phi_0) = \frac{k_0}{4} \int_{\phi'=-\pi}^{\pi} \left[-\frac{i}{k_0} \frac{\partial E_z^{sc}(\rho_2,\phi')}{\partial \rho} - E_z^{sc}(\rho_2,\phi') \right]$$

$$\cdot \exp[-ik_0\rho_2\cos(\phi - \phi')]\rho_2 \, d\phi' \tag{6.10}$$

In the computer program, the radius ρ_2 was taken to be slightly larger than w, or more precisely, one element width out from the dielectric cylinder. Although the closed contour could be on the surface of the cylinder, in general, for an inhomogeneous body with a less distinct boundary the contour must be outside the body. Further, for a body with a noncircular cross section, it is desirable to place a circular contour outside the body for ease of computation of the far scattered field.

6.2 Selection of an Incident Field

In order to demonstrate the use of this formulation without extensive modification of the computer program used to solve the problem of Chapters II and III, an incident wave is selected so that

the scattered field has the symmetry properties (2.24) and (2.27). This allows the solution to be obtained in the upper half space as before.

In general, a scattered field can be interpreted as resulting from electric and magnetic current sources induced by the incident wave in the scattering body. In the present case $\mu = \mu_o$ everywhere so that no magnetic current sources will be induced. For an incident field which excites only E-wave fields as discussed in Chapter II, the only possible electric currents must be in the z-direction. In order to maintain $H_x^{sc}(x,0)$ equal to zero for $|x| > w/2$ as implied by (2.27), the induced electric current distribution must be an even function of y. For example, the electric current element $I(x_1,y_1)\hat{z}$ produces an x-component of the magnetic field on the x-axis which is cancelled by an x-component of the magnetic field of a current element $I(x_1,-y_1)\hat{z}$.

The incident field must then have the property that

$$E_z^i(x,y) = E_z^i(x, -y)$$

in order that the symmetry properties (2.24) and (2.27) hold. Here the incident field chosen with this property consists of two plane waves

$$E_z^i = \frac{1}{2}\exp[-ik_o(x\cos\phi_o + y\sin\phi_o)] + \frac{1}{2}\exp[-ik_o(x\cos\phi_o - y\sin\phi_o)] \quad , \qquad (6.11)$$

whose angles of incidence are ϕ_o and $-\phi_o$, respectively.

6.3 Implementation of the Solution Procedure

The selection of the particular incident field (6.11) leads to a symmetric scattered field which is obtained by solution in the upper half space only. The weak form integral statement (6.8) becomes

$$\int_{\Omega} [\nabla_t v \cdot \nabla_t u - k_o^2(1 + \chi_e(x,y))vu]d\Omega + \int_{\Gamma_B} \left(\frac{1}{2\rho_1} - ik_o\right) vu \, d\Gamma$$

$$- \frac{ik_o}{2} \int_{x=-w/2}^{w/2} \left[\frac{vu}{R(x)}\right]_{y=o} dx = \frac{ik_o}{2} \int_{x=-w/2}^{w/2} \left[\frac{vu^i}{R(x)}\right]_{y=o} dx$$

$$+ k_o^2 \int_{\Omega} \chi_e(x,y) vu^i \, d\Omega \quad , \qquad (6.12)$$

where Ω refers to the region in the upper half plane bounded by Γ_B and the line $y = 0$.

Following the procedure of Chapter III, the element matrix coefficients are given by

$$K_{mn}^e = \int_{\Omega^e} \left[\frac{\partial N_m}{\partial x}\frac{\partial N_n}{\partial x} + \frac{\partial N_m}{\partial y}\frac{\partial N_n}{\partial y} - k_o^2(1 + \chi_e(x,y))N_m N_n\right] d\Omega$$

$$- \frac{ik_o}{2} \int_{\Gamma_P^e} \frac{N_m N_n}{R(x)} \, d\Gamma + \left(\frac{1}{2\rho_1} - ik_o\right) \int_{\Gamma_B^e} N_m N_n \, d\Gamma \quad . \qquad (6.13)$$

and the incident field terms are given by

$$f_m^e = \frac{ik_o}{2} \int_{\Gamma_P^e} \frac{N_m u^i}{R(x)} \, d\Gamma + k_o^2 \int_{\Omega^e} \chi_e(x,y) \, N_m u^i \, d\Omega \quad . \qquad (6.14)$$

6.4 Numerical Results

With these modifications of the computer program the radar cross section and the phase of the scattered field are computed for $w/\lambda_0 = 0.25$ and $\varepsilon_R = 2$. Figures 6.2 and 6.3 show that the bistatic scattering from the quarter wavelength width strip without the dielectric cylinder to be relatively independent of scattering angle. The magnitude and phase of the induced currents on the strip are relatively uniform. However, when the dielectric cylinder is present the scattering action becomes more complicated. On the one hand, there is scattering off the surface of the cylinder. Also the incoming field which does penetrate the dielectric, interacts with the strip and the cylindrical surface setting up standing waves inside the cylinder and producing a second scattered field which combines with that scattered off the cylindrical surface. In this process, the orientation of the strip relative to the scattering direction becomes more important.

Figures 6.4 and 6.5 show bistatic scattering for three angles of incidence. From these figures it is clear that the scattering is primarily characterized by radiation from the leading and trailing edges of the strip. For a scattering angle of $\phi \approx 90$ degrees interference between leading and trailing edge radiation produces a null in the radar cross section.

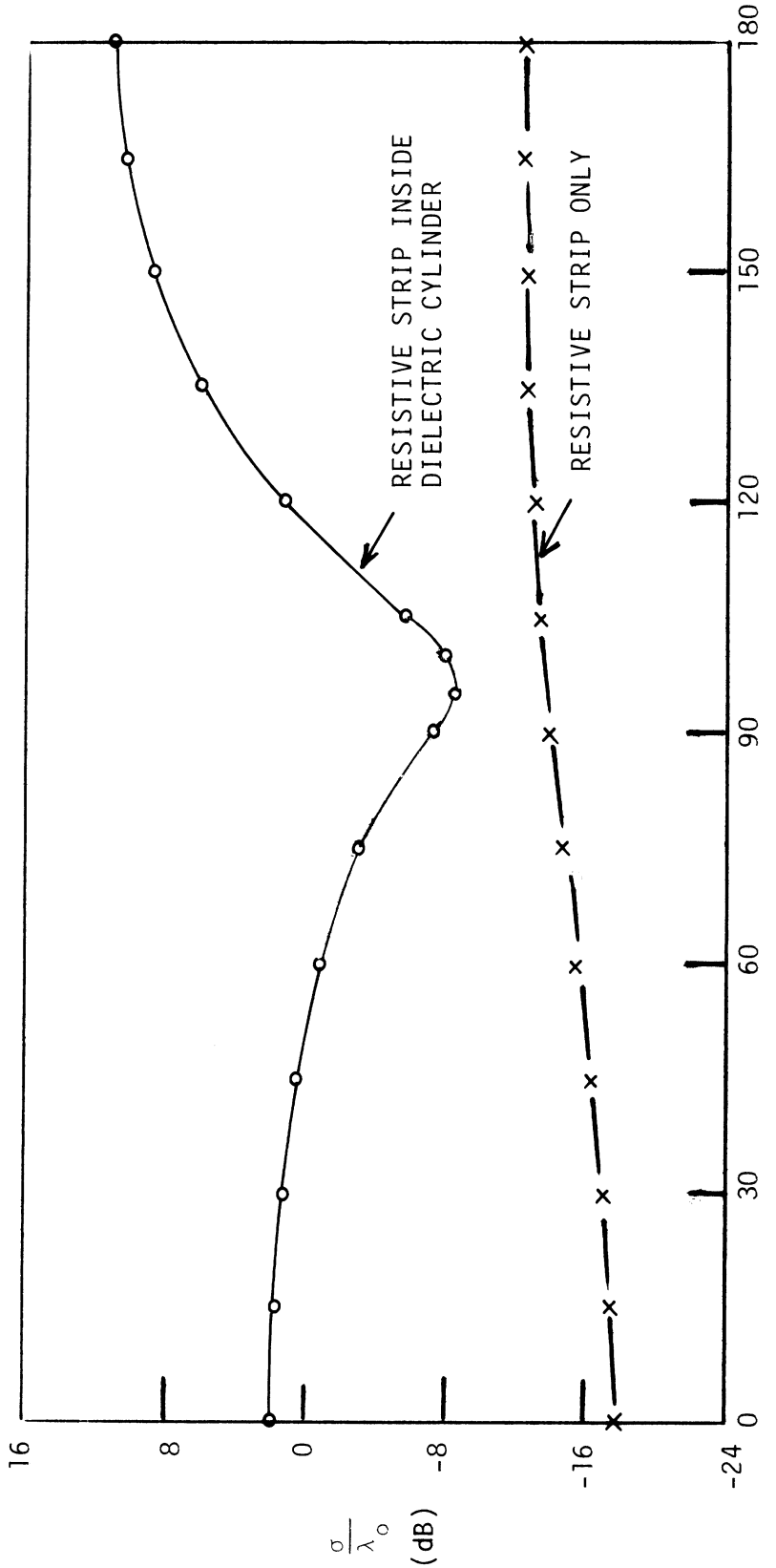

Fig. 6.2: σ/λ_o vs. ϕ for bistatic scattering, $\phi_o = 0°$, R = 1.0, $w/\lambda_o = 0.25$.

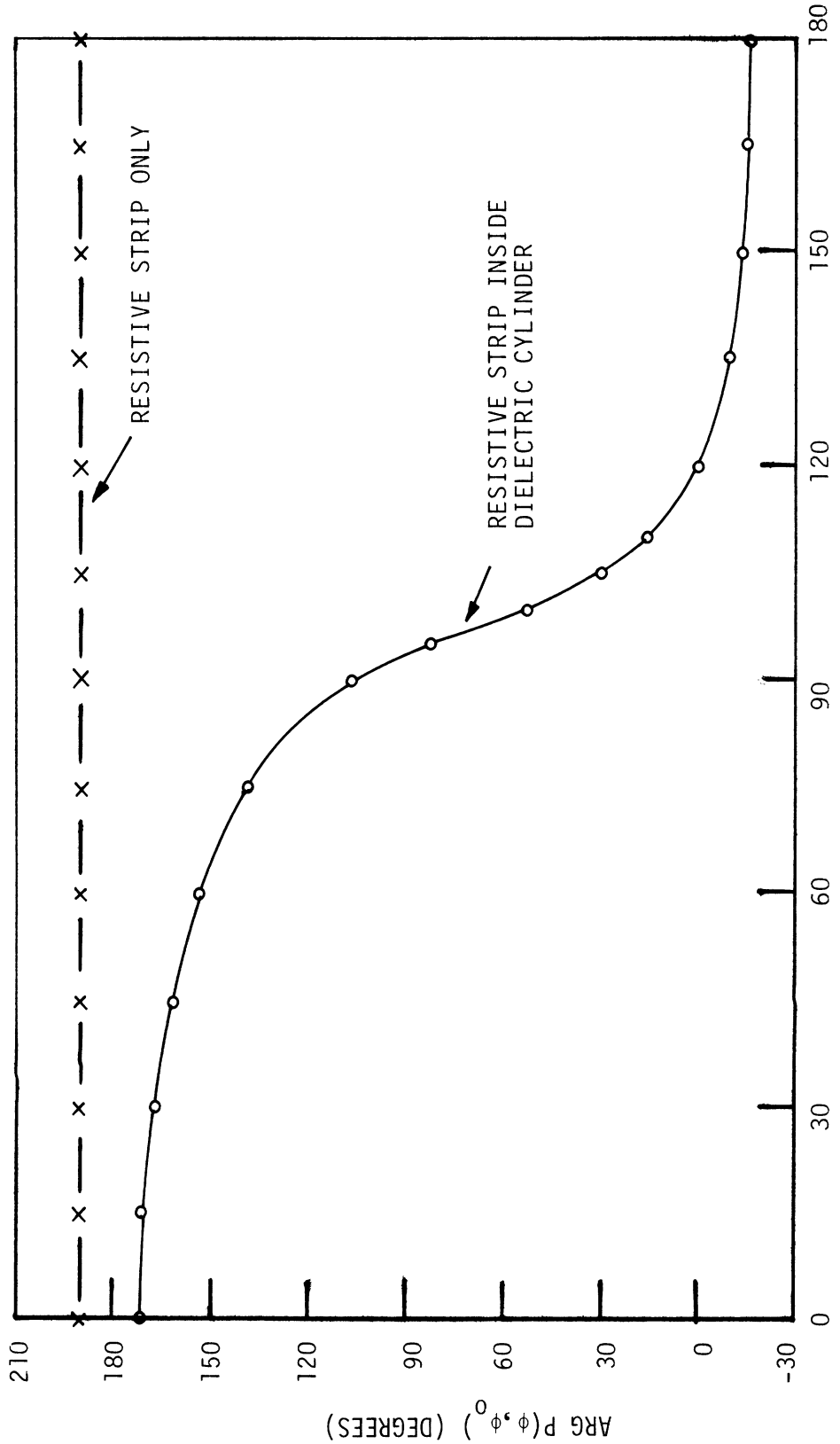

Fig. 6.3: Arg $P(\phi,\phi_o)$ vs. ϕ for bistatic scattering, $\phi_o = 0°$, R = 1.0, $w/\lambda_o = 0.25$.

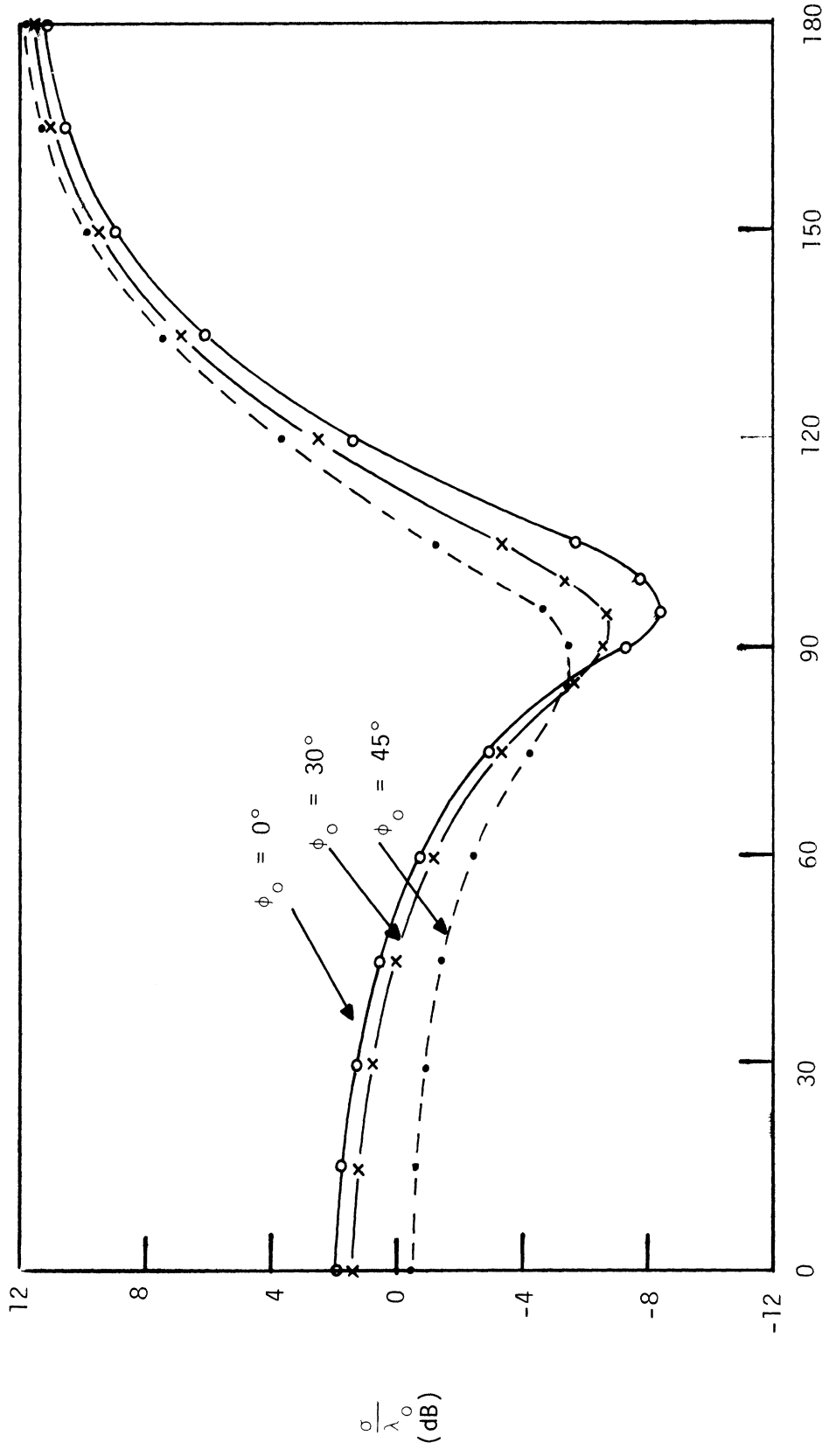

Fig. 6.4: σ/λ_o vs. ϕ for bistatic scattering, R = 1.0, w/λ_o = 0.25, dielectric cylinder (ε_R = 2) radius/λ_o = 0.25.

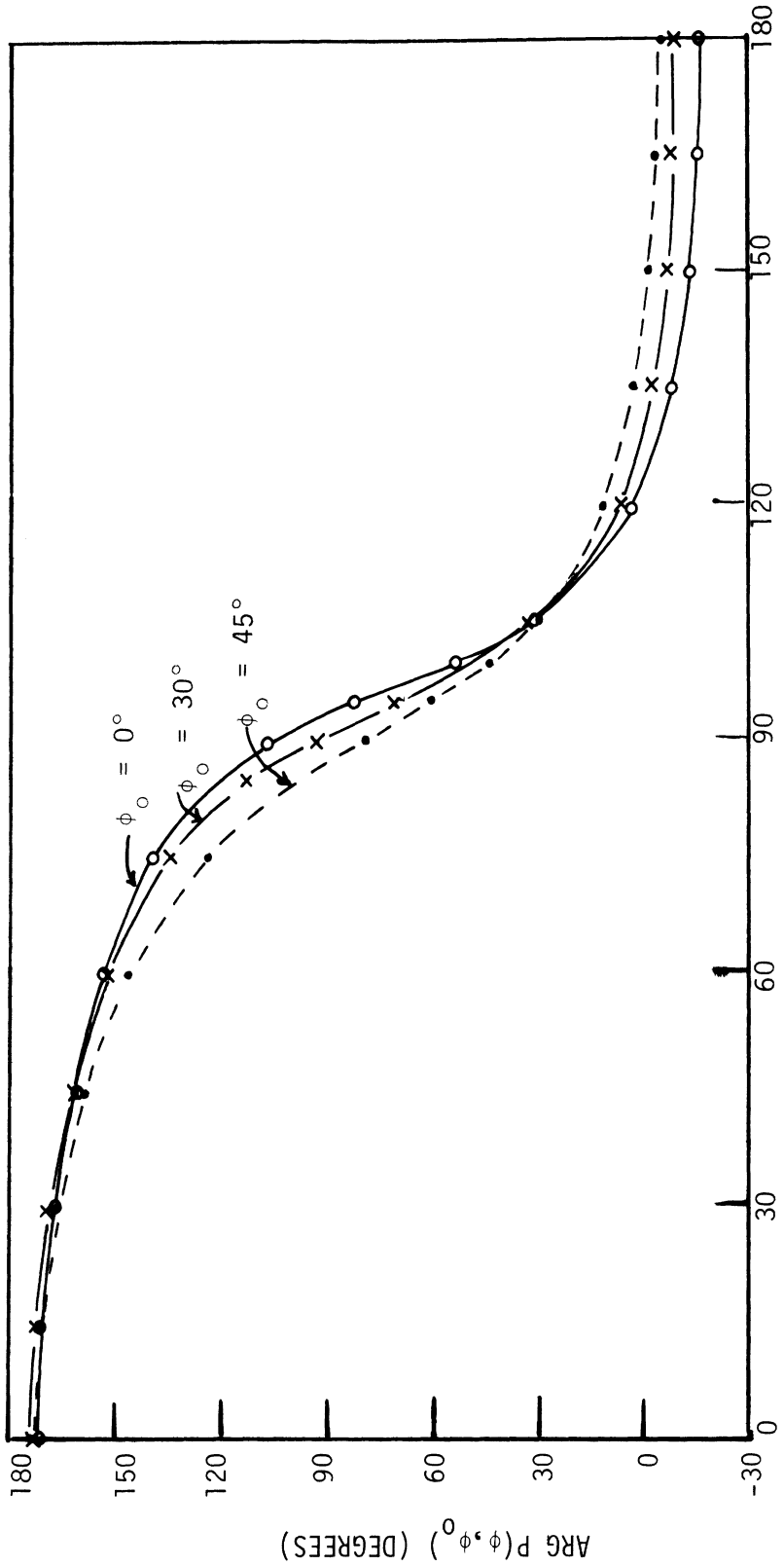

Fig. 6.5: Arg $P(\phi,\phi_o)$ vs. ϕ for bistatic scattering, R = 1.0, w/λ_o = 0.25, dielectric cylinder (ε_R = 2) radius/λ_o = 0.25.

CHAPTER VII. CONCLUSIONS AND RECOMMENDATIONS

7.1 Overview of the Work

The finite element method was applied to the solution of two-dimensional electromagnetic scattering from bodies in unbounded space. The technique combined Green's first identity and the differential equation to form a weak integral statement equivalent to that obtained by the weighted residual method. Galerkin's method was used in the selection of the weighting functions. The finite element solution region was extended outward so that its outer boundary lay in the far field region of the scattering body. The boundary condition on the outer boundary was evaluated by using the asymptotic expression for the scattered field in the far-field region. The finite element mesh consisted primarily of quadrilaterals with linear shape functions and was generated by a computer program. Two special cases were solved using this approach: a thin resistive strip and a resistive strip embedded in a dielectric cylinder. Special triangular elements were used at the edge of the thin strip for the case of zero resistivity to model the singularity occurring in the magnetic field.

Numerical results for scattering by the resistive strip were compared with results of a moment method integral equation solution known to produce highly accurate values of radar cross section and scattered field in the far field region. Results

indicate the element densities in the radial direction and adjacent to the strip should be kept equal. For an element density of 16 elements per wavelength in both directions, a strip width of a half wavelength, and a normalized resistivity R = 1.0, the magnitude of the far scattered field differed by less than four percent from the moment method result at all angles of incidence, except at deep nulls in the radiation pattern. The phase of the scattered field differed by less than six degrees at all angles of incidence.

For low resistivity strips, pronounced standing waves appeared in the computed values of the scattered field. These standing waves were apparently due to multiple reflections between the strip and the outer boundary. The standing waves led to large errors in the radar cross section and the far scattered field. Their presence in the results prevented an evaluation of the effectiveness of the special triangular elements in modeling the field at the edge of a perfectly conducting strip. Another effect occurring for low (non-zero) resistivity was the ill-conditioning of the system of algebraic equations resulting in highly inaccurate results for most angles of incidence. This effect can be partially offset by increasing the element density.

The finite element method was applied to the case of the resistive strip embedded in the dielectric cylinder. No moment method results are available for comparison, but the numerical results obtained here appear to be reasonable.

7.2 Limitations of the Method

The formulations and the computer program used here have some limitations. First, all work was done assuming an incident plane wave which excited only an E-wave. The formulation for H-wave excitation has not been developed. Second, the boundary condition on the outer boundary (Γ_B) is not accurate enough to prevent standing waves from occurring in the computed scattered field, particularly for low resistivity. Increasing the element density will improve the boundary condition and reduce the standing waves but at increased computation cost (see Appendix B). Third, the memory requirement for the computer system increases rapidly with the size of the scattering body due to the need to extend the finite elements into the far field region. As an example, for the resistive strip in free space, if a certain element density is to be maintained, the band storage requirement for the global matrix in the finite element method increases as the fifth power of the strip width for $w/\lambda_o > 1$ but only as the second power in the moment method. Fourth, the system of linear algebraic equations becomes ill-conditioned for low (non-zero) strip resistivities. A partial solution to this problem involves increasing the element density.

The second, third and fourth items above are either not limitations for a moment method solution or are less of a limitation. Because of this the finite element method is not competitive with the method of moments for scattering from a thin body in a homogeneous unbounded space. On the other hand, for a thick

penetrable body or a body in an inhomogeneous medium, the moment method may be less attractive. This may be due either to increased memory requirements or to difficulties with an integral equation formulation in an inhomogeneous medium. The finite element method has been demonstrated to be a feasible approach for these cases.

7.3 Recommendations for Further Work

1. In order that scattering due to arbitrarily polarized incident plane waves may be determined, the formulation for H-wave excitation should be developed.

2. The use of quadrilateral elements with higher order shape functions should be investigated. It is expected that the same accuracy of solution could be achieved with significantly fewer elements of a higher order.

3. Element and global matrix coefficients should be interpreted in energy and circuit terms. Such interpretations could lead to a nonreflecting boundary condition for the outer boundary of the finite element region as was done for a one-dimensional case in Appendix C. The work of Engquist and Majda (1977) on absorbing boundary conditions should also be considered in improving the boundary conditions.

4. Three dimensional scattering problems could be formulated using methods similar to those described in this work.

APPENDIX A. APPROXIMATE RELATIONSHIP BETWEEN ELEMENT MESH PARAMETERS

In selecting the values of the mesh parameters that are to be used for a particular computer run it is useful to know approximately the relationship between the parameters. The number of elements in the radial direction M_y is directly proportional to the product of EL and M_x where M_x (called NUMELS in the computer program) is the number of elements adjacent to the strip and EL is an aspect ratio for the elements. The parameter EL is the ratio of the dimension of a quadrilateral element in the direction parallel to the strip to the dimension in the direction perpendicular to the strip.

The relationship in more precise form is

$$M_y = A(EL)(M_x) + B \quad , \tag{A.1}$$

where A and B are constants yet to be determined. Figure A.1 shows the results of a number of computer runs. From this graph it can be seen that B is approximately unity and A is actually a function of SMEC. The parameter SMEC is approximately the eccentricity of the largest ellipse of the mesh, which forms the outer boundary at $\rho = \rho_1$. Figure A.2 is a plot of the slopes of the lines in Fig. A.1 vs. SMEC. This shows that

$$A \approx -0.83 \log_{10} \text{SMEC} + 0.17 \quad . \tag{A.2}$$

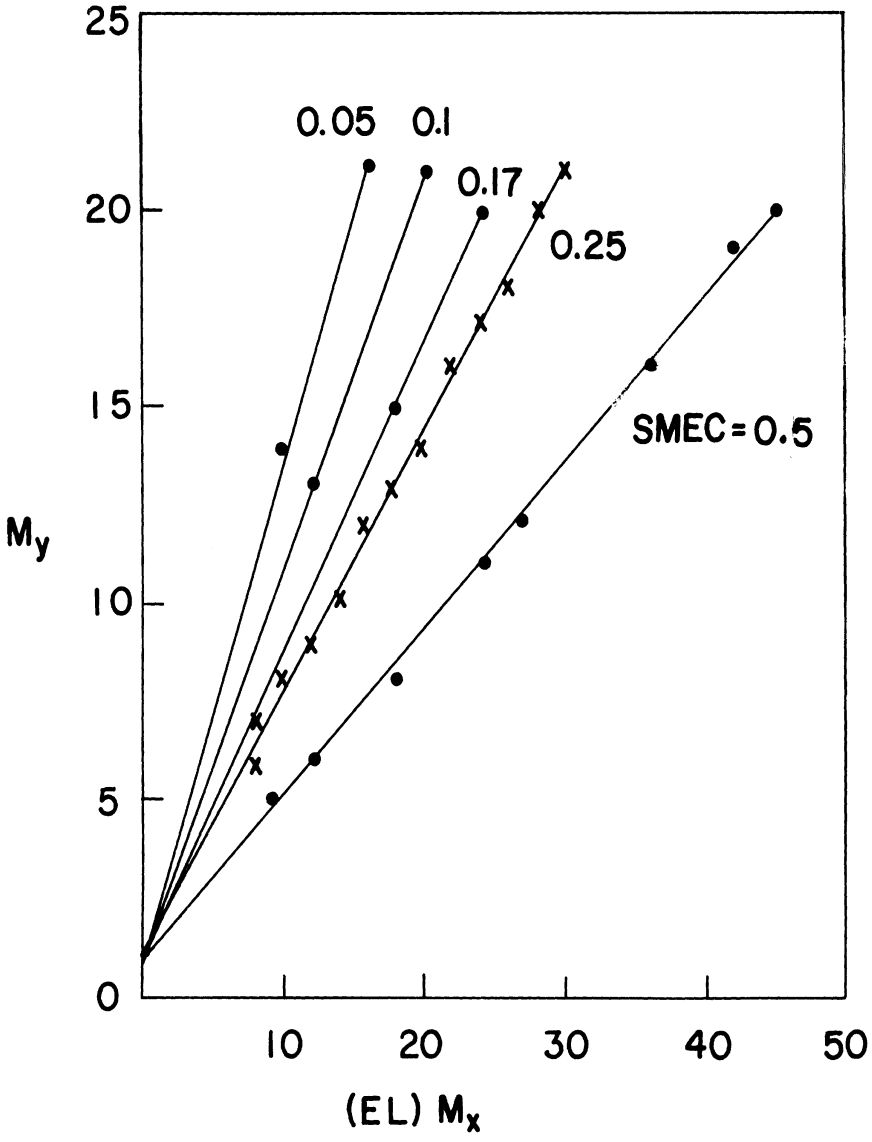

Fig. A.1: M_y vs. $(EL)M_x$.

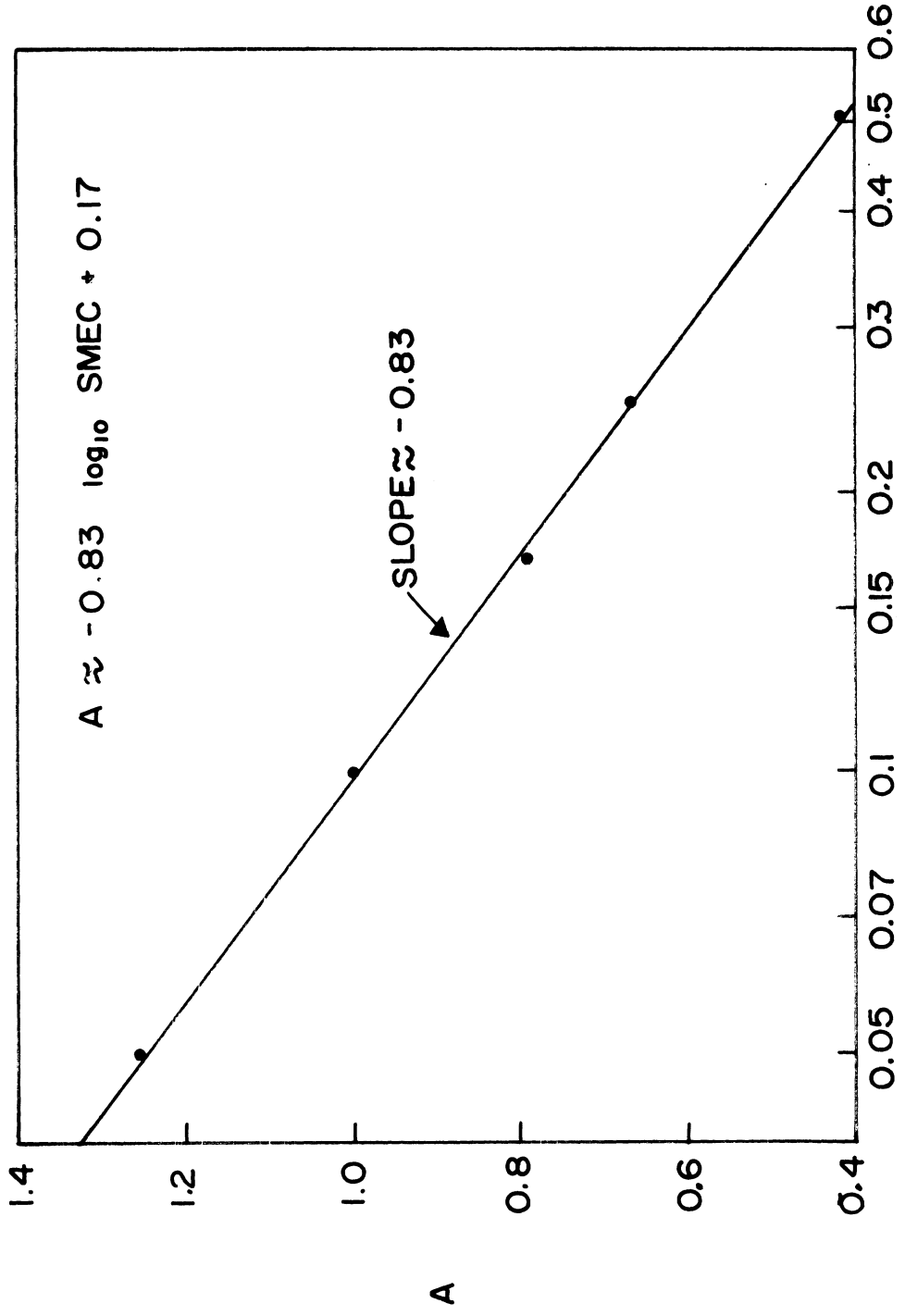

Fig. A.2: A vs. SMEC.

The desired approximate relation is then

$$M_y = A(EL)(M_x) + 1 \quad . \tag{A.3}$$

APPENDIX B. TRANSMISSION LINE INTERPRETATION FOR NUMERICAL RESULTS

B.1 The Finite Element Mesh as a Transmission Line

The resemblance of the set of linear algebraic equations for the nodal values in the finite element procedure to a set of node voltage equations for a two-dimensional electrical transmission line structure suggests that the results of the finite element solution be interpreted in terms of a transmission line. The use of electrical networks for the solution of electromagnetic field problems is well established. A great deal of work has been done in the past on the subject of wave propagation through two-dimensional periodic structures (Brillouin, 1953). Although the finite element mesh in the present work is not uniform and not perfectly periodic, the transmission line characteristics are evident in the numerical results.

As an aid in the transmission line interpretation, the finite element solution for the problem of a plane wave normally incident on a plane resistive sheet of infinite extent is provided in Appendix C. This problem is analogous to that of a uniform one-dimensional transmission line and the method of solution generally parallels that used for the two-dimensional problem which is the subject of Chapters III through V. It is found that the characteristic impedance Z_c of the transmission line is always less than the characteristic impedance of free space Z_o. This means that the boundary condition

(C.5) acts as an imperfect termination for the line and that standing waves appear in the numerical results. Further, the one-dimensional problem shows the phase constant k for the line is always less than the phase constant of free space k_0 so that the phase of the computed scattered field is always less than that of the exact value, except at the resistive sheet. If the density of the finite elements is increased, Z_c approaches Z_0 and k approaches k_0. This reduces the standing waves and the phase errors.

These results for the one-dimensional uniform line apply qualitatively to the two-dimensional line extending outward from the resistive strip. However, since the two-dimensional line is not uniform in the direction of wave propagation, the impedance mismatch will depend on the local density of elements at the edge of the finite element region. An additional consequence of the non-uniformity of the line is the dependence of the standing-wave ratio on the impedance of the strip. A larger standing-wave ratio is observed for strips of low resistivity.

For the two-dimensional problem, backscattering for normal incidence most closely resembles the one-dimensional problem of Appendix C. The transmission line characteristics are clearly apparent for this case. For example, Fig. B.1 is a plot of the magnitude of the scattered field as a function of the distance from the strip. The results of a method of moments (MOM) calculation are plotted for comparison. Figure B.1 shows that increasing the number of elements (M_y) results in a lower standing-wave ratio. The element mesh

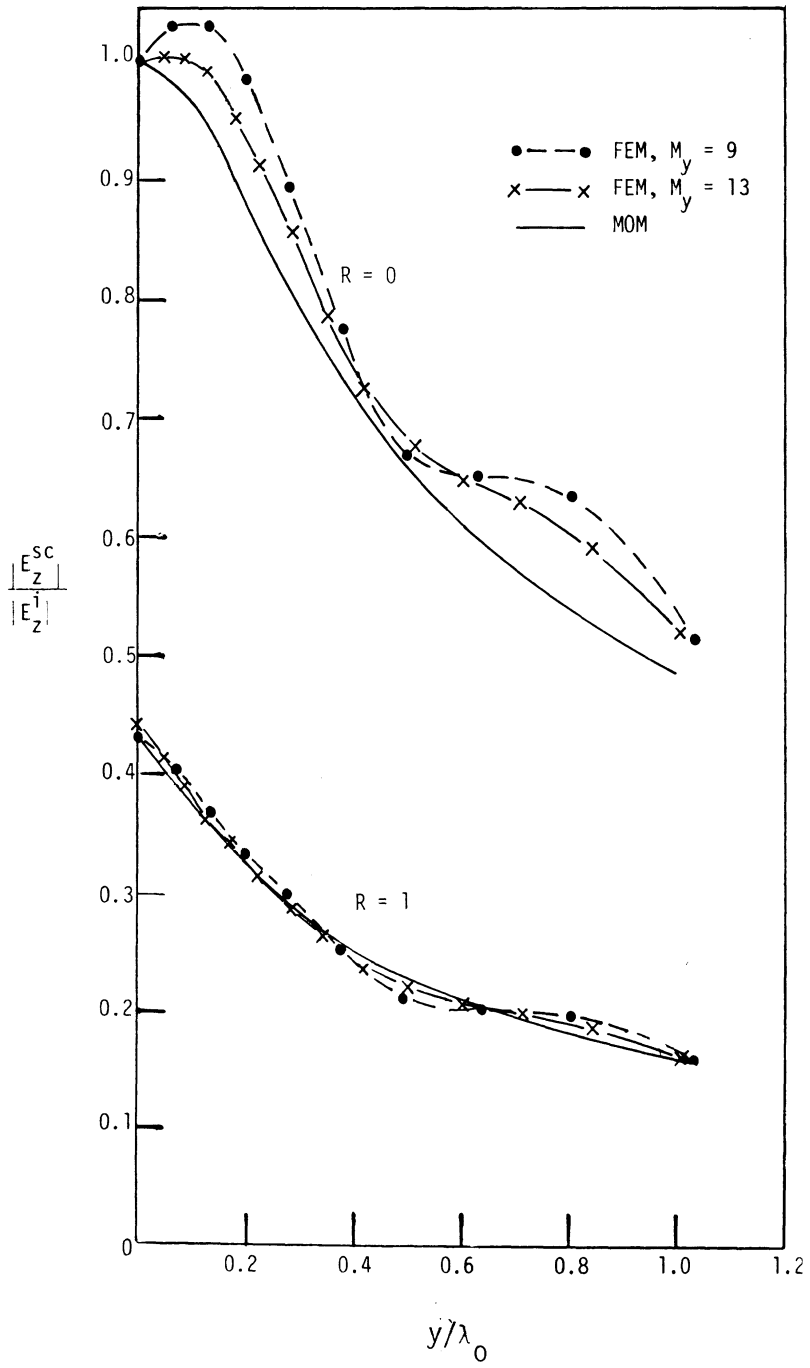

Fig. B.1: Scattered field magnitude vs. distance outward from the strip center ($\phi_0 = 90°$, $w/\lambda_0 = 0.5$, $M_x = 6$, $x = 0$).

parameters for the curves of Fig. B.1 were selected so that the standing waves could be easily seen in the data; the selection rules given in Section 5.2 were not used. Figure B.2 is a plot of the phase of the scattered field versus distance from the strip with MOM curves for comparison. It is evident that the error in phase for the FEM results increases with distance. Increasing (M_y) provides a small improvement in the phase accuracy.

B.2 Effect of Standing Waves

The value of the radar cross section of the strip may be obtained directly from the scattered field values computed in the far field region such as at $\rho = \rho_1$, or it may be obtained by means of a computation of the induced current on the strip followed by an integration over the strip (2.38). The numerical results obtained using the first method are generally less accurate than those having the second method when standing waves are present.

To examine the effect of the standing waves on the current calculation in the second method, assume that near the strip

$$E_z^{sc} \approx [A(x) + B(x)y]\exp[i(k_o y + \theta_o(x))] \qquad (B.1)$$

where A, B and θ_o are respectively the magnitude of $|E_z^{sc}|$, the slope of $|E_z^{sc}|$, and the phase of E_z^{sc} at the strip (y = 0). Using (4.66)

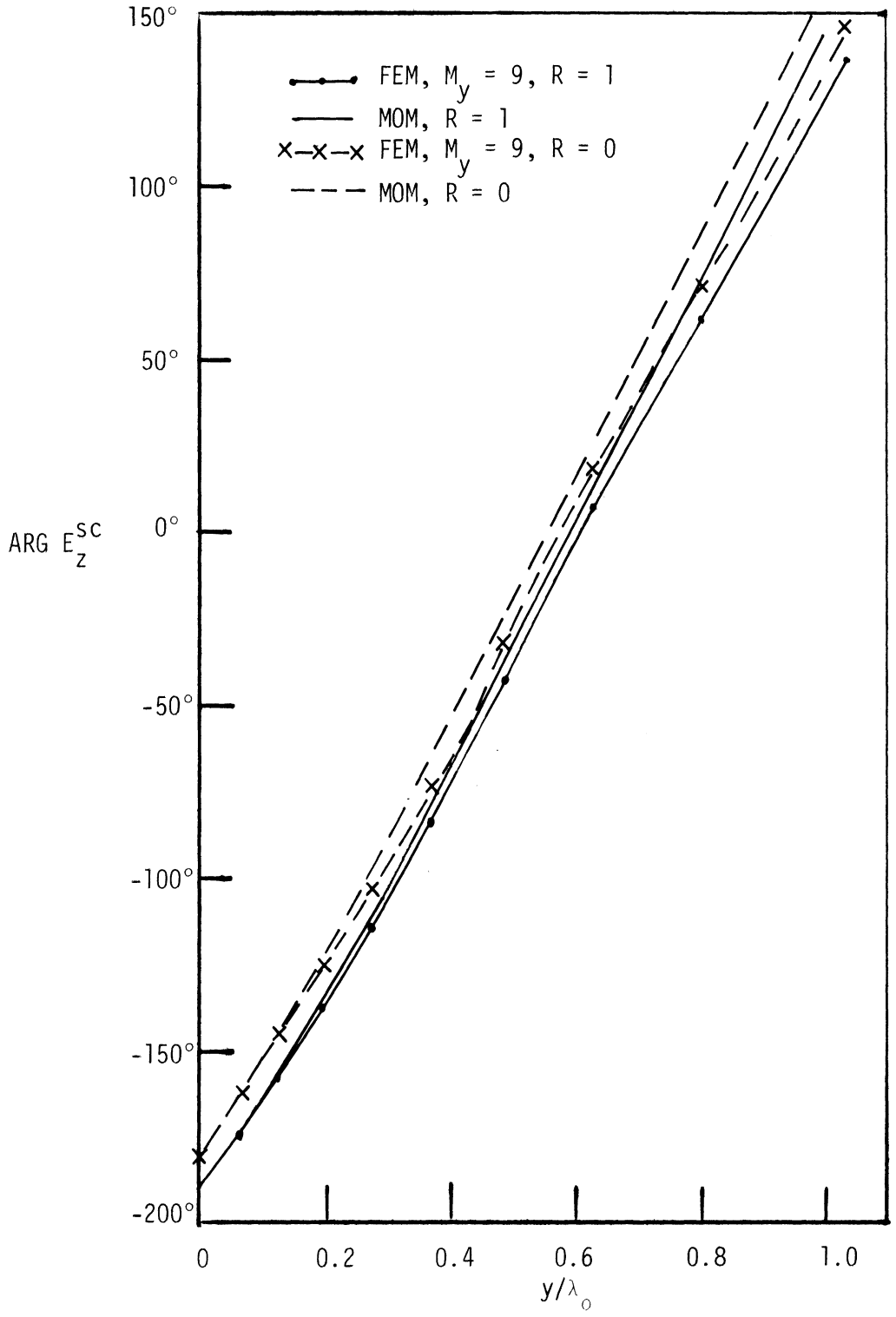

Fig. B.2: Scattered field phase vs. distance outward from the strip center (ϕ_o = 90°, w/λ_o = 0.5, λ_o = 1.0, M_x = 6, x = 0).

$$K_z \approx \frac{2A}{Z_o}\sqrt{1+\left(\frac{B}{Ak_o}\right)^2}\,\exp i\left(\theta_o + \tan^{-1}\frac{B}{-Ak_o}\right) \quad . \quad (B.2)$$

To apply this to the current calculation at the center (x = 0) of the strip for R = 0, λ_o = 1, and normal incidence, the following values are obtained from Figs. B.1 and B.2:

MOM: A = 1.0 , B ≈ -0.2 , θ_o = -180 degrees

FEM: A = 1.0 , B ≈ 0.6 , θ_o = -180 degrees

Then (B.2) yields

MOM: $Z_o K_z = 2.001\, e^{i(1.82°)}$

FEM: $Z_o K_z = 2.009\, e^{i(-5.42°)}$

It can be seen from this that the error in the slope of $|E_z^{sc}|$ at the strip caused by the standing wave results primarily in a phase error in $Z_o K_z$. Such phase errors for current in each element adjacent to the strip enter into the integration of $Z_o K_z$ (2.38) to obtain $P(\phi,\phi_o)$.

APPENDIX C. COMPUTATION OF THE SCATTERED FIELD FROM PLANE WAVE NORMAL INCIDENCE ON AN INFINITE RESISTIVE SHEET

C.1 Introduction

In this appendix a one-dimensional problem closely related to the problem stated in Chapter II is discussed. An infinitesimally thin, infinite sheet lying in the $y = 0$ plane is immersed in free space. The sheet is a resistive sheet having boundary conditions given by (2.1) and (2.2). An incident plane wave is polarized so that its electric field is

$$\underline{E}^i = E_z^i \hat{z} = e^{-ik_o y} \hat{z} \quad , \tag{C.1}$$

where an $e^{-i\omega t}$ time dependence is assumed. The direction or propagation of $\underline{E}^i$ is in the negative y direction. The scattered field E_z^{sc} propagates in the positive y direction and satisfies

$$\frac{d^2 E_z^{sc}}{dy^2} + k_o^2 E_z^{sc} = 0 \quad . \tag{C.2}$$

At the sheet the boundary condition for a resistive sheet is, using (2.26)

$$\frac{2iR}{k_o} \left. \frac{dE_z^{sc}}{dy} \right|_+ = E_z^i + E_z^{sc} \tag{C.3}$$

and for a perfectly conducting sheet is

$$E_z^i + E_z^{sc} = 0 \quad . \tag{C.4}$$

Since the scattered field is an outgoing wave, a condition must be satisifed for any $y > 0$:

$$\frac{dE_z^{sc}}{dy} = ik_o E_z^{sc} \quad . \tag{C.5}$$

C.2 Finite Element Formulation

From this point on, let $u = E_z^{sc}(y)$. The solution for u is to be obtained in the region $0 \leq y \leq L$. A one-dimensional version of Green's first identity for scalars u and v is

$$\int_{y=o}^{L} v \frac{d^2u}{dy^2}\, dy = - \int_{y=o}^{L} \frac{dv}{dy}\frac{du}{dy}\, dy + \left[v \frac{du}{dy} \right]_{y=o}^{L} \quad . \tag{C.6}$$

Use of (C.2), (C.3) and (C.5) yields

$$\int_{y=o}^{L} \frac{dv}{dy}\frac{du}{dy}\, dy - k_o^2 \int_{y=o}^{L} vu\, dy - ik_o[vu]_{y=L} - \frac{ik_o}{2R}[v(u + u^i)]_{y=o} = 0 \tag{C.7}$$

for a resistive sheet.

For a perfectly conducting sheet (C.7) cannot be used since R is in the denominator. Instead, the use of (C.2) and (C.5) in (C.6) yields

$$\int_{y=0}^{L} \frac{dv}{dy}\,\frac{du}{dy}\,dy - k_o^2 \int_{y=0}^{L} vu\,dy - ik_o[vu]_{y=L} - \left[v\,\frac{du}{dy}\right]_{y=0} = 0 \quad . \tag{C.8}$$

The value of (du/dy) at y = 0 is unknown, however (C.4) indicates that at y = 0

$$u = -u^i \quad . \tag{C.9}$$

This condition is imposed later.

In order to solve for u, the region $0 \leq y \leq L$ is divided into J equal length elements e with nodes n at the element boundaries (Fig. C.1). For each node there is an interpolation function which is unity at that node and zero at all other nodes. The scalar u is approximated by

$$u(y) \simeq \bar{u}(y) = \sum_{n=1}^{I} N_n(y)a_n \quad , \tag{C.10}$$

where $a_n = u(y_n)$ and I = J + 1.

The function v is restricted to be

$$v(y) = w_m(y) \quad , \quad m = 1,\ldots,I \quad , \tag{C.11}$$

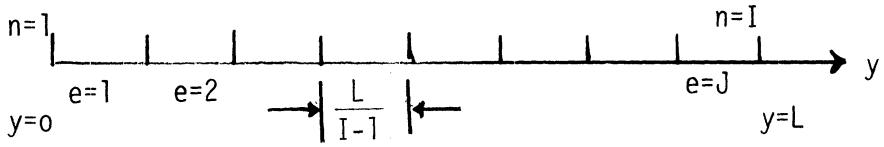

Fig. C.1: Finite elements.

where $w_m(y)$ is one of a set of weight functions yet to be specified. Using Galerkin's method,

$$w_m(y) = N_m(y) \quad . \tag{C.12}$$

Using (C.10), (C.11) and (C.12) in (C.7) yields

$$\int_{y=o}^{L} \frac{dN_m(y)}{dy} \frac{d}{dy} \left\{ \sum_{n=1}^{I} N_n(y) a_n \right\} dy - k_o^2 \int_{y=o}^{L} N_m(y) \left\{ \sum_{n=1}^{I} N_n(y) a_n \right\} dy$$

$$- ik_o \left[N_m(y) \sum_{n=1}^{I} N_n(y) a_n \right]_{y=L} - \frac{ik_o}{2R} \left[N_m(y) \sum_{n=1}^{I} N_n(y) a_n \right]_{y=o}$$

$$= \frac{ik_o}{2R} [N_m(y) u^i]_{y=o} \quad , \quad m = 1,\ldots,I \quad . \tag{C.13}$$

Interchanging the order of integration and summation, (C.13) is written as

$$\sum_{n=1}^{I} K_{mn} a_n = f_m \quad , \quad m = 1,\ldots,I \quad , \tag{C.14}$$

where

$$K_{mn} = \int_{y=o}^{L} \left[\frac{dN_m}{dy} \frac{dN_n}{dy} - k_o^2 N_m N_n \right] dy - ik_o [N_m N_n]_{y=L} - \frac{ik_o}{2R} [N_m N_n]_{y=o} \tag{C.15}$$

and

$$f_m = \frac{ik_o}{2R} u_1^i [N_m]_{y=o} \quad . \tag{C.16}$$

Equation (C.14) represents a set of linear algebraic equations to be solved for the unknown a_n's.

Calculation of the coefficients K_{mn} in the finite element method is done by an element-by-element procedure. The global integration over the entire region is replaced by a sum of integrals over individual elements lying within the interval. Thus

$$K_{mn} = \sum_{e=1}^{J} K_{mn}^e \quad , \tag{C.17}$$

where

$$K_{mn}^e = \int_e \left[\frac{dN_m}{dy} \frac{dN_n}{dy} - k_o^2 N_m N_n \right] dy - ik_o [N_m N_n]_{y=L} - \frac{ik_o}{2R} [N_m N_n]_{y=o} \quad . \tag{C.18}$$

For a perfectly conducting sheet, the set of algebraic equations should be modified by removing the equation corresponding to the node at the sheet where the field strength a_1 is known. Using (C.9),

$$a_1 = -u^i(0) = -u_1^i \quad . \tag{C.19}$$

In this case (C.10) is written as

$$u(y) \approx \bar{u}(y) = -N_1(y) u_1^i + \sum_{n=2}^{I} N_n(y) a_n \quad . \tag{C.20}$$

Using (C.20), (C.11) and (C.12) in (C.8) yields

$$\int_{y=o}^{L} \frac{dN_m}{dy} \frac{d}{dy}\left[-N_1(y)u_1^i + \sum_{n=2}^{I} N_n(y)a_n\right] dy - k_o^2 \int_{y=o}^{L} N_m \left[-N_1(y)u_1^i + \sum_{n=2}^{I} N_n(y)a_n\right] dy - ik_o\left[N_m\left(-N_1(y)u_1^i + \sum_{n=2}^{I} N_n(y)a_n\right)\right]_{y=L}$$

$$- \left[N_m \frac{d}{dy}\left(-N_1(y)u^i + \sum_{n=2}^{I} N_n(y)a_n\right)\right]_{y=o} = 0 \quad , \quad m = 2,\ldots,I \quad . \tag{C.21}$$

After interchanging the order of integration and summation, and transferring the term corresponding to the node on the sheet to the right-hand side, the resulting set of linear algebraic equations is

$$\sum_{n=2}^{I} K_{mn}a_n = g_m \quad , \quad m = 2,\ldots,I \quad , \tag{C.22}$$

where

$$K_{mn} = \sum_{e=1}^{J} K_{mn}^e \quad , \tag{C.23}$$

$$K_{mn}^e = \int_e \left[\frac{dN_m}{dy} \frac{dN_n}{dy} - k_o^2 N_m N_n\right] dy - ik_o[N_m N_n]_{y=L} \tag{C.24}$$

and

$$g_m = K_{m1}u_1^i \quad . \tag{C.25}$$

C.3 Element Matrix Coefficient K^e_{mn}

Linear interpolation functions are used for the elements:

$$N_n(y) = 1 - \left[\frac{y - y_n}{y_{n+1} - y_n}\right], \quad y_n \leq y \leq y_{n+1}$$

$$= \frac{y - y_n}{y_n - y_{n-1}}, \quad y_{n-1} \leq y \leq y_n \ . \tag{C.26}$$

In a typical element between $y = y_k$ and y_{k+1} the interpolation functions can be written in a general form

$$N_n(y) = \frac{1}{2}\left[1 + \alpha_n \frac{\left(y - \frac{y_k + y_{k+1}}{2}\right)}{\frac{y_{k+1} - y_k}{2}}\right], \tag{C.27}$$

where $\alpha_n = -1$ for $n = k$ and $\alpha_n = 1$ for $n = k + 1$. The integral in K^e_{mn} (C.18) or (C.24) is now evaluated.

$$\int_e \left[\frac{dN_m}{dy}\frac{dN_n}{dy} - k_o^2 N_m N_n\right] dy = \frac{\alpha_m\alpha_n}{L/(I-1)} - \frac{k_o^2}{4}\frac{L}{I-1}\left(1 + \frac{1}{3}\alpha_m\alpha_n\right), \tag{C.28}$$

where m and n can each be "k" or "k + 1". Thus (C.18) becomes

$$K^e_{mn} = \frac{\alpha_m\alpha_n}{L/(I-1)} - \frac{k_o^2}{4}\left(\frac{L}{I-1}\right)\left(1 + \frac{1}{3}\alpha_m\alpha_n\right) - ik_o[N_m N_n]_{y=L} - \frac{ik_o}{2R}[N_m N_n]_{y=o} \tag{C.29}$$

and K^e_{mn} for the perfectly conducting strip case is given by

$$K^e_{mn} = \frac{\alpha_m \alpha_n}{L/(I-1)} - \frac{k_o^2}{4}\left(\frac{L}{I-1}\right)\left(1 + \frac{1}{3}\alpha_m\alpha_n\right) - ik_o[N_m N_n]_{y=L} \cdot \tag{C.30}$$

For a general element between nodes k and k + 1 (element not adjacent to y = 0 or y = L) element matrix coefficients are

$$\left.\begin{aligned} K^e_{k,k} &= \frac{I-1}{L} - \frac{k_o^2}{3}\frac{L}{I-1} \\ K^e_{k,k+1} &= -\frac{I-1}{L} - \frac{k_o^2}{6}\frac{L}{I-1} \\ K^e_{k+1,k} &= -\frac{I-1}{L} - \frac{k_o^2}{6}\frac{L}{I-1} \\ K^e_{k+1,k+1} &= \frac{I-1}{L} - \frac{k_o^2}{3}\frac{L}{I-1} \end{aligned}\right\} \tag{C.31}$$

For the element adjacent to y = 0 (e = 1) the coefficients are

$$\left.\begin{aligned} K'_{11} &= \frac{I-1}{L} - \frac{k_o^2}{3}\frac{L}{I-1} - \frac{ik_o}{2R} \\ K'_{12} &= -\frac{I-1}{L} - \frac{k_o^2}{6}\frac{L}{I-1} \\ K'_{21} &= -\frac{I-1}{L} - \frac{k_o^2}{6}\frac{L}{I-1} \\ K'_{22} &= \frac{I-1}{L} - \frac{k_o^2}{3}\frac{L}{I-1} \end{aligned}\right\} \tag{C.32}$$

For the element adjacent to y = L (e = J) the coefficients are

$$\left.\begin{aligned} K^J_{I-1,I-1} &= \frac{I-1}{L} - \frac{k_o^2}{3}\,\frac{L}{I-1} \\ K^J_{I-1,I} &= -\frac{I-1}{L} - \frac{k_o^2}{6}\,\frac{L}{I-1} \\ K^J_{I,I-1} &= -\frac{I-1}{L} - \frac{k_o^2}{6}\,\frac{L}{I-1} \\ K^J_{I,I} &= \frac{I-1}{L} - \frac{k_o^2}{3}\,\frac{L}{I-1} - ik_o \end{aligned}\right\} \quad . \tag{C.33}$$

In the case of a perfectly conducting strip, the coefficients for the elements are the same as (C.31), (C.32) and (C.33) except that K^1_{11} in (C.32) does not have the term with R in it.

C.4 Set of Linear Algebraic Equations

Using (C.17), the coefficients for the set of equations (C.14) are written. If $m \neq 1$ and $m \neq I$, the mth equation is

$$K^{m-1}_{m,m-1} a_{m-1} + (K^{m-1}_{mm} + K^m_{mm}) a_m + K^m_{m,m+1}\, a_{m+1} = 0 \quad . \tag{C.34}$$

If m = 1, the equation is

$$K^1_{11}\, a_1 + K^1_{12}\, a_2 = \frac{ik_o}{2R}\, u^i_1 \tag{C.35}$$

and if m = I, the equation is

$$K^J_{I,I-1}\, a_{I-1} + K^J_{II} a_I = 0 \quad . \tag{C.36}$$

As an example, if there are six nodes (I = 6) and five elements (J = 5) the set of equations in matrix form is

$$\begin{bmatrix} K^1_{11} & K^1_{12} & 0 & 0 & 0 & 0 \\ K^1_{21} & (K^1_{22}+K^2_{22}) & K^2_{23} & 0 & 0 & 0 \\ 0 & K^2_{32} & (K^2_{33}+K^3_{33}) & K^3_{34} & 0 & 0 \\ 0 & 0 & K^3_{43} & (K^3_{44}+K^4_{44}) & K^4_{45} & 0 \\ 0 & 0 & 0 & K^4_{54} & (K^4_{55}+K^5_{55}) & K^5_{56} \\ 0 & 0 & 0 & 0 & K^5_{65} & K^5_{66} \end{bmatrix} \begin{bmatrix} a_1 \\ a_2 \\ a_3 \\ a_4 \\ a_5 \\ a_6 \end{bmatrix} = \begin{bmatrix} \frac{ik_o}{2R} u^i_1 \\ 0 \\ 0 \\ 0 \\ 0 \\ 0 \end{bmatrix} \tag{C.37}$$

for a resistive sheet.

For a perfect conductor (C.22) and (C.23) are used. For example, with I = 6 and J = 5, the system of equations is

$$\begin{bmatrix} (K^1_{22}+K^2_{22}) & K^2_{23} & 0 & 0 & 0 \\ K^2_{32} & (K^2_{33}+K^3_{33}) & K^3_{34} & 0 & 0 \\ 0 & K^3_{43} & (K^3_{44}+K^4_{44}) & K^4_{45} & 0 \\ 0 & 0 & K^4_{54} & (K^4_{55}+K^5_{55}) & K^5_{56} \\ 0 & 0 & 0 & K^5_{65} & K^5_{66} \end{bmatrix} \begin{bmatrix} a_2 \\ a_3 \\ a_4 \\ a_5 \\ a_6 \end{bmatrix} = \begin{bmatrix} u^i_1 K^1_{21} \\ 0 \\ 0 \\ 0 \\ 0 \end{bmatrix} \tag{C.38}$$

C.5 Transmission Line Interpretation

The set of linear algebraic equations (C.14) may be interpreted in terms of a transmission line made up of discrete

components. A typical equation such as (C.34) resembles a node voltage equation if the coefficients K_{mn} are divided by $-\omega\mu_o$. Each coefficient is then an admittance. The equation for node n is

$$\frac{i}{\omega\mu_o} K^{n-1}_{n,n-1} a_{n-1} + \frac{i}{\omega\mu_o} [K^{n-1}_{nn} + K^{n}_{nn}] a_n + \frac{i}{\omega\mu_o} K^{n}_{n,n+1} a_{n+1} = 0 \quad . \tag{C.39}$$

The node voltage equation for node n written in terms of the circuit components (Fig. C.2) is

$$-Y_1 a_{n-1} + (Y_1 + Y_2 + Y_3) a_n - Y_3 a_{n+1} = 0 \quad . \tag{C.40}$$

Upon comparing (C.39) and (C.40), it is apparent that

$$Y_1 = -\frac{i}{\omega\mu_o} K^{n-1}_{n,n-1} \quad , \tag{C.41}$$

$$Y_3 = -\frac{i}{\omega\mu_o} K^{n+1}_{n,n+1} \quad , \tag{C.42}$$

and

$$Y_1 + Y_2 + Y_3 = \frac{i}{\omega\mu_o} (K^{n-1}_{nn} + K^{n}_{nn}) \quad . \tag{C.43}$$

From these

$$Y_2 = \frac{i}{\omega\mu_o} (K^{n-1}_{nn} + K^{n}_{nn} + K^{n-1}_{n,n-1} + K^{n+1}_{n,n+1}) \quad . \tag{C.44}$$

Using (C.31) yields

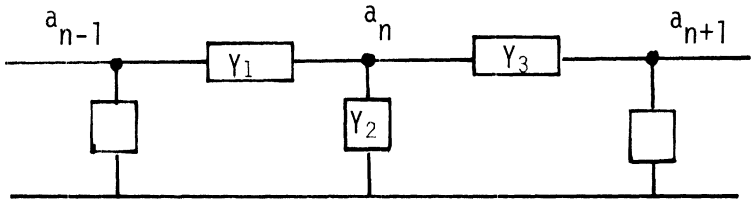

Fig. C.2: Transmission line.

$$Y_1 = Y_3 = \frac{i}{\omega\mu_o}\left[\frac{I-1}{L} + \frac{k_o^2}{6}\,\frac{L}{I-1}\right] \tag{C.45}$$

and

$$Y_2 = -i\omega\varepsilon_o\left(\frac{L}{I-1}\right) . \tag{C.46}$$

The characteristic impedance of a transmission line made up of T sections (Fig. C.3) is (Johnson, 1950, p. 42)

$$Z_c = \sqrt{Z_1 Z_2 + \frac{Z_1^2}{4}} . \tag{C.47}$$

Using (C.45) and (C.46) yields

$$Z_1 = -\frac{i\omega\mu_o\left(\frac{L}{I-1}\right)}{1 + \frac{k_o^2}{6}\left(\frac{L}{I-1}\right)^2} \tag{C.48}$$

and

$$Z_2 = \frac{i}{\omega\varepsilon_o\left(\frac{L}{I-1}\right)} . \tag{C.49}$$

Also

$$Z_c = \sqrt{\frac{\mu_o}{\varepsilon_o}\left\{\frac{1}{1 + \frac{k_o^2}{6}\left(\frac{L}{I-1}\right)^2} - \frac{k_o^2\left(\frac{L}{I-1}\right)^2}{4\left[1 + \frac{k_o^2}{6}\left(\frac{L}{I-1}\right)^2\right]^2}\right\}} \tag{C.50}$$

for which

$$\lim_{I \to \infty} Z_c = \sqrt{\frac{\mu_o}{\varepsilon_o}} . \tag{C.51}$$

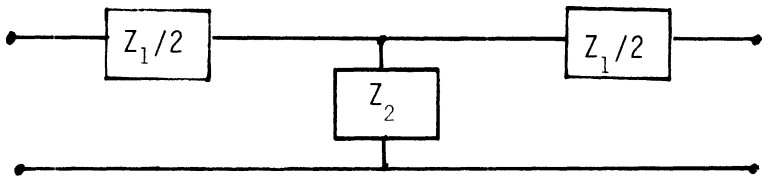

Fig. C.3: Symmetrical T network.

Thus the characteristic impedance of the finite element transmission line is always less than the free space value, but approaches 377 ohms as the density of elements is increased.

Continuing the transmission line analogy, the proper termination of the line to prevent reflections and standing waves may now be determined. The transmission line (Fig. C.2) is terminated in its characteristic impedance Z_c (Fig. C.4). The node voltage equation for node I is

$$-Y_1 a_{I-1} + \left[Y_1 + Y_2 + \frac{1}{\frac{Z_1}{2} + Z_c} \right] a_I = 0 \quad . \tag{C.52}$$

The finite element equation for the last node is

$$\frac{i}{\omega\mu_0} K^J_{I,I-1} a_{I-1} + \frac{i}{\omega\mu_0} K^J_{I,I} a_I = 0 \quad . \tag{C.53}$$

Comparing (C.52) and (C.53) indicates that

$$Y_1 = -\frac{i}{\omega\mu_0} K^J_{I,I-1} \tag{C.54}$$

and

$$Y_1 + Y_2 + \frac{1}{\frac{Z_1}{2} + Z_c} = \frac{i}{\omega\mu_0} K^J_{II} \quad . \tag{C.55}$$

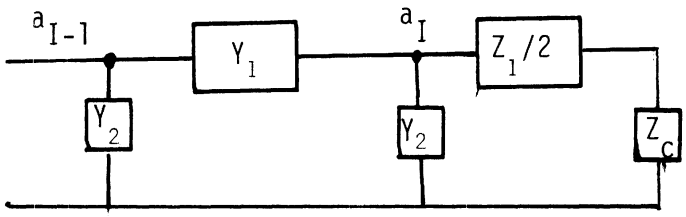

Fig. C.4: Terminated transmission line.

Then using (C.45) and (C.46) in (C.55) yields

$$K^J_{I,I} = \left[\frac{I-1}{L} - \frac{k_o^2}{3}\,\frac{L}{I-1}\right] - \frac{k_o^2}{2}\,\frac{L}{I-1} - \frac{i\omega\mu_o}{\frac{Z_1}{2} + Z_c} \quad . \quad \text{(C.56)}$$

Using (C.48) and (C.50) in (C.56) yields

$$K^J_{I,I} = \left[\frac{I-1}{L} - \frac{k_o^2}{3}\,\frac{L}{I-1}\right] - \frac{k_o^2}{2}\,\frac{L}{I-1}$$

$$+ \frac{1}{\dfrac{L/(I-1)}{2\left[1 + \dfrac{k_o^2}{6}\left(\dfrac{L}{I-1}\right)^2\right]} + \dfrac{i}{k_o}\sqrt{\dfrac{1}{1 + \dfrac{k_o^2}{6}\left(\dfrac{L}{I-1}\right)^2} - \dfrac{k_o^2 L^2/(I-1)^2}{4\left[1 + \dfrac{k_o^2}{6}\left(\dfrac{L}{I-1}\right)^2\right]^2}}} \quad . \quad \text{(C.57)}$$

Use of K^J_{II} given by (C.57) corresponds to a transmission line terminated in its characteristic impedance. This expression should be compared with that given in (C.33) for $K^J_{I,I}$. The value $K^J_{I,I}$ of (C.57) approaches $K^J_{I,I}$ of (C.33) as $I \to \infty$. Thus use of K^J_{II} in (C.33) corresponds to having an impedance mismatch at the termination of the transmission line. The greater the density of the elements, the less the mismatch is. The mismatch will cause standing waves in the numerical results for the scattered field. On the other hand, use of $K^J_{I,I}$ of (C.57) always leads to numerical results without standing waves.

The propagation constant k for the transmission line is given by (Watkins, 1958, p. 28)

$$\cos k\left(\frac{L}{I-1}\right) = 1 + \frac{Y_2}{2Y_1} \quad . \tag{C.58}$$

Use of (C.45) and (C.46) yields

$$\cos k\left(\frac{L}{I-1}\right) = 1 - \frac{1}{2}\,\frac{k_o^2\left(\frac{L}{I-1}\right)^2}{1 + \frac{k_o^2}{6}\left(\frac{L}{I-1}\right)^2}$$

or

$$k \approx \frac{k_o}{\sqrt{1 + \frac{k_o^2}{6}\left(\frac{L}{I-1}\right)^2}} \tag{C.59}$$

for $(L/I\text{-}1) \ll \lambda_o$. Thus the propagation constant is always less than that of free space k_o, and the phase angle of numerical results will always be less than that of the actual scattered plane wave. The greater the density of elements, the less the phase error will be.

Sample numerical results are given in Fig. C.5 through [C.7] for various values of the element density $(I\text{-}1)\lambda_o/L$ in elements per wavelength. The magnitude of the scattered field is plotted versus distance from the resistive sheet in Figs. C.5 and C.6. Figure C.5 shows the standing waves resulting from the imperfect termination of the transmission line and Fig. C.6 shows the result when the line is terminated in its characteristic impedance. The phase of the

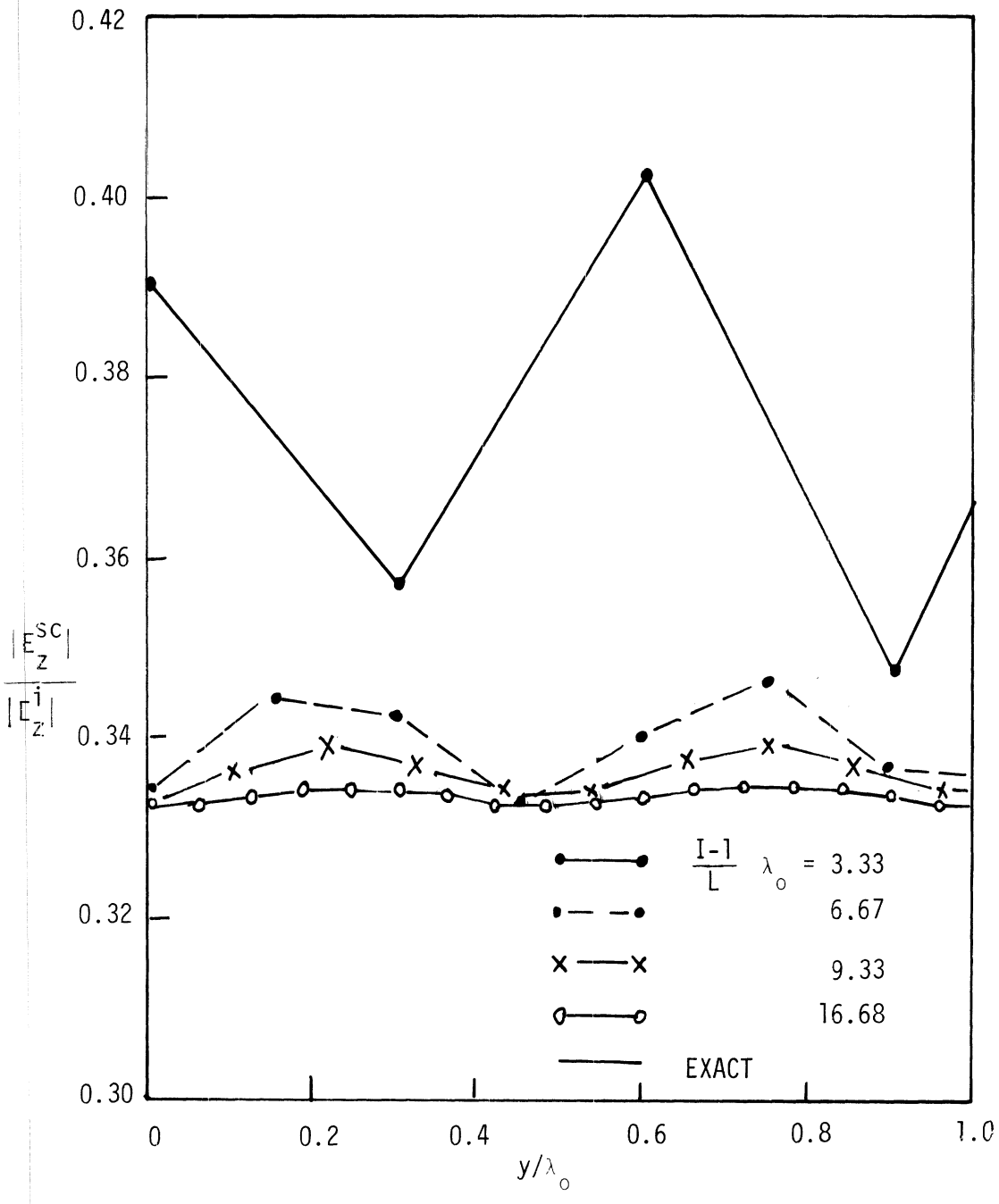

Fig. C.5: $|E_z^{sc}|$ vs. y/λ_o for resistive sheet (R = 1.0), λ_o = 1.0 and "free space termination" (K_{II}^J given by C.33).

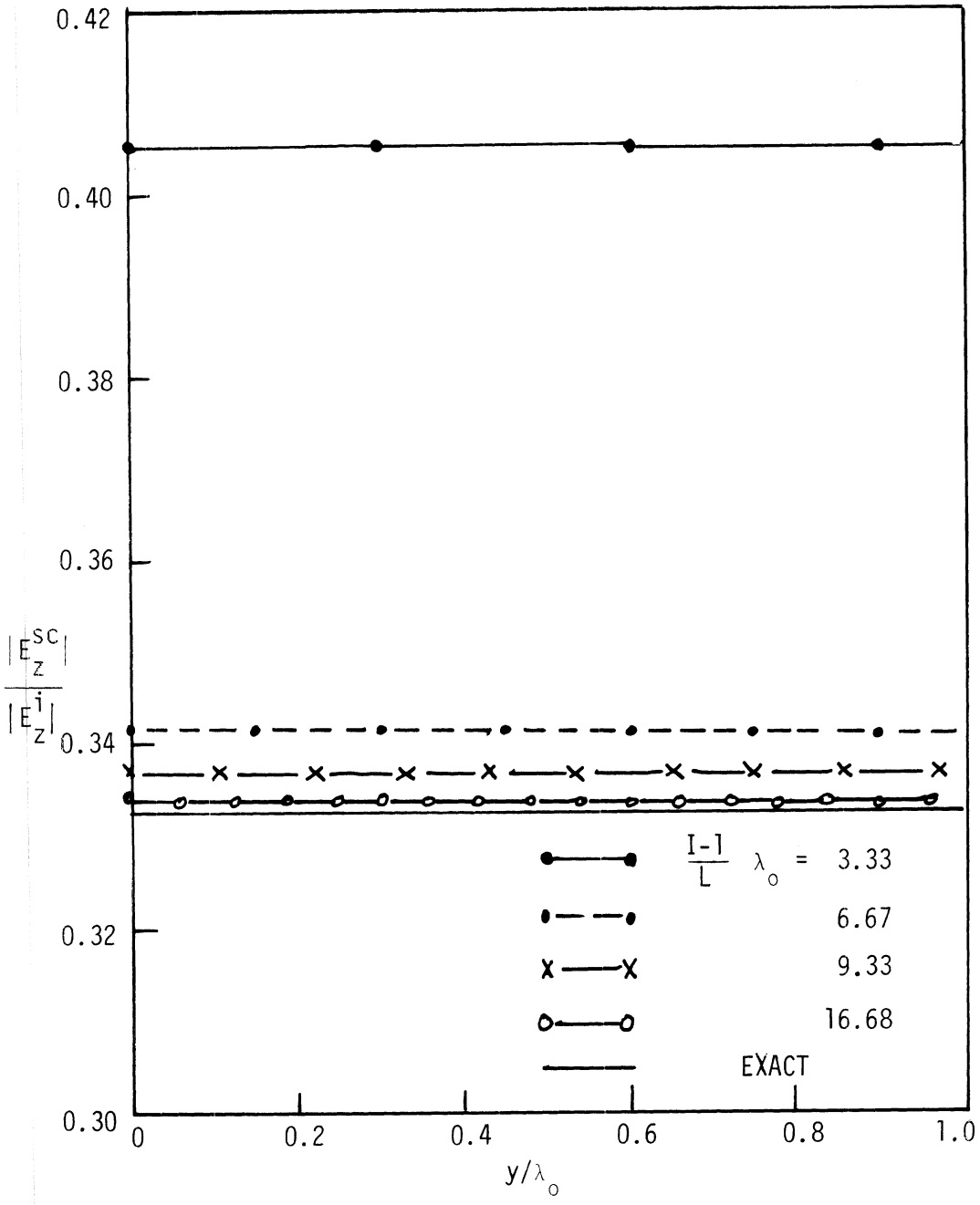

Fig. C.6: $|E_z^{sc}|$ vs. y/λ_o for resistive sheet (R = 1.0), λ_o = 1.0 and "characteristic impedance termination" (K_{II}^J given by C.57).

scattered field versus distance from the sheet is shown in Fig. C.7 for the imperfect termination. The location of the exact values, if plotted, would essentially coincide with the line for 16.68 elements per wavelength. A set of phase curves for the characteristic impedance termination differs only slightly from Fig. C.7.

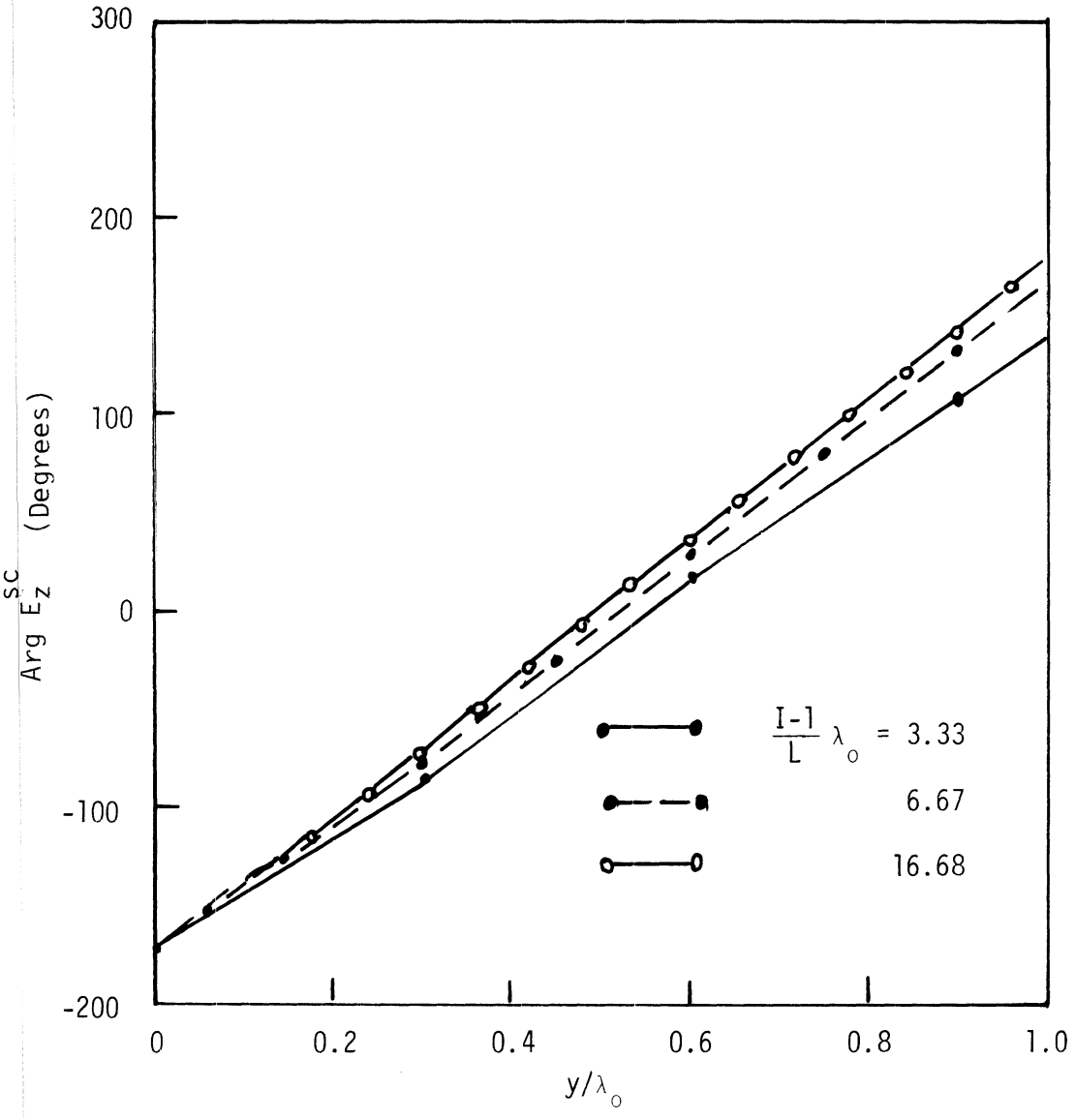

Fig. C.7: Arg E_z^{sc} vs. y/λ_o for resistive sheet (R = 1.0), λ_o = 1.0 and "free space termination" (K_{II}^J given by C.33).

BIBLIOGRAPHY

Arlett, P. L., Bahrani, A. K., and Zienkiewicz, O. C. (1968), "Application of Finite Elements to the Solution of Helmholtz's Equation," Proc. IEE 115, 1762-1766.

Bettess, P. (1977), "Infinite Elements," Int. Jour. Num. Meth. Eng. 11, 53-64.

Bettess, P. and Zienkiewicz, O. C. (1977), "Diffraction and Refraction of Surface Waves Using Finite and Infinite Elements," Int. Jour. Num. Meth. Eng. 11, 1271-1290.

Blackburn, W. S. (1973), "Calculation of Stress Intensity Factors at Crack Tips Using Special Finite Elements," in the Mathematics of Finite Elements and Applications (Whiteman, J. R., ed.), Academic Press.

Bouwkamp, C. J. (1946), "A Note on Singularities Occurring at Sharp Edges in Electromagnetic Diffraction Theory," Physica 12, 467-474.

Bowman, J. J., Senior, T.B.A., and Uslenghi, P.L.E., editors (1969), Electromagnetic and Acoustic Scattering by Simple Shapes, North-Holland Publishing Company.

Brebbia, C. A. and Walker, S. (1980), "Boundary Element Techniques in Engineering," Newnes-Butterworths, London.

Brillouin, L. (1953), Wave Propagation in Periodic Structures, Dover Publications, New York.

Chang, S. K. and Mei, K. K. (1976), "Application of the Unimoment Method to Electromagnetic Scattering of Dielectric Cylinders," IEEE Trans. on Antennas and Propagation AP-24, 35-42.

Engquist, B. and Majda, A. (1977), "Absorbing Boundary Conditions for the Numerical Simulation of Waves," Mathematics of Computation 31, 629-651.

Fawzi, T. H. and Burke, P. E. (1974), "Edge Effects in Induction Problems," IEEE Trans. on Magnetics MAG-10, 429-430.

Franz, W. (1948), "Zur Formulierung des Huygensschen Prinzips," Z. Naturforschung, Part 3a, 500-506.

Franz, W. (1949), "Zur Theorie der Beugung," Z. Physik 125, 563-596.

Hanson, M. E. and Petschek, A. G. (1976), "A Boundary Condition for Significantly Reducing Boundary Reflections with a Lagrangian Mesh," Jour. Comp. Phys. 21, 333-339.

Harrington, R. F. (1968), Field Computation by Moment Methods, MacMillan Co., New York.

Jeng, G. and Wexler, A. (1977), "Isoparametric, Finite Element, Variational Solution of Integral Equations for Three-Dimensional Fields," Int. Jour. Num. Meth. Eng. 11, 1455-1471.

Johnson, W. C. (1950), Transmission Lines and Networks, McGraw-Hill, New York.

Jones, D. S. (1956), "A Critique of the Variational Method in Scattering Problems," IRE Trans. on Antennas and Propagation AP-4, 297-301.

Klein, C. A. and Mittra, R. (1975), "An Application of the 'Condition Number' Concept to the Solution of Scattering Problems in the Presence of the Interior Resonant Frequencies," IEEE Trans. on Antennas and Propagation AP-23, 431-435.

Knott, E. F., Liepa, V. V., Senior, T.B.A., (1973), "Non-Specular Radar Cross-Section Study," AFAL-TR-73-70, University of Michigan Radiation Laboratory Report 011062-1-F.

Kouyoumjian, R. G. and Peters, L. (1965), "Range Requirements in Radar Cross-Section Measurements," Proc. IEEE 53, 920-928.

Maue, A. W. (1949), "Zur Formulierung eines allgemeinen Beugungs-problems durch eine Integralgleichung," Z. Physik 126, 601-618.

McDonald, B. H. and Wexler, A. (1972), "Finite-Element Solution of Unbounded Field Problems," IEEE Trans. on Microwave Theory and Techniques MTT-20, 841-847.

McDonald, B. H. and Wexler, A. (1980), "Mutually Constrained Partial Differential and Integral Equation Field Formulations," in Finite Elements in Electrical and Magnetic Field Problems (Chari, M.V.K. and Silvester, P. P., editors), John Wiley and Sons, New York.

Mei, K. K. (1974), "Unimoment Method of Solving Antenna and Scattering Problems," IEEE Trans. on Antennas and Propagation AP-22, 760-766.

Meixner, Josef (1949), "Die Kantenbedingung in der Theorie der Beugung Electromagnetischer Wellen an Vollkommen Leitenden Ebenen Schirmen," Ann. Physik 6, 2-9.

Meixner, Josef (1972), "The Behaviour of Electromagnetic Fields at Edges," IEEE Trans. on Antennas and Propagation AP-20, 442-446.

Morgan, M. A. and Mei, K. K. (1979), "Finite-Element Computation of Scattering by Inhomogeneous Penetrable Bodies of Revolution," IEEE Trans. on Antennas and Propagation AP-27, 202-214.

Orlanski, I. (1976), "A Simple Boundary Condition for Unbounded Hyperbolic Flows," Jour. Comp. Phys. 21, 251-269.

Poggio, A. J. and Miller, E. K. (1973), "Integral Equation Solutions of Three-Dimensional Scattering Problems," in Computer Techniques for Electromagnetics (Mittra, R., ed.), Pergamon Press.

Sankar, A. and Tong, T. C. (1975), "Current Computation on Complex Structures by Finite-Element Method," Electronics Letters 11, 481-482.

Senior, T.B.A. (1979), "Backscattering from Resistive Strips," IEEE Trans. on Antennas and Propagation AP-27, 808-813.

Silvester, P. and Hsieh, M. S. (1971), "Finite-Element Solution of 2-Dimensional Exterior-Field Problems," Proc. IEE 118, 1743-1747.

Smith, W. D. (1974), "A Nonreflecting Plane Boundary for Wave Propagation Problems," Jour. Comp. Phys. 15, 492-503.

Stratton, J. A. and Chu, L. J. (1939), "Diffraction Theory of Electromagnetic Waves," Physical Review 56, 2nd Series, 99-107.

Stratton, J. A. (1941), Electromagnetic Theory, McGraw-Hill, New York.

Thatcher, R. W. (1978), "On the Finite Element Method for Unbounded Regions," SIAM Jour. Num. Anal. 15, 466-477.

Ungless, R. F. (1973), "An Infinite Finite Element," M.Sc. Thesis, Department of Civil Engineering, University of British Columbia, Canada.

Watkins, D. A. (1958), Topics in Electromagnetic Theory, John Wiley and Sons, New York.

Wexler, A. (1969), "Computation of Electromagnetic Fields," IEEE Trans. on Microwave Theory and Techniques MTT-17, 416-439.

Zienkiewicz, O. C. (1977), The Finite Element Method, 3rd edition, McGraw-Hill, London.

Zienkiewicz, O. C., Kelly, D. W., and Bettess. P. (1977), "The Coupling of the Finite Element Method and Boundary Solution Procedures," Int. Jour. Num. Meth. Eng. 11, 355-375.